2-27-2010

Geodetic Imaging of Plate Motions, Slip Rates, and Partitioning of Deformation in Japan

John P. Loveless
Smith College, jloveles@smith.edu

Brendan J. Meade
Harvard University

JOURNAL OF GEOPHYSICAL RESEARCH, VOL. 115, B02410, doi:10.1029/2008JB006248, 2010

Geodetic imaging of plate motions, slip rates, and partitioning of deformation in Japan

John P. Loveless[1] and Brendan J. Meade[1]

Received 11 December 2008; revised 21 July 2009; accepted 11 September 2009; published 27 February 2010.

[1] Interseismic deformation in Japan results from the combined effects of tectonic processes including rotation of crustal blocks and the earthquake cycle process of elastic strain accumulation about upper plate faults and subduction zone interfaces. We use spherical linear block theory constrained by geodetic observations from densely spaced Global Positioning System (GPS) stations to estimate plate motions, fault slip rates, and spatially variable interplate coupling on the Japan-Kuril, Sagami, and Nankai subduction zones. The reference model developed in this paper consists of 20 blocks, produces a mean residual velocity magnitude of 1.84 mm/yr at 950 stations, and accounts for 96% of the observed interseismic deformation signal. We estimate fault slip rates in excess of 15 mm/yr along the Niigata-Kobe Tectonic Zone and Itoigawa-Shizuoka Tectonic Line through central Japan, confirming their hypothesized roles as major tectonic boundaries. Oblique convergence across the Nankai Trough is partitioned, with 3/4 of the ~30 mm/yr of trench-parallel motion accommodated by strike-slip motion on the subduction interface and the remaining 1/4 accommodated by right-lateral slip on the Median Tectonic Line. In contrast, our models suggest negligible slip partitioning in eastern Hokkaido, where oblique slip on the Japan-Kuril subduction interface accommodates all of the trench-parallel component of relative plate motion. Inferred spatial variations in the rake and magnitude of slip deficit on subduction zone interfaces reflect the influences of megathrust geometry and earthquake cycle processes such as enhanced elastic strain accumulation about seismic asperities and coseismic sense fault motion indicative of silent slip events or afterslip following large earthquakes.

Citation: Loveless, J. P., and B. J. Meade (2010), Geodetic imaging of plate motions, slip rates, and partitioning of deformation in Japan, *J. Geophys. Res.*, *115*, B02410, doi:10.1029/2008JB006248.

1. Introduction

[2] Over the last two decades, Global Positioning System (GPS) measurements of crustal motion have provided unprecedented insight into tectonic processes including plate motions, fault system activity, and the earthquake cycle [e.g., *Feigl et al.*, 1993; *Hager et al.*, 1991]. Modern wide aperture GPS networks comprise hundreds of continuously recording stations capable of tracking spatial and temporal variations in surface motions across entire plate boundary zones, providing insight into on the underlying tectonic forces that drive them. The GEONET network of Japan [*Sagiya et al.*, 2000, 2004] is a type example of such an array, consisting of 1224 GPS stations spaced ~20 km apart recording daily position estimates with time series durations up to 15 years. The long recording period and dense station spacing make these data ideal for understanding active plate boundary processes and, in particular, the interactions between subduction zones and crustal faults in and around Japan.

1.1. Plate Tectonic Setting Models

[3] The plate tectonic setting of Japan is a debated topic, with proposed models differing in the number, names, sizes, and interactions of tectonic plates [e.g., *Bird*, 2003; *DeMets*, 1992b; *Seno et al.*, 1993, 1996]. This ambiguity stems primarily from difficulty in precisely determining the boundary between the North American (NAM) and Eurasian (EU) plates in northeast Asia [*Seno et al.*, 1996, and references therein]. All models are similar in that the Pacific Plate (PAC) subducts beneath central northern Honshu and Hokkaido at the Japan-Kuril Trench, and the Philippine Sea Plate (PS) subducts obliquely beneath southwestern Honshu and Shikoku along the Nankai Trough, beneath central Honshu but above PAC at the Sagami Trough, and beneath Kyushu and the Ryukyu Islands (Figure 1) [*Seno and Takano*, 1989]. Some models suggest that northern Honshu and Hokkaido belong to NAM [*Nakamura*, 1983], while others [e.g., *Chapman and Solomon*, 1976] place the boundary between NAM and EU through Hokkaido, meaning that most of Japan is part of EU. Subdivision of NAM and EU around Japan into several smaller plates forms the basis of additional plate tectonic models. The Okhotsk Plate (OK) encompasses much of the Sea of Okhotsk, with its eastern boundary defined by the Japan-Kuril Trench and the

[1]Department of Earth and Planetary Sciences, Harvard University, Cambridge, Massachusetts, USA.

0148-0227/10/2008JB006248$09.00

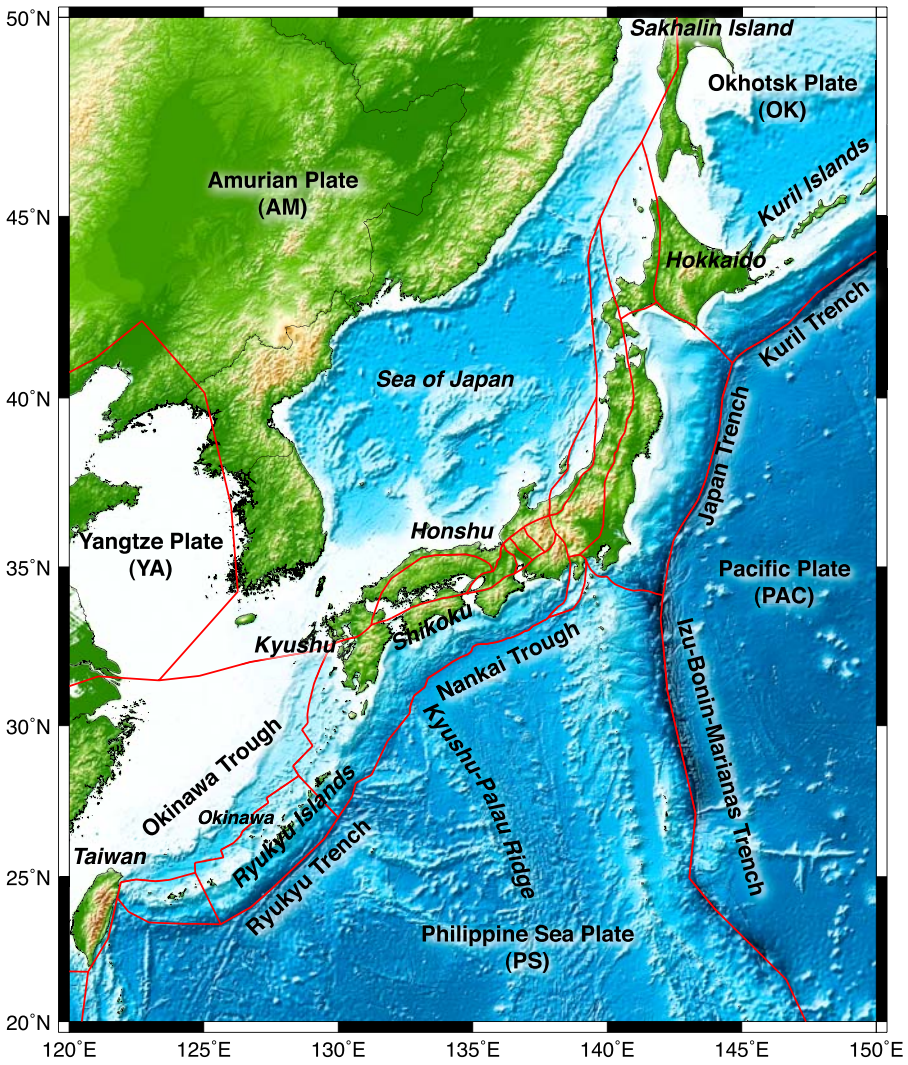

Figure 1. Shaded relief map of the East Asia–Pacific region, labeled with geographic (italicized) and tectonic features discussed in this paper. Red lines show the block boundaries used in model JB1.

western boundary striking roughly parallel to the long axis of Sakhalin Island (Figure 1). The western boundary of OK near Japan has been proposed to cross Hokkaido [*Chapman and Solomon*, 1976] or, alternatively, follow the eastern edge of the Sea of Japan and through central Honshu [e.g., *Cook et al.*, 1986], with the Sea of Japan portion of the boundary representing a zone of "incipient subduction" [*Nakamura*, 1983]. *Seno* [1985] employs both of these boundaries in proposing a new microplate comprising northern Honshu and southwest Hokkaido. The Amurian Plate (AM) has been subdivided from EU and lies between the Baikal Rift Zone in Russia and OK (or NAM [*Zonenshain and Savostin*, 1981]) and, based on the analysis of *Tamaki and Honza* [1985], AM is beginning to subduct beneath OK (or NAM) at the incipient subduction zone. This plate boundary has been highlighted by the occurrence of several moderate to large earthquakes, including the 2007 M_w = 6.8 Niigata Prefecture reverse faulting event. *Kimura and Tamaki* [1986] suggest that much of Japan is part of AM, but the eastern part of Hokkaido belongs to OK. They argue that much of northern Honshu is part of a "strike-slip duplex," with numerous NNW striking right-lateral faults dividing the island into distinct blocks. The easternmost of these faults extends north from the prominent bend in the Japan-Kuril subduction zone (41°N) across Hokkaido and Sakhalin Island, consistent with previous interpretations of the AM-OK boundary [e.g., *Chapman and Solomon*, 1976]. *Apel et al.* [2006] find that contemporary GPS velocities in northeast Asia favor inclusion of AM and OK as distinct plates with boundaries similar to those proposed previously [e.g., *Cook et al.*, 1986; *Zonenshain and Savostin*, 1981].

1.2. Elastic Deformation Signals

[4] In addition to rotational motion of tectonic plates, elastic deformation from both offshore subduction zones and the onshore network of crustal faults produces distinct signatures in the geodetic velocity field. Interseismic elastic strain accumulation due to locking at a subduction zone gives rise to a surface velocity field directed approximately in the direction of plate convergence, with speeds that in general decay with distance away from the plate boundary [*Savage*, 1983]. Where convergence is oblique to the strike of the subduction zone, geodetic velocities show enhanced deflection away from the trench-perpendicular direction

[*Bevis and Martel*, 2001; *McCaffrey*, 2002]. Accommodation of deformation at obliquely converging plate boundaries can occur in a variety of ways, including (1) complete partitioning of the convergence vector, with the trench-perpendicular component accommodated by dip slip on the subduction interface and the trench-parallel component taken up by an upper plate strike-slip fault parallel to the plate boundary [*Fitch*, 1972], (2) no partitioning, with interplate earthquake slip opposite the direction of plate convergence, and (3) distributed plastic deformation of the upper plate combined with thrust earthquakes with nearly trench-perpendicular slip vectors [e.g., *McCaffrey*, 1992, 1993]. Strain accumulation about upper plate strike-slip faults produces the classic arctangent signature that typifies the interseismic geodetic velocity fields near the Dead Sea, north Anatolian, and San Andreas fault zones [e.g., *Savage and Burford*, 1973; *Reilinger et al.*, 2006; *Gomez et al.*, 2007]. The complicated tectonics of Japan produce an elastic deformation signal that includes the combined effects of interseismic strain accumulation from perpendicular subduction, oblique subduction, and upper plate faults.

[5] Many previous modeling studies of geodetic data in Japan focused exclusively on the dip-slip component of coupling on subduction zones [e.g., *Ito et al.*, 2000; *Le Pichon et al.*, 1998; *Mazzotti et al.*, 2000; *Sagiya et al.*, 2000], although some work has also addressed the influence of upper plate faults [e.g., *Kanaori et al.*, 1993; *Matsuzaki et al.*, 1996; *Miyazaki and Heki*, 2001; *T. Nishimura et al.*, 2004, 2007]. Efforts to model the integrated effects of both subduction zone and upper plate faults were pioneering in the application of block-and-fault models to study both historical geodetic data [*Hashimoto and Jackson*, 1993] and the GEONET GPS velocity field [*Hashimoto et al.*, 2000]. However, the latter model features several surprising results, including (1) a slip rate on the Japan-Kuril Trench (136–150 mm/yr) that far exceeds many long-term estimates across the plate boundary (75–95 mm/yr [*Bird*, 2003; *Seno et al.*, 1996]), (2) no opening resolved across the Beppu-Shimabara Graben on the island of Kyushu, and (3) large (~10 mm/yr) differences between modeled and observed velocities on Hokkaido. Regional microplate and block modeling studies have suggested several important tectonic characteristics, including the segmentation of the Ryukyu fore arc into distinct blocks [*Nakamura*, 2004; *S. Nishimura et al.*, 2004], the presence of a fault cross cutting southern Kyushu [*Nishimura and Hashimoto*, 2006; *Wallace et al.*, 2009], and the complicated interactions amongst faults in the Kanto-Tokai region of central Japan [*Nishimura et al.*, 2007]. We extend these previous studies by using interseismic GEONET GPS observations nationwide, in addition to measurements elsewhere in the world, to assess the modern tectonics at scales ranging from individual structures to interacting tectonic plates.

2. Block Modeling

[6] Nominally interseismic GPS velocities record the combined effects of plate motions, permanent deformation, and elastic strain accumulation. Using linear spherical block theory [*Meade and Loveless*, 2009], we simultaneously estimate the rotation vectors of crustal blocks, kinematically consistent slip rates on block bounding faults, spatially variable fault slip rates on subduction zone interfaces, and strain rate tensor components within deforming blocks, and we focus on the former three contributions in this paper.

[7] Through an idealized earthquake cycle, interseismic elastic strain accumulation complements coseismic strain release, so that there is no net elastic strain accumulation in the crust surrounding seismogenic faults [e.g., *Savage and Burford*, 1973]. In modern block theory, nominally interseismic velocities, $\mathbf{v}_I$, are given by the difference between long-term block motion, $\mathbf{v}_B$, homogeneous internal block strain, $\mathbf{v}_{\dot{\epsilon}}$, and the elastic deformation from the coseismic slip deficit (CSD) associated with both kinematically consistent slip rates on the block bounding faults, $\mathbf{v}_{CSD}$, and partially coupled regions, $\mathbf{v}_{TDE}$, described by triangular dislocation elements (TDEs): $\mathbf{v}_I = \mathbf{v}_B(\boldsymbol{\Omega}) - [\mathbf{v}_{CSD}(\boldsymbol{\Omega}) + \mathbf{v}_{TDE}(\mathbf{t})] + \mathbf{v}_{\dot{\epsilon}}(\dot{\boldsymbol{\epsilon}})$, where the velocity components are functions of block rotation parameters, $\boldsymbol{\Omega}$, TDE slip rate components, $\mathbf{t}$, or intrablock strain tensors, $\dot{\boldsymbol{\epsilon}}$. We use a linear estimator to simultaneously estimate the block rotation vectors $\boldsymbol{\Omega}^{est}$, smoothly varying TDE slip vectors $\mathbf{t}^{est}$, and intrablock strain tensors $\dot{\boldsymbol{\epsilon}}^{est}$ using a weighted least squares inversion. Fault slip rates are calculated by projecting the rotational block motions onto the geometry of the bounding faults, thus ensuring kinematic consistency. Uncertainties on fault slip rates are calculated by the direct linear propagation of data uncertainties while Euler pole location and rotation rate uncertainties are determined by a Monte Carlo propagation of formal rotation vector uncertainties. Smooth variation of $\mathbf{t}^{est}$ is enforced by simultaneously minimizing the data misfit and gradient of the TDE slip distribution, carried out by setting the discrete second derivative of TDE slip equal to zero. The weighting matrix used in the inversion includes data and pseudodata variance, the latter of which is expressed by a coefficient β, which controls the extent to which TDE smoothness is enforced [e.g., *Maerten et al.*, 2005]. A small value of β permits a better fit to the GPS data at the expense of an oscillating, physically unreasonable TDE slip distribution, while a very large β value strongly enforces smoothing such that $\mathbf{t}^{est}$ on each TDE approaches a homogeneous value (see discussion in section 5.7.1).

3. GPS Data

[8] The principal goal of this paper is to assess the tectonic processes in Japan that contribute to the geodetically observed interseismic deformation signal. Our block models are constrained by GPS velocities from the GEONET array in Japan (Figure 2) [*Sagiya et al.*, 2000] along with several other network across east Asia and the Pacific [*Kogan et al.*, 2000; *Wang et al.*, 2001; *Zhang et al.*, 2004; *Shen et al.*, 2005; *Apel et al.*, 2006; *Calais et al.*, 2006]. We combine these velocities into the nominal stable Eurasian reference frame of *Apel et al.* [2006] by solving for rotation and translation vectors that minimize differential velocities at collocated stations (Appendix A).

[9] We determine the velocity field in Japan using the GEONET processed daily position estimates (Geographical Survey Institute, ftp://terras.gsi.go.jp). For each component of the time series, we correct position offsets introduced by antenna changes (marked by abrupt changes on the order of 10–100 m) and then fit an equation comprising a linear

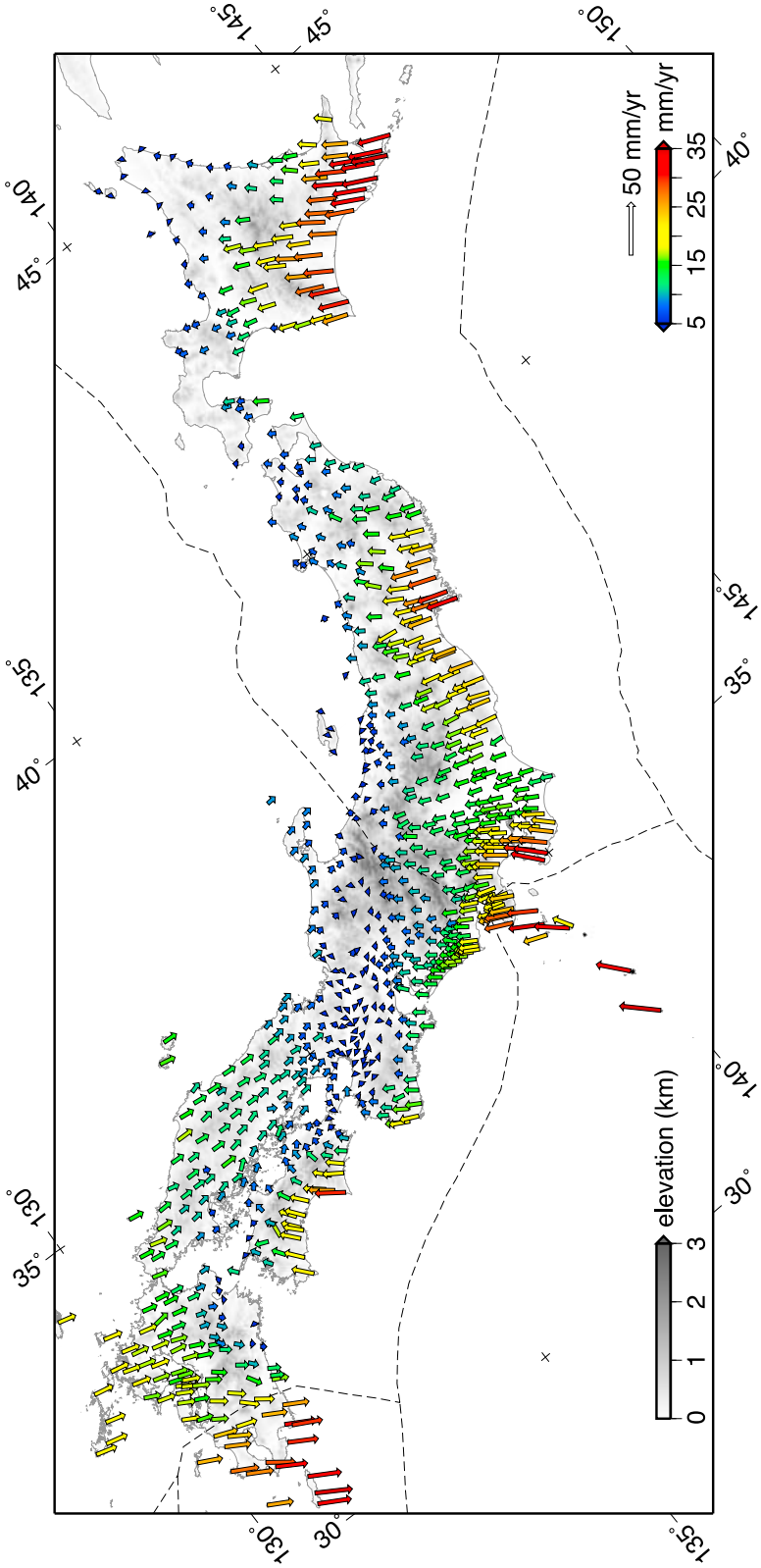

Figure 2. Nominally interseismic GPS velocity field in Japan derived from GEONET data between 1997 and 2000, expressed in a stable Eurasian reference frame [*Apel et al.*, 2006]. Velocity magnitude is indicated both by vector length and color. Dashed lines show plate boundaries from *Bird* [2003].

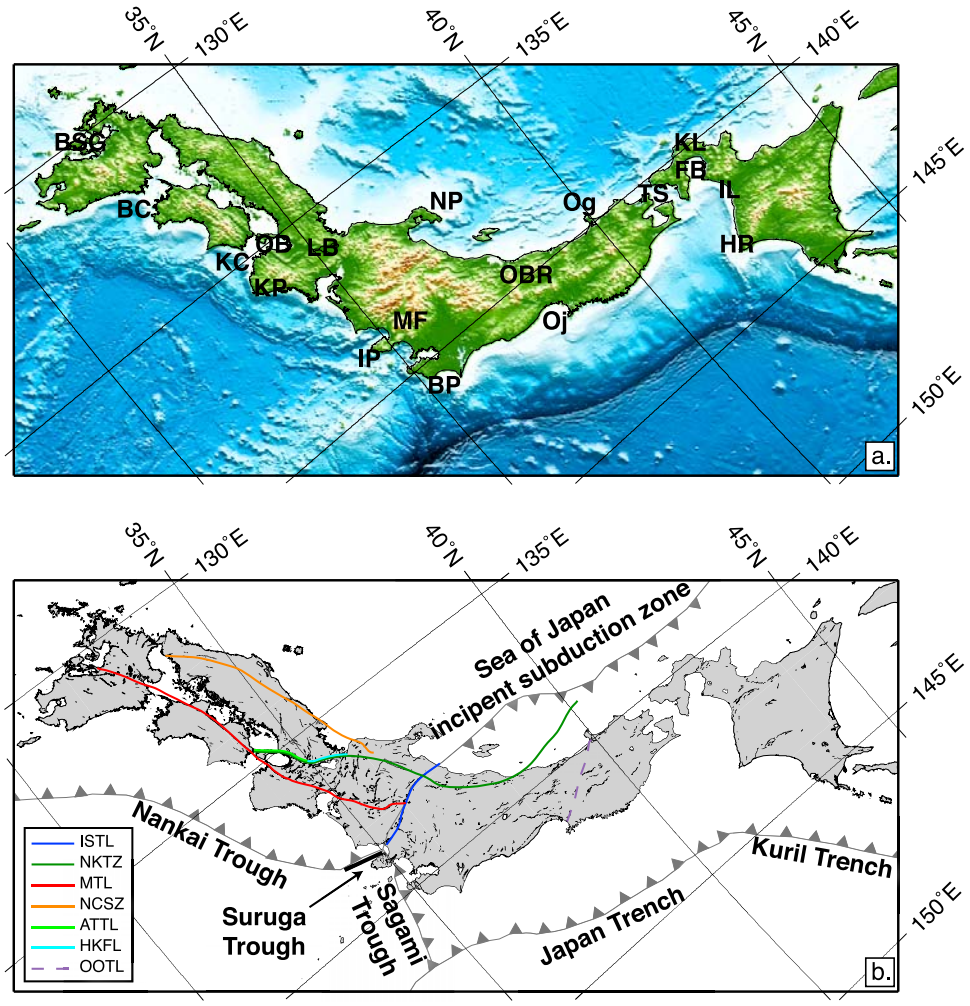

Figure 3. Local base maps showing prominent geologic and geographic features discussed throughout this paper. (a) Shaded relief map showing the four main Japanese Islands and smaller geographic features used as points of reference in the text. BSG, Beppu-Shimabara Graben; BC, Bungo Channel; KC, Kii Channel; OB, Osaka Bay; KP, Kii Peninsula; LB, Lake Biwa; IP, Izu Peninsula; MF, Mount Fuji; BP, Boso Peninsula; NP, Noto Peninsula; OBR, Ou Backbone Range; Oj, Ojika Peninsula; Og, Oga Peninsula; TS, Tsugaru Straits; FB, Funka Bay; KL, Kuromatsunai Lowlands; IL, Ishikari Lowlands; HR, Hidaka Range. (b) Prominent tectonic lines discussed in the text. ISTL, Itoigawa-Shizuoka Tectonic Line; NKTZ, Niigata-Kobe Tectonic Zone [*Sagiya et al.*, 2000]; MTL, Median Tectonic Line [*Fitch*, 1972]; NCSZ, North Chugoku Shear Zone [*Gutscher and Lallemand*, 1999]; ATTL, Arima-Takatsuki Tectonic Line [*Kanaori et al.*, 1994]; HKFL, Hanaore-Kongo Tectonic Line [*Kanaori et al.*, 1994]; OOTL, Oga-Ojika Tectonic Line [*Hashimoto and Jackson*, 1993]. Subduction zones are shown as barbed gray lines and are based on the geometry of *Bird* [2003]; our model varies in the location of these boundaries (see Figure 1).

trend (velocity component) and an annual periodic signal. We examine a time series spanning January 1997 to May 2000, limited in temporal extent to avoid contamination of the interseismic signal from coseismic deformation related to several strong to great earthquakes that have occurred throughout the GEONET observation period of 1994 to present. The two M = 6.7 Hyuga-nada earthquakes of October and December 1996 each induced up to 20–30 mm of coseismic displacement on the east shore of Kyushu [*Yagi et al.*, 1999]. The signal caused by postseismic deformation and a slow slip event following these earthquakes [e.g., *Hirose et al.*, 1999] was not explicitly removed and therefore remains as a contribution to the velocity field in the Kyushu-Bungo Channel region ("BC" in Figure 3a). Consideration of the time series ending in 2000 avoids effects from the seismic swarm offshore central Japan in 2000, the great M_w = 8.3 Tokachi-oki earthquake offshore Hokkaido in 2003, and the series of $M_w \sim 7.5$ earthquakes offshore Sendai between 2003–2005. We account for effects on the velocity field of two episodes (March 1997 and May 1998 [*Nishimura et al.*, 2007, and references therein]) of coupled seismic and volcanic activity near the Izu Peninsula ("IP" in Figure 3a), and two earthquakes that occurred near the southwest Kyushu coast (26 March 1997 and 13 May 1997 [*S. Nishimura et al.*,

2004]) by solving for a shift in station position following onset of the events.

[10] To further avoid contamination by nontectonic effects, we neglect stations whose component velocity uncertainties exceed 5 mm/yr, those whose speeds differ from the mean of all stations within 20 km by more than 5 mm/yr and those within 30 km of the Aira caldera in southern Kyushu and Usu volcano in southwest Hokkaido, following *S. Nishimura et al.* [2004]. If we include the stations near Aira caldera in the block model, their residual velocity vectors point radially outward from the caldera, indicating the influence of the volcano on the local velocity field. Velocities surrounding Usu volcano show no such pattern, likely because volcanic activity began in latest March 2000, near the end of the time series that we use to construct the velocity field. We use a total of 950 velocities (907 in Japan; Figure 2) with mean uncertainties in the east and north velocity components of 2.30 mm/yr (2.42 mm/yr in Japan) and 2.41 mm/yr (2.53 mm/yr in Japan). Station positions, velocities, uncertainties, and a list of omitted stations appear in the auxiliary material Data Set S1.[1] The quoted uncertainties are on par with those reported by *Sagiya et al.* [2000] and are given as the mean residual between the data and the fit equation. Much smaller uncertainties are estimated by examining the square root of the model covariance matrix used in fitting the velocity equation to the data. In either case, the uncertainties on the velocities show approximately Gaussian distributions, and so the effect of using one mode of uncertainty estimation versus the other should be similar in terms of the weighting in the block model inversion.

4. Block Geometry

[11] We construct the block geometry (red lines of Figure 1) of a reference model of the greater Japan region, hereinafter referred to as JB1, based on plate boundary models [e.g., *Bird*, 2003], the digital active fault map of Japan (DAFMJ) [*Nakata and Imaizumi*, 2002], and previous block model studies [*Hashimoto and Jackson*, 1993; *Nakamura*, 2004; *Nishimura and Hashimoto*, 2006; *Nishimura et al.*, 2007]. To constrain the three-dimensional geometry of the Japan-Kuril, Sagami, and Nankai subduction zones, we use contour maps of the subduction interfaces constrained by seismic reflection, microseismicity, and gravity data. For the Japan and Nankai subduction zones, we estimate spatially variable fault slip (using TDEs) only on the portion of the interface that lies offshore Japan where GPS velocities are dense; to the northeast of Hokkaido and southwest of Kyushu, we use dipping rectangular fault segments because GPS data are sparse in these regions. The Japan Trench geometry between 0 and 100 km depth is based on the results of *Furuse and Kono* [2003] and is consistent with previous geodetic analyses of subduction zone locking [e.g., *Mazzotti et al.*, 2000; *T. Nishimura et al.*, 2004; *Suwa et al.*, 2006], while the Nankai geometry follows *Hirose et al.* [2008], using slab contours between 0 and 50 km depth. The Sagami Trough geometry has been disputed [e.g., *Ishida*, 1992; *Sato et al.*, 2005], and we digitize the geometry presented by *Toda et al.* [2008] to generate the TDE mesh. Although the modeled Japan Trench interface extends to 100 km depth, we note that the smoothing constraints and boundary conditions that we impose (zero slip deficit allowed on the updip and downdip extent of the fault) limit substantial slip to between 20 and 60 km depth (see section 5.7).

[12] The large-scale tectonic plate boundaries in general follow the configuration suggested by *Bird* [2003], including consideration of the Pacific (PAC), Okhotsk (OK), Amurian (AM), Eurasian (EU), Yangtze (YA), Okinawan (ON), and Philippine Sea (PS) plates. Some deviation between the boundaries in JB1 and those of *Bird* [2003] exists near Kyushu: we consider the northeastern extreme of the Ryukyu arc as part of the same block as the Nankai fore arc, while *Bird* [2003] shows a NW trending boundary between ON and AM through southernmost Kyushu. We adopt a multiblock geometry for the majority of the Ryukyu arc block, with southern and central Ryuyku blocks defined by structures striking approximately perpendicular to the trench between the islands of Tokara and Amami, and between Miyako and Okinawa [*Nakamura*, 2004; *S. Nishimura et al.*, 2004]. While the exact structures defining these boundaries are unclear [*Nakamura*, 2004], the bathymetry of the region shows several linear features that can be traced across the Ryukyu Trench, roughly orthogonal to its strike (Figure 1). Furthermore, offshore and onshore geology indicates extension directed oblique to orthogonal to the spreading Okinawa Trough [*Fournier et al.*, 2001]. *Nakamura* [2004] estimated Euler poles for the southern, central, and northern Ryukyu blocks testing several different boundary locations; our model geometry varies slightly from the best fitting configuration of that study based on our own analysis of the nationwide velocity field.

[13] The boundary between AM and YA in the East China Sea is similar in the *Bird* [2003] model and JB1. We merge this boundary with the Okinawa Trough at 130°E and the merged structure continues east through Kyushu, representing the Beppu-Shimabara Graben ("BSG" on Figure 3a). The BSG continues through northern Shikoku, where it represents the Median Tectonic Line (MTL, red line on Figure 3b). North of the MTL and isolating much of western Honshu, northernmost Shikoku, and central Kyushu as a distinct block is a structure representing the North Chugoku Shear Zone, which we model as following the general trend of the active volcanic arc and several faults in the channel between northern Kyushu and Honshu (NCSZ, orange line on Figure 3b) [*Gutscher and Lallemand*, 1999]. Just east of Shikoku, the MTL branches into two faults: one that strikes NE toward Kobe and the other that continues along the ENE strike of the MTL (Figure 3b). The NE striking fault represents the SW extent of the Niigata-Kobe Tectonic Zone (NKTZ, dark green line on Figure 3b), which has been defined as a region of high shear strain in analyses of GPS data [e.g., *Sagiya et al.*, 2000; *Sagiya*, 2004; *Toya and Kasahara*, 2005]. Both branches off of the MTL intersect with the Itoigawa-Shizuoka Tectonic Line (ISTL, blue line on Figure 3b) in central Honshu, and the Chubu region lying between these faults (red, green, and blue lines on Figure 3b) is divided into four blocks by three NW striking faults. The ISTL has been proposed to represent a major tectonic boundary through central Honshu [*Hashimoto and Jackson*, 1993; *Sagiya et al.*, 2002], stretching from the Izu

[1] Auxiliary materials are available at ftp://ftp.agu.org/apend/jb/2008jb006248.

Collision Zone to the Japan Sea. The southern extent joins with the Suruga Trough (the northernmost part of the Nankai Trough) offshore southern central Honshu near the Izu Peninsula ("IP," Figure 3a). That peninsula itself is modeled as a distinct block, the Izu Microplate, as has been proposed previously [*Hashimoto and Jackson*, 1993; *Sagiya*, 1999; *Nishimura et al.*, 2007]. Trending east from the ISTL-Izu-Nankai intersection region is the Sagami Trough, which meets the Japan and Marianas trenches at a trench-trench-trench triple junction [*Seno and Takano*, 1989]. The northern extent of the ISTL is modeled as continuing along the eastern margin of the Sea of Japan, as has been proposed in several previous plate tectonic setting models [e.g., *Cook et al.*, 1986; *Seno et al.*, 1996], although we model the Sea of Japan margin as crossing east of Sado Island, on the basis of GPS velocities on the island, which are consistent with motion of AM. Extending NE from the central and northern part of the ISTL are two N striking faults that line the west coast of northern Honshu and the Ou Backbone Range (OBR). These faults are roughly parallel through northern Honshu and intersect just north of western Hokkaido; the merged fault continues north to intersect with the eastern Japan Sea margin fault southwest of the tip of Sakhalin Island (Figure 1). We model an east striking fault branching from the OBR fault in southwest Hokkaido. This fault intersects a N striking fault and the SSE striking, NE dipping fault that represents the Hidaka Fold-and-Thrust Belt in southeast Hokkaido. The N striking fault crosses central Hokkaido to Sakhalin Island, while the Hidaka Fault intersects the Japan Trench at the prominent bend offshore Hokkaido. With the exception of a 40 km section of fault near Nagano (see section 5.4.6), we model all crustal faults with a locking depth of 15 km.

5. Results

[14] Here we describe the kinematic features of reference model JB1, providing an integrated image of present-day deformation across Japan. Where appropriate, we describe differences between the results shown and those generated by models using alternate block and fault parameters. In general, the upper plate faults chosen to represent the block geometry are those that are estimated to have long-term slip rates >1 mm/yr based on the online active fault database of Japan maintained by the National Institute of Advanced Industrial Science and Technology (AIST, available online at http://riodb02.ibase.aist.go.jp/activefault/index_e.html). In many test cases, we used alternate block configurations that employ faults with slower estimated long-term slip rates in order to explore sensitivity of results to changes in fault network geometry. We represent closely spaced, subparallel faults with a single trace meant to characterize the cumulative deformation across the set of structures.

[15] We evaluate the model fit by examining the residual velocity field estimated by the block model analysis, choosing JB1 as the realization of the block geometry that minimizes the GPS residuals while remaining consistent with geological constraints on the sense and rate of fault slip. The mean residual magnitude of model JB1 is 1.84 mm/yr, while the mean magnitude of the observation uncertainties is 3.35 mm/yr. In general, the orientations of residual velocity vectors are random (Figure 4b), suggesting that the misfit of our model primarily reflects anomalous or noisy station velocities. Residual velocities showing regional or clustered consistency in their orientations could suggest that the model misrepresents, for example, the local fault geometry. In addition to analyzing the model fit to the constraining GPS data, we also compare the model-predicted fault slip rates (shown with formal uncertainties in Figures 5–10) to those indicated by studies of modern, historical, and paleoseismicity, and in some cases we compare our estimated Euler poles of block motion (Table 1) to previous plate tectonic models.

5.1. Okinawa Trough

[16] We note a northward decrease in magnitudes of opening along the Okinawa Trough, consistent with previous studies based on analysis of fault azimuths and seismic reflection data [*Bird*, 2003, and references therein]. We estimate an Euler pole describing motion between the Okinawa (central Ryukyu) and Yangtze blocks (27.9 ± 10.1°N, 141.7 ± 13.7°E, 1.0 ± 0.2°/Myr) similar to that calculated by *Bird* [2003] for the equivalent plates (29.8°N, 133.9°E, 2.42°/Myr). Between the southwest Ryukyu and Yangtze blocks, we estimate an Euler pole of 24.5 ± 2.8°N, 126.1 ± 3.6°E, 13.1 ± 0.8°/Myr, in line with previous analyses that divide the Ryukyu fore arc into distinct blocks (24.4°N, 126.5°E, 11.2°/Myr (relative to EU) and 25.6°N, 128.1°E, 11.0°/Myr (relative to AM) as estimated by *Nakamura* [2004] and *S. Nishimura et al.* [2004], respectively). Spreading along the Okinawa Trough decreases from very fast rates (37–75 mm/yr) along the northern boundary of the southwest Ryukyu block to between 28.6 ± 2.6 mm/yr and 19.7 ± 1.5 mm/yr on the Okinawa block, to 6.1 ± 1.2 mm/yr on the southwest extent of the Nankai-Kyushu fore-arc block. We suggest that the fastest rates of opening estimated in southwesternmost Ryukyu may be an artifact due to the fact that there are few constraining data. We discuss the pattern of shortening rates across the Ryukyu Trench in section 5.6.3.

5.2. Kyushu

[17] Two major block boundaries, AM-YA and the Okinawa Trough, merge off the western coast of Kyushu and continue as a single structure, which becomes the Median Tectonic Line on the island of Shikoku, consistent with the interpretation of *Takayama and Yoshida* [2007]. On Kyushu, this structure represents the Beppu-Shimabara Graben (BSG), across which N–S extension occurs, demonstrating consistency in the sense of deformation from an offshore spreading center to an onshore system of normal faults. We estimate up to 8.9 ± 0.8 mm/yr of opening across the graben near the western islands and peninsulas of Kyushu, decreasing to a rate of 2.4 ± 0.9 mm/yr in eastern Kyushu (Figure 5). The structure also accommodates an estimated 5–9 mm/yr of right-lateral slip as it continues eastward to become the Median Tectonic Line, discussed below. Intersecting this structure in eastern Kyushu is the western extension of the North Chugoku Shear Zone (NCSZ) [*Gutscher and Lallemand*, 1999], across which we estimate an additional 1.3 ± 1.7 mm/yr of opening and 3.2 ± 1.7 mm/yr of right-lateral slip, consistent with the general sense of north-south extension indicated by the long-term behavior of faults on Kyushu [*Nakata and Imaizumi*, 2002].

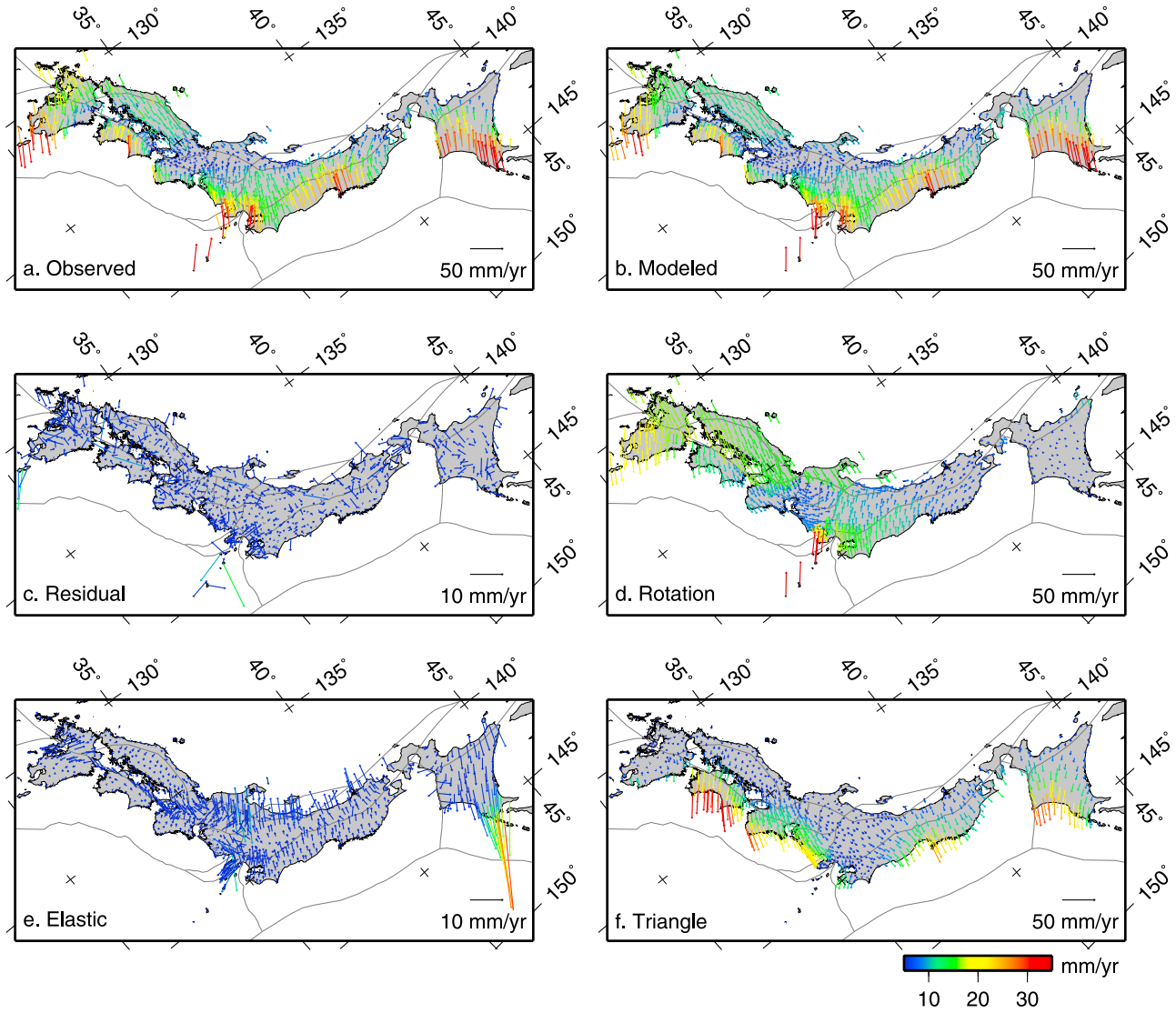

Figure 4. Decomposition of the velocity field into the constituent parts estimated by the block modeling theory. (a) Velocities as observed in the GPS field. (b) JB1 model velocity field. (c) Residual velocities (observed minus modeled). (d) Velocities due to long-term rotational block motion. (e) Velocities due to elastic strain accumulation about faults modeled using rectangular dislocation sources. (f) Velocities due to elastic strain accumulation from locking on the subduction zone interfaces modeled with triangular dislocation elements. The velocity color scale in Figure 4f applies to all plots, but the vector scale in each plot applies only to those velocities. Coastal elastic velocities (Figures 4e and 4f) are directed trenchward because they represent motion due to coseismic slip deficit. The large elastic velocities at the northeast tip of Hokkaido in Figure 4e result from the transition in subduction zone parametrization, from triangular dislocation elements to rectangular fault segments.

[18] *Bird* [2003] suggested that the Nankai and Ryukyu fore arcs are distinct blocks, separated from each other by a plate boundary coincident with the subducted Kyushu-Palau Ridge that connects the Nankai Trough at ~31.5°N to the BSG. This boundary was proposed on the basis of a pronounced gradient in the GPS velocities (from SE trending in the SE part of Kyushu to NW trending in western Shikoku; Figure 2) and the occurrence of several crustal earthquakes. We test this plate configuration, modeling the boundary as a vertical fault, and find results that are broadly similar to those of JB1, but with several key differences. The opening rate across the BSG is reduced relative to JB1 to a maximum of ~6 mm/yr, and ~11 mm/yr of left-lateral slip and up to 3 mm/yr of opening are predicted on the Kyushu-Palau Fault itself, which has no surface expression on the island [*Bird*, 2003], and up to 9 mm/yr of shortening is estimated across parts of the Median Tectonic Line (see section 5.3). *Nishimura and Hashimoto* [2006] suggested that the gradient in velocities between stations in southeastern and northeastern Kyushu is indicative of relative motion across an ESE striking structure at ~32°N. As an alternative explanation, we propose that all stations on Kyushu are part of the contiguous Nankai-Kyushu fore-arc block and the discrepancy in velocity stems from the variation in interplate coupling on the subduction zone. The block rotation component of the velocity field is southeast directed for all

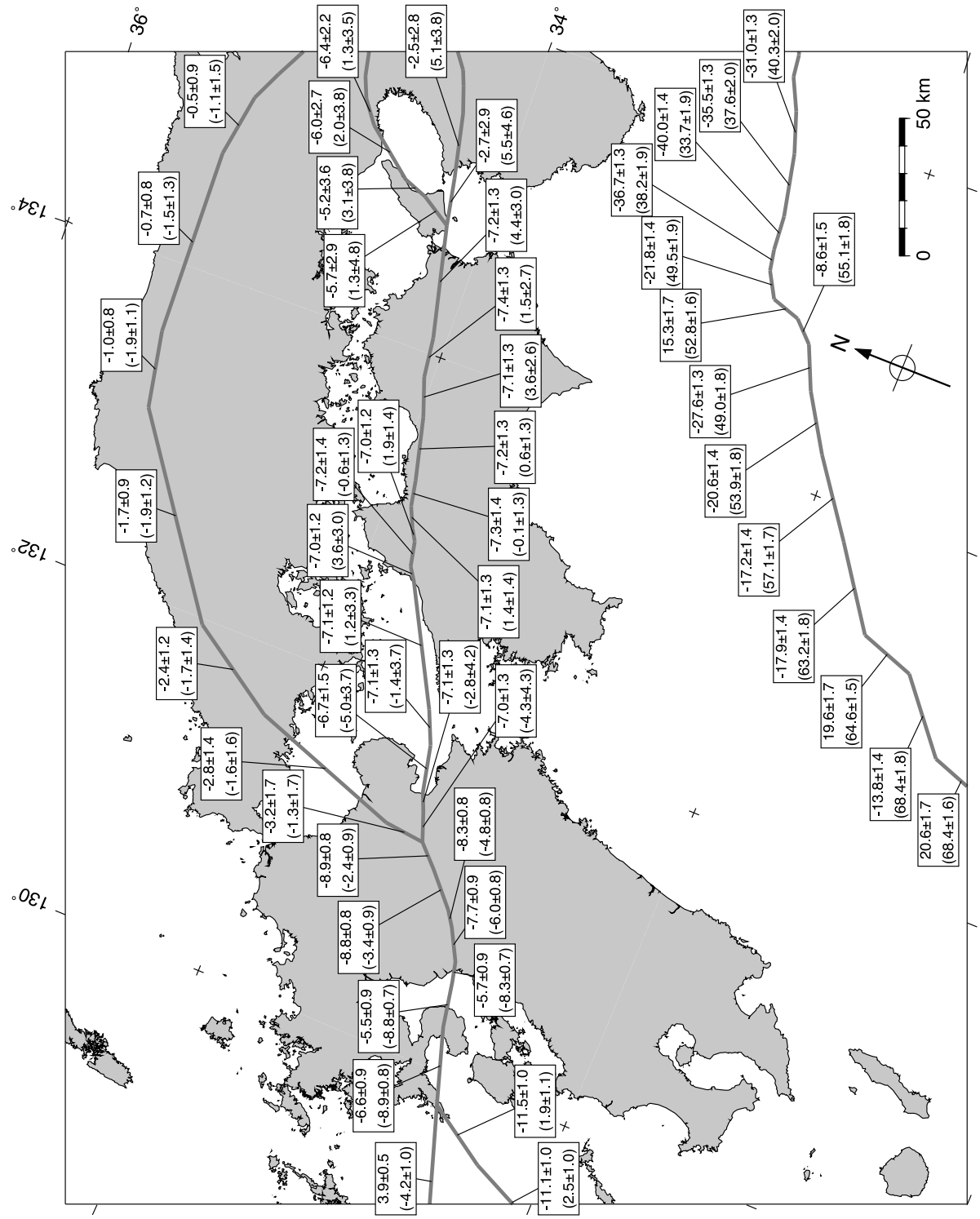

Figure 5. Estimated fault slip rates on block bounding segments of southwest Japan. Bold gray lines indicate the fault traces and corresponding labels give strike (top) and fault-normal (bottom, in parentheses) slip rates and uncertainties.

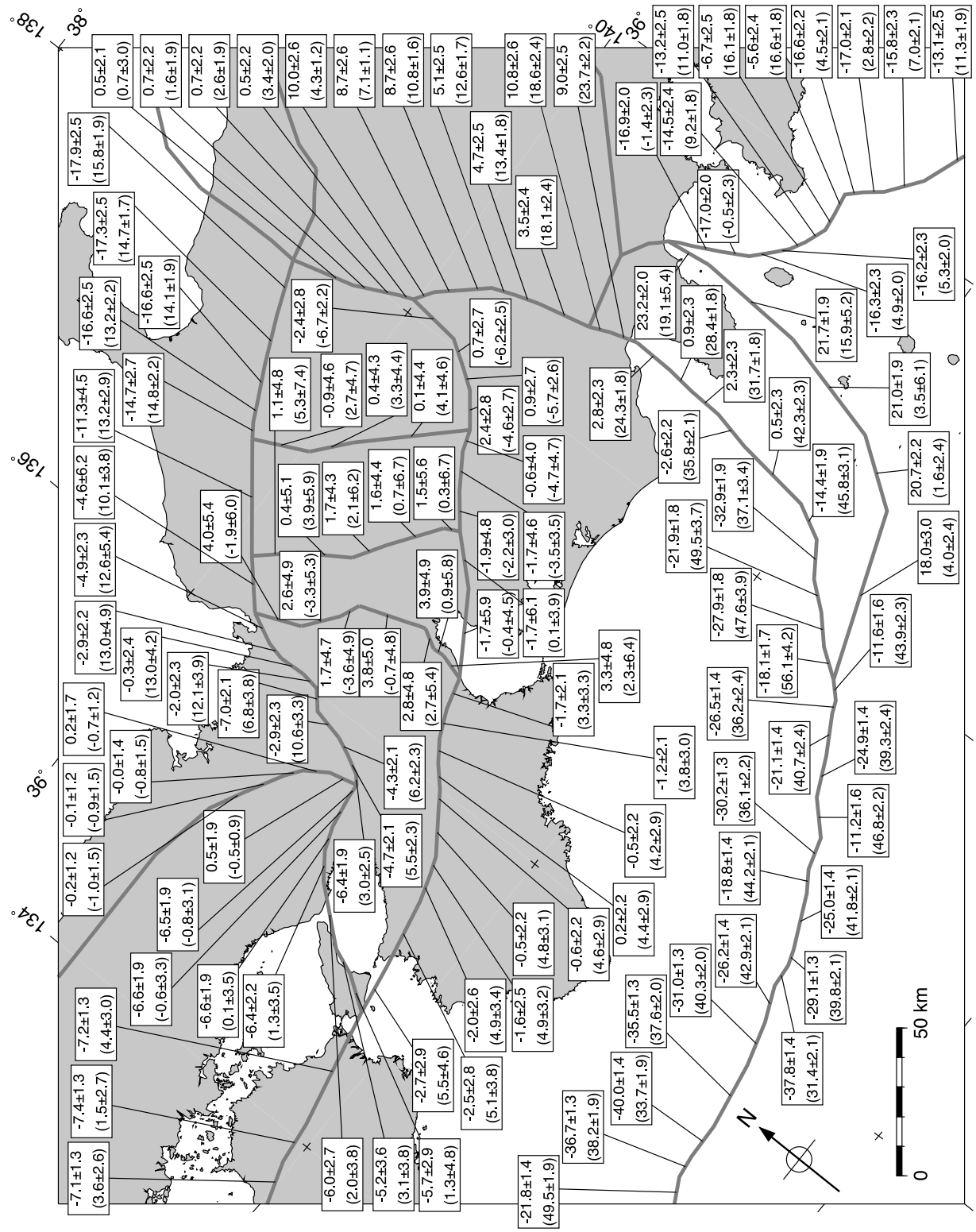

Figure 6. Same as Figure 5 but of central Japan.

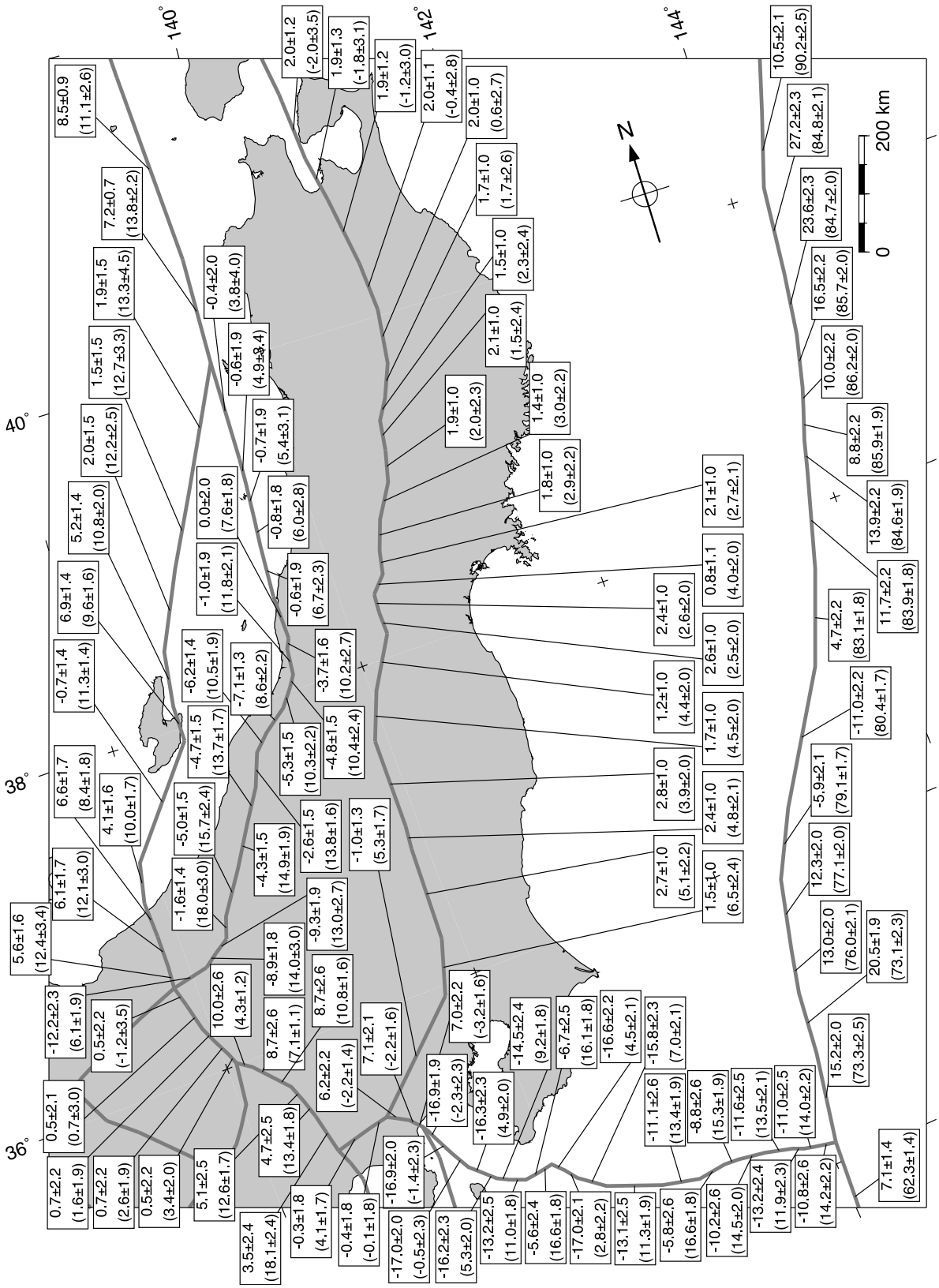

Figure 7. Same as Figure 5 but of northern Honshu.

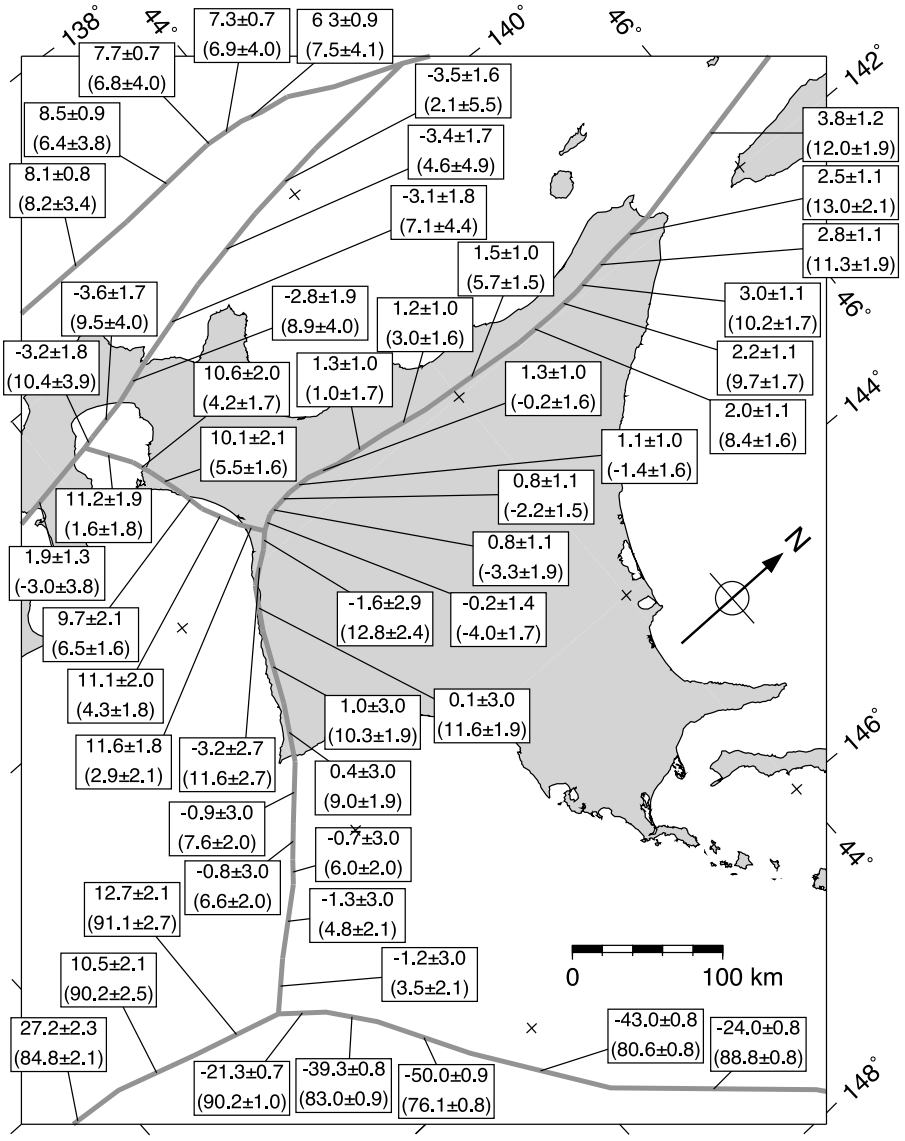

Figure 8. Same as Figure 5 but of Hokkaido.

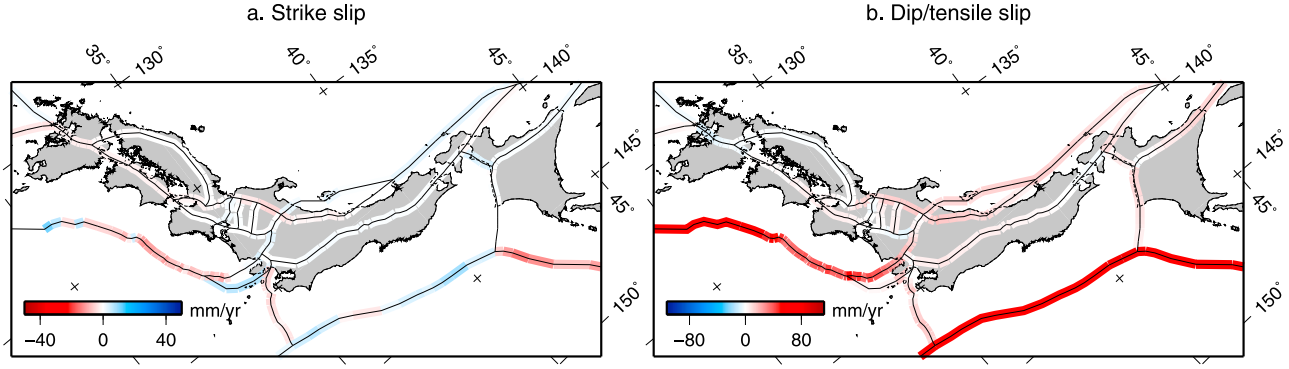

Figure 9. Slip rates estimated for model JB1. (a) Strike slip rates, with left-lateral slip shown as positive. (b) Dip (on inclined faults) or tensile (on vertical faults) slip rates, with closing or shortening taken as positive.

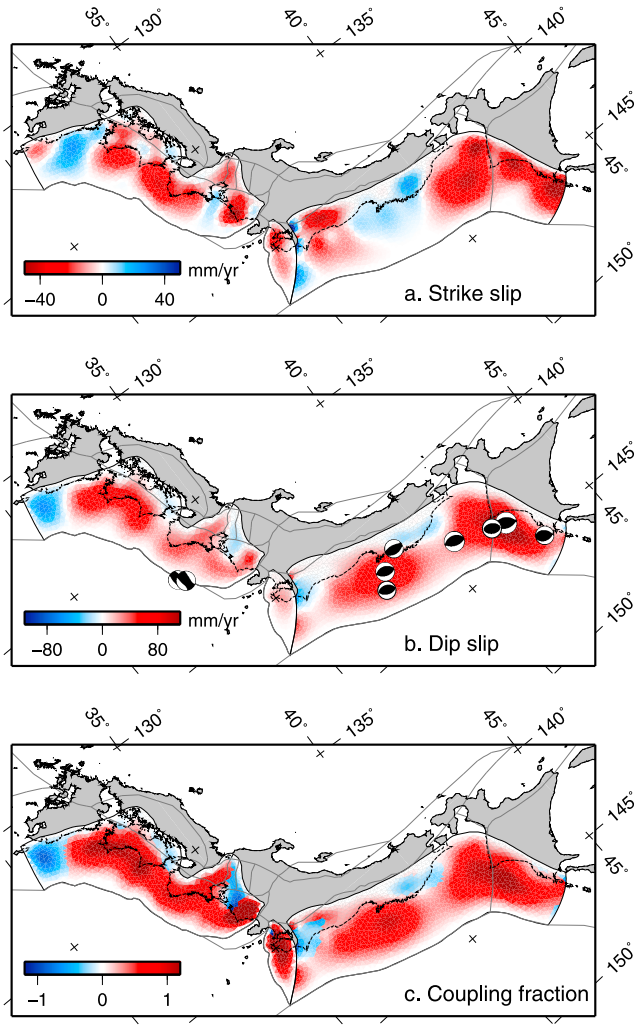

Figure 10. Slip rates and coupling fraction estimated on subduction zone interfaces for model JB1. (a) Strike slip rates, with left-lateral slip shown as positive. (b) Dip slip rates, with coseismic slip deficit (CSD) taken as positive and thrust sense slip negative. (c) Coupling fraction, defined as the speed of estimated slip divided by the speed given by projecting relative block motions onto the triangular dislocation elements. The sign is given by the sign of the dip slip rate. Thin gray lines indicate the block geometry. Focal mechanisms from the global centroid moment tensor catalog for all earthquakes shallower than 100 km with $M_w \geq 7$ since 1976 are overlain on the dip slip rate distribution. Strong correlation between the concentrations of CSD and coupling fraction with clusters of post-2000 earthquakes offshore Hokkaido (42°N) and Sendai (38°N) indicates the predictive power of detailed resolution of the slip rate distribution, while the forward slipping Sanriku-oki region (40°N) shows the afterslip following a 1994 event. The two events off the Kii Peninsula (33–34°N) occurred within the subducting Philippine Sea plate near the trench [*Seno*, 2005] and therefore are not expected to show correlation with the slip distribution on the plate interface.

stations on the Nankai-Kyushu fore-arc block (Figure 4d). These southeast velocities are countered by the effects of elastic strain accumulation due to the coupled Nankai plate interface, but the lack of coupling on the Ryukyu subduction zone means that, for stations along the eastern Kyushu coastline, there is a southwestward decrease in the contribution to the overall velocity field from elastic strain accumulation. Additionally, because postseismic deformation following the 1996 Hyuga-nada earthquakes is not explicitly removed from the position time series in our construction of the velocity field (section 3), coastal stations are also affected by that process. Thus, the transition from southeast directed velocities in southernmost Kyushu to negligible velocities in northern Kyushu to northwest directed vectors on Shikoku can be interpreted as a reflection of the underlying transition in the rate of locking on the plate boundary (see section 5.7) or may reveal a crustal structure poorly expressed at the surface [*Nishimura and Hashimoto*, 2006; *Wallace et al.*, 2009].

5.3. Shikoku and the Median Tectonic Line

[19] The Median Tectonic Line (MTL) is the most prominent feature on the island of Shikoku and serves as one of the world's type examples of a structure that allows slip partitioning at a subduction zone by accommodating right-lateral motion arising from oblique convergence at the Nankai Trough [e.g., *Fitch*, 1972; *Tabei et al.*, 2002, 2003]. We model the MTL as a structure with variable dip, ranging from 45°N to vertical, following the AIST active fault map and generally consistent with the interpretation of seismic reflection data [e.g., *Ito et al.*, 1996]. We estimate right-lateral slip rates of 7 mm/yr along the western and central parts of the fault system across Shikoku, with uncertainties of 1.2–1.5 mm/yr, and some segments show moderate shortening ($\leq$4.4 ± 3.0 mm/yr), although most segments show statistically insignificant dip-slip motion (Figure 5). Segments of the MTL on the Kii Peninsula ("KP" on Figure 3a) are modeled as vertically dipping and right-lateral slip rates on this continuation of the MTL east of Shikoku range from 0 to 2.7 ± 2.9 mm/yr, with the maximum rates along the west coast of the peninsula (Figures 5 and 6). Shortening across these segments decreases eastward from 5.6 ± 4.6 on the west coast of the Kii Peninsula to 3.3 ± 3.3 mm/yr on the east coast. Average Quaternary right-lateral slip rates vary along the length of the MTL, with the western segment (including the Bungo Channel and westernmost Shikoku) slipping at 0.5–5 mm/yr, the central segments at 5–9 mm/yr, and the eastern segments at 1–3 mm/yr (Figure 11) [*Kanaori et al.*, 1994, and references therein]. Geodetically constrained strike-slip rates from JB1 are consistent with the Quaternary rates along the central and eastern segments. Segmentation of the MTL due to the intersection with the Niigata-Kobe Tectonic Zone (dashed vertical line marked "NKTZ" on Figure 11; see section 5.4.2) at the east coast of Shikoku explains the abrupt decrease in right-lateral slip rate estimated with the block model and may explain the similar jump in the paleoseismic data. We do not resolve a slower slip rate on the western segment, as has been inferred from qualitative Quaternary paleoseismic data [*Kanaori et al.*, 1994]. Instead, the MTL and its continuation onto Kyushu slip at a nearly uniform right-lateral rate of ~7 mm/yr (Figures 5 and

Table 1. Estimated Euler Pole Locations and Rotation Rates[a]

Name	Longitude	Latitude	Rotation Rate (°/Myr)	N	$\bar{v}_{res}$ (mm/yr)
Asia	141.24° ± 2.30°	68.57° ± 0.85°	0.31° ± 0.01°	19	1.82
North America	119.39° ± 67.98°	−74.82° ± 13.97°	0.01° ± 0.01°	16	1.31
Pacific	104.78° ± 0.70°	−51.14° ± 0.27°	0.78° ± 0.00°	6	0.95
Amurian	143.93° ± 2.17°	66.80° ± 1.77°	0.26° ± 0.02°	119	2.18
Okhotsk	224.53° ± 38.85°	29.15° ± 37.72°	0.03° ± 0.02°	91	2.51
Yangtze	153.00° ± 8.63°	67.85° ± 2.83°	0.33° ± 0.02°	29	1.08
Philippine Sea	336.45° ± 2.38°	−44.85° ± 1.29°	1.07° ± 0.11°	10	5.85
SW Ryukyu	126.33° ± 0.34°	25.52° ± 0.16°	13.29° ± 1.79°	6	3.92
Okinawa	143.14° ± 6.80°	37.61° ± 3.92°	1.25° ± 0.47°	16	1.67
Nankai	135.57° ± 0.59°	36.96° ± 0.60°	1.55° ± 0.15°	185	2.00
West Honshu	138.39° ± 4.44°	47.46° ± 8.62°	0.62° ± 0.43°	91	1.40
Osaka	136.62° ± 0.86°	36.67° ± 1.58°	2.48° ± 2.11°	31	1.44
West Chubu	135.00° ± 5.61°	37.43° ± 6.28°	1.51° ± 4.66°	15	1.10
Central Chubu	136.38° ± 0.61°	35.81° ± 0.27°	4.90° ± 3.49°	10	0.71
East Chubu	136.55° ± 0.69°	35.45° ± 0.40°	3.85° ± 2.20°	13	1.11
IMP	319.40° ± 0.10°	−35.88° ± 0.15°	9.17° ± 1.18°	19	2.62
Niigata	133.59° ± 6.60°	40.49° ± 3.63°	0.80° ± 1.01°	16	1.57
OBR	325.65° ± 2.80°	−41.20° ± 1.73°	0.75° ± 0.28°	105	1.60
Central Hokkaido	320.72° ± 0.35°	−43.16° ± 0.24°	2.46° ± 0.42°	25	1.54
NE Honshu	324.70° ± 1.28°	−40.77° ± 0.83°	1.28° ± 0.26°	131	1.57

[a]Locations and rates are given in reference to the nominally stable Eurasian reference frame of *Apel et al.* [2006]. Pole locations and rotation rates were determined by converting the estimated block motion vectors, Ω^{est}, the uncertainties of which are determined by direct propagation of the data uncertainties, from Cartesian coordinates to geographic coordinates, with formal uncertainties on the converted coordinates and rates given by Monte Carlo simulation. The number of observations, *N*, on each block and the mean residual velocity magnitude, $\bar{v}_{res}$, of those stations are also given.

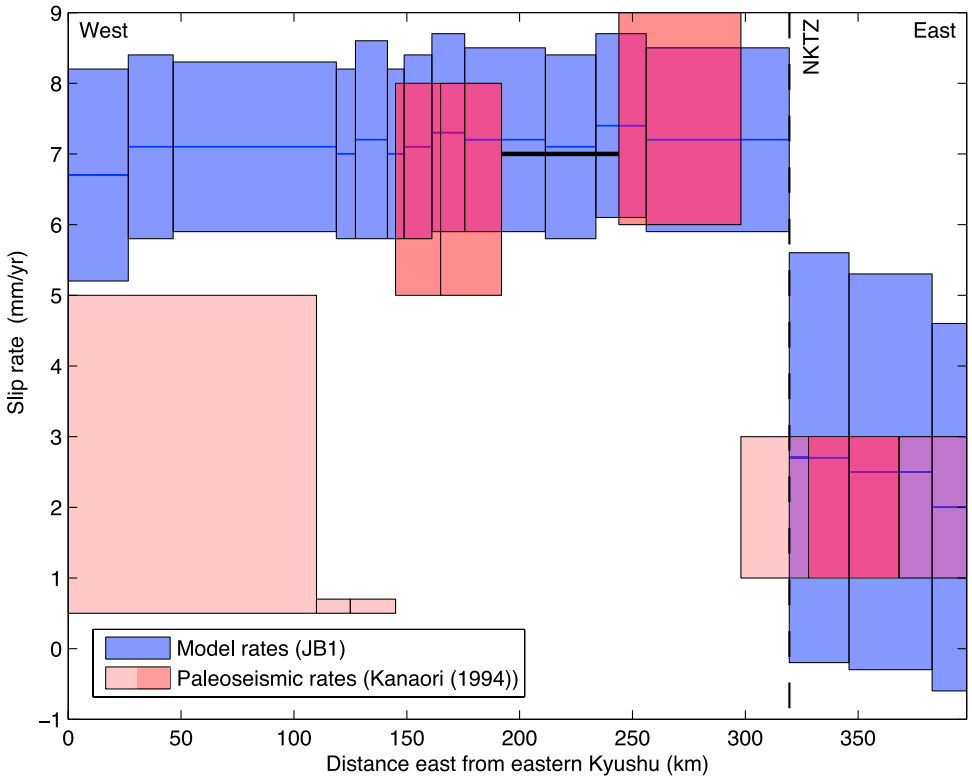

Figure 11. Right-lateral slip rates along segments of the Median Tectonic Line (MTL) as estimated by model JB1 and measured paleoseismologically throughout the Quaternary [*Kanaori et al.*, 1994, and references therein]. Blue lines indicate the slip rates estimated by model JB1, with the extent of the corresponding blue box indicating the uncertainties. Red boxes show the range of estimated Quaternary rates, with the lighter shading indicating rates that were inferred from qualitative data and the darker shading denoting dated right-lateral offsets [*Kanaori et al.*, 1994]. A single slip rate value of 7 mm/yr is given by *Kanaori et al.* [1994] for the central segment of the MTL between ∼200 and 250 km from eastern Kyushu (bold black line). The vertical dashed line labeled "NKTZ" indicates the position of the intersection between the MTL and Niigata-Kobe Tectonic Line as represented in JB1; this junction approximately coincides with the boundary between the central and eastern segments of the MTL as defined by *Kanaori et al.* [1994].

11). In model JB1, the MTL is not segmented by an intersection with the putative boundary between the Nankai and Ryukyu fore arcs, which occurs near the BSG rather than near the Bungo Channel [*Bird*, 2003; *Nishimura and Hashimoto*, 2006], and so the alternative plate geometry discussed above does not improve the agreement between the estimated geodetic and geologic slip rates.

[20] If the eastern segments of the MTL on the Kii Peninsula are modeled as dipping, the resulting slip rates are less consistent with geologic observations. In particular, we estimate left-lateral slip between ~1.5–3 mm/yr, opposite the long-term sense of lateral offset on these structures. Additionally, we find poorly constrained normal slip on the westernmost Kii Peninsula of up to ~1.5 mm/yr, where reverse slip is catalogued in the AIST active fault database. Although the fault segments that are estimated to have higher slip rates in the AIST catalog dip northward at 45°, an additional fault approximately 15 km to their north dips southward. Assuming locking depths of 10–15 km, these faults must coalesce at depth, and we so we choose to represent these segments as a vertical [e.g., *Souter*, 1998].

[21] The rate and rake of slip estimated on the MTL are affected by the location of the northernmost segmenting fault along the Ryukyu Arc. In general, the farther northeast this fault is located, and thus the smaller the Nankai fore-arc block, the faster the rate and steeper the rake of the slip vector resolved on the MTL (e.g., faster rates of dip slip), particularly on the eastern extent. We find that the fault location resulting in the best overall fit to the GPS data is near boundary "H" identified by *Nakamura* [2004], which lies between Okinawa and Amami Islands.

5.4. Honshu

5.4.1. Western Honshu

[22] The strike-slip faults of the North Chugoku Shear Zone (NCSZ) [*Gutscher and Lallemand*, 1999] in western Honshu arc from the southwest to northeast and are capable of producing damaging earthquakes as evidenced by several historical events [*Gutscher and Lallemand*, 1999; *Wesnousky et al.*, 1982] and the 2000 $M_w = 6.7$ western Tottori prefecture event [e.g., *Semmane et al.*, 2005]. This earthquake occurred in a region of no mapped active faults and low geodetic shear strain rate [*Shibutani et al.*, 2002; *Toya and Kasahara*, 2005] yet produced strong local ground motions due to its shallow hypocenter [*Semmane et al.*, 2005]. Here reference model JB1 produces right-lateral slip rates decreasing eastward along the NCSZ from 3.2 ± 1.7 to 0.1 ± 1.2 mm/yr (Figures 5 and 6), consistent with studies of previous seismicity and structure [e.g., *Wesnousky et al.*, 1982; *Shen-Tu et al.*, 1995; *Gutscher and Lallemand*, 1999]. We find slow (up to 0.5 ± 1.9 mm/yr) left-lateral motion on the W–NW striking segments on the eastern end of the shear zone (east of 135.5°E, Figure 6); the left-lateral kinematics on these faults was demonstrated by the 2000 earthquake and long-term motions of the Yamasaki and Mitoke faults [*Gutscher and Lallemand*, 1999]. Removing the NCSZ from JB1 only slightly decreases the fit to the GPS data while negligibly affecting slip rates on neighboring faults including the MTL. These results, in conjunction with the slow slip rates resolved on the structure, suggest that, while faults of the NCSZ are actively causing elastic strain accumulation and are capable of producing damaging earthquakes and, they do not play an important role in the larger-scale tectonics of western Honshu.

5.4.2. Niigata-Kobe Tectonic Zone

[23] The Niigata-Kobe Tectonic Zone (NKTZ) has been identified as a region of high shear strain rates in analyses of GPS data [e.g., *Sagiya et al.*, 2000; *Sagiya*, 2004; *Toya and Kasahara*, 2005] trending NE–SW from the Japan Sea to the MTL, which is consistent with the fast slip rates in block model JB1. Slip rates are greatest on the ENE striking segments just south of the Noto Peninsula, including the Atotsugawa Fault, with right-lateral and shortening rates reaching 17.9 ± 2.5 and 15.8 ± 1.9 mm/yr, respectively (Figure 6). Striking NE from the city of Kobe to Lake Biwa ("LB" on Figure 3a) are the faults comprising what is termed the Hanaore-Kongo Fault Line (HKFL, cyan line on Figure 3b) by *Kanaori et al.* [1994]. On these faults, we estimate reverse slip rates increasing northeastward from 3.0 ± 2.5 to 13.0 ± 4.9 mm/yr, with right-lateral slip as fast as 7.0 ± 2.1 mm/yr on the most easterly striking segments of the HKFL. Between the HKFL faults and the MTL is the Arima-Takatsuki Tectonic Line (ATTL, light green line on Figure 3b [*Kanaori et al.*, 1994]) on which we estimate dominantly reverse (0.1 ± 3.5 to 3.1 ± 3.8 mm/yr) and right-lateral slip (5.7 ± 2.9 to 6.6 ± 1.9 mm/yr).

[24] Our interpretation of the NKTZ as a structure accommodating relative motion between adjacent blocks is consistent with the view that it represents the boundary between AM and OK (or NAM) [*Sagiya et al.*, 2000; *Shimazaki and Zhao*, 2000; *Miyazaki and Heki*, 2001; *Heki and Miyazaki*, 2001; *Mazzotti et al.*, 2001]. Local studies suggest that material heterogeneity within the crust or mantle can explain the origin of the high strain zone evident in the GPS data [*Iio et al.*, 2002; *Hyodo and Hirahara*, 2003; *Yamasaki and Seno*, 2005]. As an alternative to such a proposed change in rheology, we find that we can accurately characterize the GPS velocity field using a combination of block motion and elastic strain accumulation along segments of the NKTZ.

5.4.3. Chubu-Kinki Region

[25] In the Chubu and Kinki region, we find that the ENE striking faults, such as the NKTZ and eastern extension of the MTL, experience right-lateral slip while the NW striking structures, including, from west to east, the Yoro, Neodani, and Sakashita-Atera faults, slip left laterally, consistent with previous large-scale kinematic models of this region [*Kanaori*, 1990; *Kanaori et al.*, 1991, 1992; *Matsuzaki et al.*, 1996]. We estimate left-lateral slip (1.7 ± 4.7 to 3.9 ± 4.9 mm/yr) and a variable sense of tensile motion (up to 3.6 ± 4.9 mm/yr of opening and 2.7 ± 5.4 mm/yr of closing) on the Yoro Fault, which strikes NW from Nagoya to the northern coast of Honshu, along the east side of Lake Biwa (Figure 6). To the east of the Yoro Fault, we model the trace of the Neodani Fault and its branches in accordance with the mapped surface rupture of the 1891 M_w = 7.5 Nobi earthquake [*Kaneda and Okada*, 2008]. Along this fault, we estimate left-lateral slip of 0.4 ± 5.1 to 1.7 ± 4.3 mm/yr, which is similar to the rate estimated over the past 150 kyr (1.3 ± 0.3 mm/yr [*Kaneda and Okada*, 2008]). We estimate shortening rates increasing northward from 0.3 ± 6.7 at the intersection with the MTL to 5.3 ± 7.4 mm/yr at the junction with the NKTZ. We find shortening and slow strike-slip rates (2.7 ± 4.7 to 4.1 ± 4.6 mm/yr and 0.9 ± 4.6 mm/yr

right-lateral, restricted to the northernmost segment, to 0.4 ± 4.3 mm/yr left-lateral, respectively) on the Sakashita-Atera Fault, which lies east of the Neodani Fault. Though the slip rate uncertainties on this fault are high as well, we note that the sense of motion predicted is consistent with the long-term behavior of this structure [*Kanaori et al.*, 1990].

[26] Although the MTL is mapped as continuing east of its junction with the NKTZ, across the Kii Peninsula to an intersection with the Itoigawa-Shizuoka Tectonic Line (ISTL) north of Mount Fuji [e.g., *Kanaori*, 1990; *Nakata and Imaizumi*, 2002], we find that the NKTZ is, kinematically, the more important structure through the Kinki-Chubu region. On the eastern extension of the MTL, estimated right-lateral slip rates range from 0.5 ± 2.2 to 2.7 ± 2.9 mm/yr (near the intersection with the NKTZ, described in section 5.3), while minor left-lateral slip (0.7 ± 2.7 to 2.4 ± 2.8 mm/yr) is estimated on about a 40 km long segment between the Sakashita-Atera Fault and ISTL (Figure 6). Closing sense tensile slip rates up to 5.5 ± 4.6 mm/yr are estimated along much of the eastern MTL west of its intersection with the Neodani fault, with maximum rates occurring just east of the intersection with the NKTZ, while opening of up to 6.7 ± 2.2 mm/yr is predicted between the Neodani Fault and the ISTL. The modeled fault follows the active Iida and Tagiri faults [*Nakata and Imaizumi*, 2002], but shifting the model geometry to the north along the Yomikaki-Agematsu faults [*Nakata and Imaizumi*, 2002] changes the estimated slip rates only slightly while increasing the local misfit to the GPS data. An additional test model invoking the Jurassic trace of the MTL, which lies about 20 km south of the active fault traces used in JB1, also predicts generally similar slip rates on faults in the region. Regardless of the position of this segment of the MTL, the extension estimated across it is curious, as such a sense of displacement is not commonly reported geologically, although the nearby Ho-osan Fault is identified as a normal fault with a low degree of activity in the AIST database.

5.4.4. Tokai-Kanto and the Izu Microplate

[27] The tectonics of the south central Honshu region is marked by the intersection of the Nankai and Sagami Troughs with several prominent crustal faults. The region has been studied previously using a block-and-fault model, the methodology of which differs from ours in some respects [*Nishimura et al.*, 2007]. We model the Izu Microplate (IMP) as a distinct block with a western boundary of the Suruga Trough, an eastern boundary composed of steeply (70–80°W) dipping faults that lie just west of the Izu Islands, and a northern boundary striking E–W, just south of Mount Fuji. We estimate an Euler pole for the IMP located at 139.40 ± 0.10°E, 35.86 ± 0.15°N with a clockwise rotation rate of 9.20 ± 1.17°/Myr, which is similar to that of *Nishimura et al.* [2007] (139.05°E, 35.30°N, 9.7°/Myr), despite a difference in the velocity field reference frame and modeling methodology. In fact, our pole lies approximately halfway between those of *Nishimura et al.* [2007] and *Mazzotti et al.* [2001] (139.60°E, 37.14°N, 4.52°/Myr for IMP-central Japan relative motion). Given the motion of PS, the rotation of the IMP resolved onto the eastern boundary of the IMP gives left-lateral slip that increases northward from 18.0 ± 3.0 to 23.2 ± 2.0 mm/yr (Figure 6), similar the 26–28 mm/yr predicted by *Nishimura et al.* [2007]. We estimate more substantial shortening across the eastern boundary of the IMP (19.1 ± 5.4 mm/yr on the northernmost segment decreasing to 4.0 ± 2.4 mm/yr on the southern 2/3 of the boundary) than do *Nishimura et al.* [2007], who find nearly pure strike-slip along the faults. The discrepancy in the rake of estimated slip likely results from the difference in our estimate of rotational motion of PS, lower resolution of our model offshore the Izu Peninsula given our rejection of GPS stations with high uncertainties (>5 mm/yr), variations in the block geometries, and our consideration of spatially variable coupling on the nearby Nankai and Sagami subduction interfaces. We estimate a PS rotation rate that is slower and about an Euler pole that lies NNE of that of *Nishimura et al.* [2007] (156.45 ± 2.38°E, 44.85 ± 1.29°N, 1.07 ± 0.11°/My compared to 150.62°E, 45.81°N, 1.59°/Myr).

[28] Along the Suruga Trough to the west of the IMP, we estimate a southward increase in the magnitude of dip slip, from 18.6 ± 2.4 mm/yr near Mount Fuji to 56.1 ± 4.2 mm/yr at the southern tip of the IMP, faster than the typical rates across much of the Nankai Trough (section 5.6.3). Additionally, we estimate up to 32.9 ± 1.9 mm/yr of right-lateral motion on the most easterly striking southern segments of the trough, little strike-slip motion between 34 and 35°N ($\leq$2.8 ± 2.3 mm/yr right-lateral or left-lateral), and left-lateral slip up to 10.8 ± 2.6 mm/yr along the onshore segments just south of the intersection with the E striking fault near Mount Fuji. This contrasts with the findings of *Nishimura et al.* [2007], who report a larger strike-slip component on the northern segments of the Suruga Trough. This difference is probably due to the fact that we model the GPS stations to the west of the Suruga Trough as part of the Nankai-Kyushu fore arc, separated from the Kanto region by the ISTL, while *Nishimura et al.* [2007] assume that both Tokai and Kanto are part of a single central Japan plate. Block motion velocities, which dictate the rate and rake of fault slip, are similar between our model and that of *Nishimura et al.* [2007] for the IMP, but we predict NE directed velocities for the Nankai-Kyushu block near the Suruga Trough where the central Japan block velocities of *Nishimura et al.* [2007] are nearly zero.

5.4.5. Itoigawa-Shizuoka Tectonic Line

[29] The Itoigawa-Shizuoka Tectonic Line (ISTL) has been proposed to represent a major tectonic boundary through central Honshu [*Hashimoto and Jackson*, 1993; *Sagiya et al.*, 2002], stretching from the Izu collision zone north to the Japan Sea near the Noto Peninsula. Despite Quaternary slip rate estimates up to 14 mm/yr, large earthquakes have not ruptured the fault since 841 A.D. [*Okumura*, 2001]. We find shortening decreasing from 18.1 ± 2.4 mm/yr just north of the Izu collision zone to ~0 mm/yr near the intersection of the ISTL and NKTZ, then abruptly increasing to 12.1 ± 3.0 mm/yr near the north coast of Honshu (Figure 7). In addition, we estimate left-lateral slip of up to 6.6 ± 1.7 mm/yr near the north coast of Honshu, slow rates of up to 0.7 ± 2.2 mm/yr on the segments between the NKTZ and MTL, and rates up to 10.0 ± 2.6 mm/yr just south of the intersection with the MTL, decreasing southward toward the Izu Collision Zone.

[30] Segmentation of the ISTL has been recognized in the paleoseismic record as well (Figure 12) [e.g., *Okumura*, 2001]. The Gofukuji Fault, located near the intersection

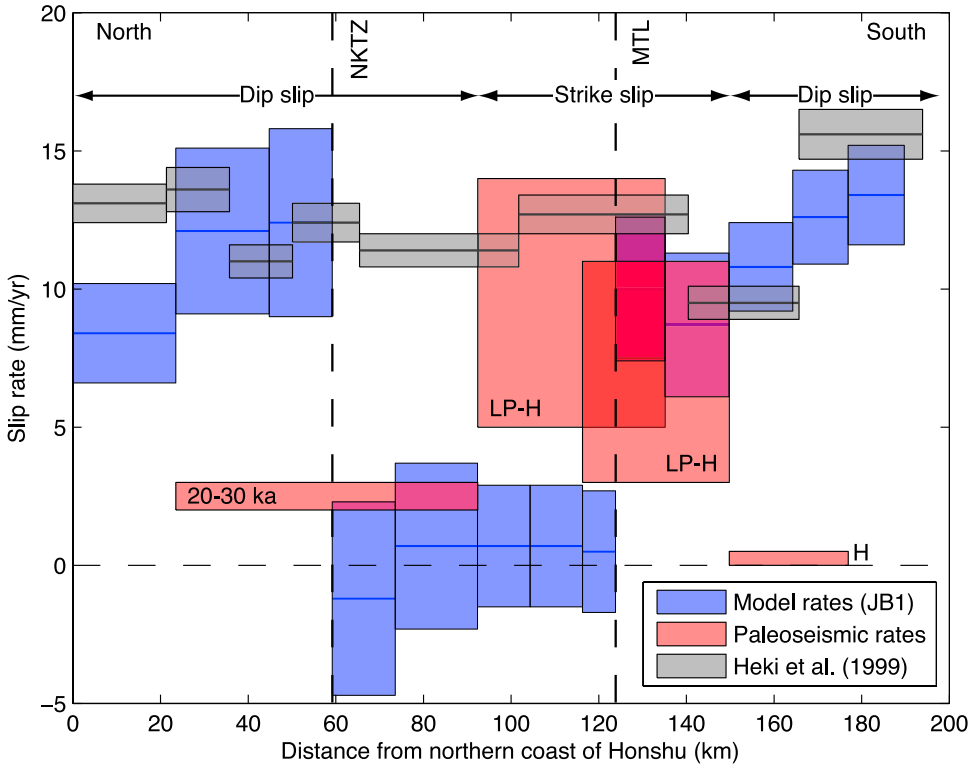

Figure 12. Comparison of slip rates along the Itoigawa-Shizuoka Tectonic Line (ISTL) from three sources: model JB1, which considers segmentation of the fault system by intersection with other faults (the eastern extension of the Median Tectonic Line (MTL) and the Niigata-Kobe Tectonic Line (NKTZ)), a model that uses a block geometry similar to that proposed by *Heki et al.* [1999], in which the ISTL represents a major tectonic plate boundary, and paleoseismic data summarized by *Okumura* [2001]. In the case of the model results, the horizontal lines show slip rate magnitude estimated for distinct segments, and the extent of the surrounding boxes shows the uncertainties on those rates. For the paleoseismic data, we show the slip rate magnitude range quoted by *Okumura* [2001] over the interval denoted by the text in each box (LP, late Pleistocene; H, Holocene). The dashed vertical lines indicate the ISTL's intersections with the NKTZ and MTL in model JB1. Because the segments of the ISTL show differences in the dominant mode of slip accumulated in the paleoseismic record, we compare the rates quoted by *Okumura* [2001] to the appropriate component of slip estimated in the block models, as shown by the interval arrows near the top. We find that the higher left-lateral slip rates south of the intersection with the MTL agree with the paleoseismically estimated rates, and it is difficult to discern exactly where the intersection occurs because of multiple, subparallel fault strands near the intersection.

between the MTL and ISTL, shows a late Pleistocene–Holocene average left-lateral slip rate of 5–14 mm/yr. Segments to the south, including the Chino Fault, slip left laterally at 3–11 mm/yr [*Okumura*, 2001]. Segments north of the Gofukuji Fault dip to the east and have slower, reverse slip rates of 2–3 mm/yr. We find mixed agreement between our estimated pattern of slip rates on the ISTL and that revealed by the longer-term records. The fastest slip rates in our model coincide with the slowest segments of the ISTL as described by *Okumura* [2001]; along the southern segment, (km ~150–180 of Figure 12), the paleoseismic record indicates a Quaternary reverse slip rate of <0.5 mm/yr [*Okumura*, 2001, and references therein], while we estimate rates of up to ~13 mm/yr. The Chino segment of the ISTL (km ~120–150 of Figure 12) shows good agreement between the paleoseismic and geodetic model rates along much of its length. Along the Gofukuji segment (km ~90–140; there is some overlap between the Gofukuji and Chino segments), we estimate slip rates on some segments that agree with the fast left-lateral paleoseismic rate, and others that do not. That geodetic rates fall below geologic estimates precludes the possibility that the JB1 fault system representation and slip estimates are incorporating multiple fault strands into a single estimate. The location of the transition from slow to fast rates in the block models depends on the intersection between the eastern extension of the MTL and the ISTL. If we model this junction farther north than in JB1, there is good agreement between the geodetic and paleoseismic rates along a greater length of the Gofukuji Fault. The location of this intersection is unknown: there are several roughly parallel faults that may represent the active trace of the eastern MTL (section 5.4.3), but current GPS data are insufficiently dense to determine which, if any, is the most kinematically significant strand. Average reverse slip rates on the northern ISTL (km ~20–90) are estimated to be ~2–3 mm/yr, which is faster than the rates predicted by model JB1 (Figure 12) south of the intersection with the NKTZ and far slower than the rates estimated north of the

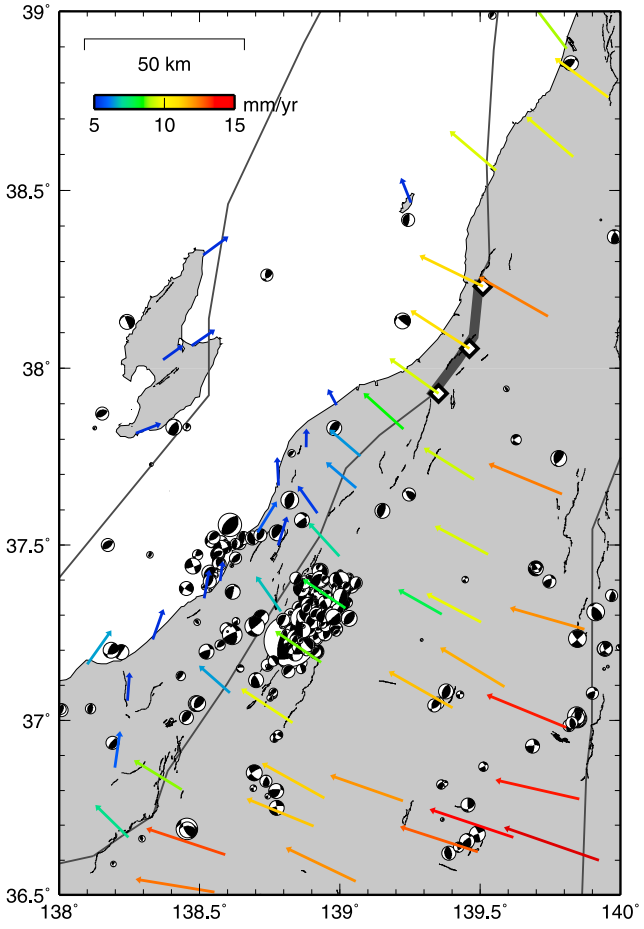

Figure 13. GPS velocities in the mid-Niigata Prefecture region. Thin black lines show the position of active faults [*Nakata and Imaizumi*, 2002], and gray lines show the segment boundaries used in model JB1, with the thick gray lines showing the fault segments modeled as creeping. Focal mechanisms are taken from the Japanese Meteorological Agency (JMA) catalog from 1997 to 2008, and the concentration of events between 37.1°N and 37.4°N marks the 2004 M_w = 6.6 earthquake and its aftershock sequence. Colored vectors show the interseismic GPS velocities. The diamonds around 38°N indicate three near-fault stations showing velocities larger than other stations that are also adjacent to the faults, which we interpret as possibly reflecting creeping behavior along the local fault segments.

NKTZ. While uncertainty in the fault system geometry along the ISTL likely contributes to some of the disagreement between short- and long-term slip rate estimates, the discrepancy may alternatively indicate temporal variation in slip rate patterns.

[31] To compare further the geodetic and geologic fault slip rates on the ISTL, we test other block model geometries. Figure 12 shows the rates predicted by a model that tests the plate boundary configuration proposed by *Heki et al.* [1999], in which the MTL and NKTZ are not considered as tectonic discontinuities. That model predicts nearly uniform high slip rates ($\geq$10 mm/yr) along the ISTL (Figure 12), emphasizing that the segmentation of the ISTL introduced by the intersections with the NKTZ and eastern extension of the MTL results in the along-strike changes in slip rate. We also test several different configurations of these intersections, one in which the MTL intersects the ISTL north of the Gofukuji segment, farther north than inferred from the DAFMJ [*Nakata and Imaizumi*, 2002], and another in which the MTL crosscuts the ISTL in the same location as in model JB1 but extends NE as the fault system that lines the western coast of northern Honshu. The former predicts a slip rate pattern similar to that of JB1, with overlap between the range of estimated and paleoseismic slip rates on the Gofukuji segment, while the latter predicts a pattern of alternating senses of slip on adjacent segments that is not observed geologically.

5.4.6. Northern Honshu and the Ou Backbone Range

[32] Northeast of its intersection with the ISTL, reverse and right-lateral slip on the NKTZ and related faults (including the Shibata-Koide and Kashiwazaki-Chiba tectonic lines) along the west coast of Honshu in Niigata Prefecture decrease with increasing latitude, with dip slip reduced from >15 mm/yr near the ISTL to ~4 mm/yr where the fault system intersects the eastern margin of the Sea of Japan, and right-lateral slip vanishing northward from about 12 mm/yr near the ISTL. Near the source region of the 2004 M_w = 6.6 mid-Niigata Prefecture earthquake (focal mechanism shown in Figure 13), we estimate 14–15 mm/yr of reverse slip on a fault dipping 45°W, consistent with focal mechanisms for the 2004 main shock and several large aftershocks [e.g., *Kato et al.*, 2005]. Just north of the 2004 earthquake region, at 38°N latitude, we find that modeling a ~40 km section of the 45°W dipping fault as a creeping structure (zero locking depth) provides an improved fit to the local GPS data, which show NW directed velocities faster than other stations adjacent to along-strike segments of this fault system (Figure 13). Considering even a shallow locking depth of 5 km on this segment of the fault substantially increases the mean residual velocity magnitude at 3 nearby stations as compared to the creeping segment model, from 0.96 mm/yr to 3.06 mm/yr. While it is possible that the locally fast velocities at these stations reflect errors in the data rather than the effects of a creeping fault, we note that the stations show fast motion in our velocity field solution, as well as those of *Sagiya et al.* [2000] and *Miura et al.* [2002]. Furthermore, recent and historical earthquakes have occurred along other segments of this fault system, but not in the immediate vicinity of where we have inferred a creeping segment (Figure 13) [*Wesnousky et al.*, 1982]. It is worth noting that disagreement between focal mechanism locations and our chosen block boundaries in Figure 13 can result from (1) our choice to represent multiple subparallel fault strands with a single boundary, (2) errors in earthquake locations, and (3) nonvertical dips of faults, such that the focal mechanism shown overlies a particular 45–60° fault plane at several kilometers depth.

[33] Parallel to the west coast fault in the interior of Honshu are faults bounding the Ou Backbone Range (OBR), which are characterized by dominantly reverse slip of several mm/yr. This region has been noted as a zone of high geodetic strain rates [*Miura et al.*, 2002, 2004; *Toya and Kasahara*, 2005] and produced the 2008 M_w = 6.9 Akita (Iwate Prefecture) reverse faulting earthquake. We estimate northward decreasing reverse slip, with rates up to 6.5 ± 2.4 mm/yr just northwest of the Boso Peninsula, while

segments of the fault in northernmost Honshu and southern Hokkaido (40.0–42.0°N) are estimated to experience minor normal slip up to 3.0 ± 3.8 mm/yr (Figures 7 and 8). We note that normal slip is inconsistent with geologic observations but may be related to afterslip following the 1994 Sanriku-oki earthquake (section 5.7). Additionally, the high formal uncertainty, as compared to the estimated rate, indicates that the sense of dip slip is poorly constrained.

[34] We test several block geometries in northern Honshu, including some that invoke the Oga-Ojika Tectonic Line (OOTL), which was proposed on the basis of aligned shallow earthquake epicenters in the absence of an obvious surface trace to represent a major tectonic boundary in the block model of *Hashimoto and Jackson* [1993]. Our models that include the OOTL connecting the Japan Trench at 38°N to the Sea of Japan trench at 41°N produce several curious estimates of fault slip rates throughout northern Honshu. Dip slip on the structure marking the eastern boundary of the Sea of Japan decreases abruptly south of where it intersects the OOTL, with the latter structure accommodating ~7.5 mm/yr of NE–SW shortening. Near Sendai, where the OOTL crosses the Pacific coast of Honshu, we estimate ~15 mm/yr of left-lateral slip, providing a prediction testable with paleoseismic observations. Modeling the OOTL between the Japan Trench and the OBR faults provides minor improvement in the fit to the GPS data but does not substantially change the slip rates throughout northern Honshu and Hokkaido compared to JB1 (generally <1–2 mm/yr difference), although normal faulting is predicted at a faster rate (up to ~5 mm/yr) than is predicted by JB1.

5.5. Hokkaido

[35] We model the OBR fault as continuing across the Tsugaru Straits and through the Kuromatsunai Lowland ("TS" and "KL", respectively, in Figure 3a) in western Hokkaido, where the Kuromatsunai Fold-and-Thrust Belt has been recognized [e.g., *Azuma et al.*, 2003, 2004]. We estimate not only shortening of 7.1 ± 4.4 to 10.4 ± 3.9 mm/yr across this structure, consistent with the sense of slip from paleoseismological findings, but also ~3–3.5 mm/yr of right-lateral slip (Figure 8). We note that, given the uncertainty in the geometry of the fault lining the eastern margin of the Sea of Japan, our estimate of shortening across the Kuromatsunai structure, particularly its offshore extension, may represent some of the shortening between the Amurian Plate and Hokkaido. Furthermore, uncertainty in block motions in western Hokkaido arise due to the lack of stations unaffected by postseismic deformation from the 1993 Nansei-oki earthquake [*Ueda et al.*, 2003]. On the fault striking N–S through central Hokkaido, we estimate minor left-lateral slip up to 3.0 ± 1.1 mm/yr, and southward decreasing dip-slip rates, from 13.0 ± 2.1 mm/yr of shortening at the northern tip of Hokkaido to 4.0 ± 1.7 mm/yr of normal faulting near the south coast of the island. As with the Kuromatsunai Fault, estimated slip rates on the Central Hokkaido Fault may be affected by the sparsity of stations on the western part of the island, and we note that the extension observed across the southern section of this fault is at odds with the reverse slip observed in the geological record [e.g., *Itoh et al.*, 2005]. The fault branch striking WNW in SE Hokkaido represents the Hidaka Fold-and-Thrust Belt and is modeled as a NE dipping structure between central Hokkaido and the major bend in the Japan-Kuril Trench. We estimate reverse slip rates on this structure, decreasing trenchward from 12.8 ± 2.4 to 3.5 ± 2.1 mm/yr, and up to 3.2 ± 2.7 mm/yr of right-lateral slip. The sense of lateral motion on the Hidaka structures has changed through time [*Kusunoki and Kimura*, 1998], and paleomagnetic data documenting Oligocene rotation of the hanging wall suggest a complicated history of faulting [*Itoh et al.*, 2005].

[36] In southwestern Hokkaido, just north of the Tsugaru Straits, we model an ENE striking fault from the OBR fault across Funka Bay ("FB" in Figure 3a), following the general trend of the active volcanic arc [e.g., *Kusunoki and Kimura*, 1998]. The fault connects to the Hidaka Fault [*Kusunoki and Kimura*, 1998] near the south end of the Ishikari Lowland ("IL" in Figure 3a) in the west central part of Hokkaido and serves as a boundary between a block comprising the northern Honshu fore arc and a central Hokkaido–Sea of Japan block to the north. We find that the inclusion of this fault is necessary in order to estimate fault slip senses that agree with those known from geologic data: in JB1, shortening is predicted across the Sea of Japan faults (see section 5.6.4), the Kuromatsunai Fold-and-Thrust Belt, the Hidaka Collision Zone in southeast Hokkaido ("HR" in Figure 3a), and faults in western and central Honshu. Without this fault, we predict normal motion in the Hidaka Fold-and-Thrust Belt region, although slip rates along many other faults bounding the relevant blocks are similar to those of JB1. Additionally, the mean residual GPS velocity at stations in the Kuromatsunai region is notably increased from 1.54 to 3.32 mm/yr when the fault is omitted. On the other hand, we estimate up to ~11 mm/yr of left-lateral reverse slip along the proposed Funka Bay fault, although it is unclear as to whether or not this fault exists. Seismic reflection profiling across the Yufutsu anticline offshore the Ishikari Lowland indicates the presence of a blind thrust fault whose trend strike is locally interpreted as SSW and therefore may project across Funka Bay to northern Honshu [*Kato et al.*, 2004]. Additionally, *Hashimoto and Jackson* [1993] suggest several submarine faults and monoclines in this region that together may comprise a boundary between northeast Honshu and west central Hokkaido. Finally, *Toya and Kasahara* [2005] show high geodetic strain rates in southwest Hokkaido, as well as a trend in crustal seismicity that follows the trace of the proposed fault, both of which support the existence of this putative structure.

[37] The east coast of Hokkaido has been proposed to be part of the Kuril fore-arc sliver [e.g., *Fitch*, 1972; *Kimura*, 1986; *DeMets*, 1992a], accommodating oblique convergence across the Japan-Kuril Trench through translation toward the southwest relative to central Hokkaido. We tested models with a Kuril block, the northern and eastern boundaries of which are marked by vertical faults striking ENE and NW, respectively [e.g., *Kimura*, 1986; *Kusunoki and Kimura*, 1998]. Models including the Kuril sliver but employing block geometries otherwise identical to JB1 show fault kinematics resolved on these structures that do not agree with the long-term sense of motion recorded in the geology, and only a slight improvement in the fit to the data; the 24 stations on the modeled sliver show improvement in the mean residual speed from 1.71 mm/yr in JB1 to

1.45 mm/yr in the Kuril sliver model. The Kuril strike-slip fault, which strikes parallel to the subduction zone, has experienced right-lateral motion throughout the Cenozoic [*Kimura*, 1986], yet our test model resolves 10–20 mm/yr of left-lateral slip. Similarly, the opening noted beneath the Bussol Straits, which is thought to drive the motion of the Kuril sliver [*Kimura*, 1986], is in disagreement with the ~20 mm/yr of closing estimated by the test block model. Convergence between PAC and OK that occurs exclusively on the subduction zone in reference model JB1 is partitioned in the Kuril sliver test models, with up to 40 of the ~80 mm/yr of shortening accommodated across the Kuril fault instead of the subduction zone. Finally, the Kuril sliver test model predicts normal fault motion on the Hidaka Fold-and-Thrust Belt, at odds with the geologically documented collision and contraction [*Kimura*, 1986; *Kusunoki and Kimura*, 1998; *DeMets*, 1992a]. In JB1, we estimate significant right-lateral slip across the Japan-Kuril Trench (see section 5.6.1), indicating that the margin-parallel component of relative plate motion may be accommodated by oblique slip on the subduction interface. However, the sparsity of GPS stations in coastal Hokkaido may preclude resolution of slip on the distinct crustal structures that take up some of the lateral motion.

5.6. Subduction Zones

5.6.1. Japan-Kuril Trench

[38] We estimate reverse dip-slip rates along the Japan Trench that increase northward from 73.3 ± 2.5 mm/yr near the Japan-Marianas-Sagami triple junction east of Kanto (34°N) to 91.1 ± 2.7 mm/yr just south of the prominent bend in the trench near Hokkaido (41°N; Figures 7, 8, and 9b). North of this bend, we estimate reverse slip rates of 76.1 ± 0.8 to 90.2 ± 1.0 mm/yr along the Kuril Trench northeast to Kamchatka, with most rates around 85 mm/yr. We note opposite senses of strike-slip motion on either side of the Hokkaido bend, with generally left-lateral slip between 4.7 ± 2.2 and 27.2 ± 2.3 mm/yr south of the bend and right-lateral slip between 21.3 ± 0.7 and 50.0 ± 0.9 mm/yr north of the bend, reflecting the along-strike variation in angle between the WNW trending block motion vectors of PAC and the subduction zone fault segments (Figures 7, 8, and 9a). The pattern is consistent with clockwise-counterclockwise paired rotation on Hokkaido noted by *Toya and Kasahara* [2005] in an analysis of the GPS-derived velocity gradient field. The rate and sign of strike-slip motion resolved along the Japan-Kuril Trench is sensitive to the strike of the fault segments, with the fastest left-lateral slip offshore northern Honshu occurring on the more northerly striking segments, and even some right-lateral slip estimated on those segments that strike more easterly. On the Kuril Trench, the right-lateral component of slip generally decreases northeastward. The overall magnitude of slip across the subduction zone is consistent with previous estimates of PAC-NAM (PAC-OK) convergence (~75–95 mm/yr [*Bird*, 2003; *DeMets*, 1992a; *Seno et al.*, 1996]).

5.6.2. Sagami Trough

[39] There have been several interpretations suggested for the configuration of tectonic plates beneath Kanto. At the Sagami Trough, *Seno and Takano* [1989] described the Philippine Sea plate as being subducted northward beneath Kanto yet above the Pacific slab, which itself is subducting westward beneath Kanto. *Toda et al.* [2008] suggested that a fragment of the Pacific plate, detached upon collision of two subducting Pacific plate seamount chains around 2 Ma, is sandwiched between the Pacific, Philippine Sea, and crustal Japan plates and influences the seismicity beneath greater Tokyo. Along the Sagami Trough, we estimate right-lateral slip rates between 5.6 ± 2.4 and 17.0 ± 2.1 mm/yr, with most rates >10 mm/yr, and reverse slip rates of 2.8 ± 2.2 to 16.6 ± 1.8 mm/yr, with most segments slipping 11–15 mm/yr (Figures 6, 7, and 9), giving a total convergence velocity of ~20 mm/yr, which is considerably slower than the 28–30 mm/yr estimated by *Seno et al.* [1993] for the oblique convergence between PS and what is interpreted as NAM at the Sagami Trough.

5.6.3. Nankai Trough-Ryukyu Trench

[40] Along the Nankai Trough in the Tokai-Tonankai region, south of the Suruga Trough (discussed in section 5.4.4), we estimate reverse slip rates ranging from 36.2 ± 2.4 mm/yr immediately south of the intersection with the eastern boundary of the IMP to 63.2 ± 1.8 mm/yr off the Bungo Channel (Figures 5, 6, and 9b), with a mean of 44.2 ± 2.0 mm/yr, consistent with the 40–46 mm/yr rates predicted by *Seno et al.* [1993] for PS-EU convergence. Oblique slip on the subduction thrust is demonstrated by right-lateral slip at rates between 8.6 ± 1.5 and 40.0 ± 1.4 mm/yr, averaging 22.9 ± 1.4 mm/yr along the Tokai-Tonankai part of the trough (Figures 5, 6, and 9a). Offshore Kyushu, from the Bungo Channel southwest to the northeastern boundary of the Okinawa block, we find a mix of right-lateral and left-lateral strike-slip rates (up to 37.5 ± 1.7 mm/yr left-lateral and 33.6 ± 1.5 mm/yr right-lateral) that are sensitive to short-wavelength changes in strike of the trench. Shortening rates along this segment of the trench increase southwestward, from the 63.1 mm/yr rate quoted above to 93.8 ± 2.5 mm/yr at the intersection with the Okinawa block fault. The average dip-slip rate along this stretch of trench is 76.1 ± 1.9 mm/yr.

[41] We modeled the Ryukyu Arc proper as comprising two blocks, with the northeastern reaches of the arc as part of the Nankai-Kyushu fore-arc block, the boundaries of which are based on our own assessment of GPS magnitudes and azimuths as well as previous analyses focused on the arc alone [*Nakamura*, 2004; *S. Nishimura et al.*, 2004]. If the entire Ryukyu Arc is included as part of Nankai-Kyushu fore-arc block, residual velocities on the Ryukyu Islands are large in magnitude and systematically oriented, with distinct clustering of the residual orientations in the central and southern islands; dividing the region into smaller blocks by introducing structures striking perpendicular to the trench substantially decreases residual velocities (from a mean of 8.05 mm/yr for 35 Ryukyu stations, defined as all stations southwest of Kyushu, in a single fore-arc block model to 3.46 mm/yr for the segmented fore-arc block model) while not substantially modifying the slip rates on the Ryukyu Trench and the Okinawa Trough spreading center. While the geology of the region shows numerous structures striking oblique or orthogonal to the Ryukyu and Okinawa plate boundaries [e.g., *Fournier et al.*, 2001], the process that serves to physically segment the fore-arc/arc and allow distinct blocks to rotate independently is unclear. We speculate that a combination of the changing strike of the Ryukyu Trench and Okinawa Trough with respect to the

direction of PS subduction, in addition to the subduction of bathymetric highs such as the Daito Ridge beneath the thin crust of the Ryukyu Arc, may explain the local block geometry.

[42] Along the eastern margin of the Okinawa block (ON), reverse slip rates are relatively homogeneous along strike, ranging 102.2 ± 2.8 to 118.2 ± 3.9 mm/yr. This maximum rate is substantially faster than the ~65 mm/yr estimated by *Seno et al.* [1993] for PS-EU convergence along the Ryukyu near Okinawa, because it represents convergence between PS and ON. Factoring in the 20–30 mm/yr of opening we estimate along the boundary between ON and the Yangtze block (YA) (section 5.1), the relative convergence between PS and YA is reduced to ~80 mm/yr. This summed rate, a result of the net effects of motion across two roughly parallel block boundaries (PS-ON and ON-YA), is ~15 mm/yr faster than the *Seno et al.* [1993] estimate. No elastic strain accumulation across the Ryukyu plate boundary is modeled in JB1, where fault segments are assumed to creep. This is based upon a previous analysis of GPS velocities along the arc [*S. Nishimura et al.*, 2004], which suggested that the paucity and moderate size of thrust-sense earthquakes along the Ryukyu plate boundary is due to generally low seismic coupling between the two plates with isolated patches where sufficient locking occurs to generate seismic events. We tested models in which a locking depth of 30 km was assigned to all subduction fault segments along the Ryukyu Trench and found relative slip rates between PS and the Ryukyu arc blocks of up to 130 mm/yr, with opening rates along the Okinawa Trough of up to 40 mm/yr. We prefer the slower rates estimated by the model in which interplate creep is allowed along the Ryukyu Trench, as they are more consistent with previous plate motion studies [e.g., *Seno et al.*, 1993] and rates estimated from geodetic inference of block rotations [*Nakamura*, 2004; *S. Nishimura et al.*, 2004].

5.6.4. Sea of Japan

[43] The eastern margin of the Sea of Japan is seismically active, yet the geometry of the plate boundary is ambiguous [e.g., *Fukao and Furumoto*, 1975; *Okamura et al.*, 2005]. We therefore model this boundary using a vertical fault, as the elastic deformation field resulting from motion normal to a vertical fault is similar to that due to dip slip on a pair of faults dipping toward each other at 45° [*Souter*, 1998; *McClusky et al.*, 2000]. *Seno et al.* [1996] estimate a relative convergence rate for EU-OK (or EU-NAM) across the eastern margin of the Sea of Japan of ~5–13 mm/yr, increasing southward from Sakhalin Island to the Noto Peninsula, consistent with the closing sense rates predicted by JB1, which range from 6.4 ± 3.8 mm/yr off the west coast of Hokkaido to 13.8 ± 2.2 mm/yr offshore northern Honshu, with rates of 10–12 mm/yr farther south off central Honshu. In addition to the closing sense slip, we also estimate left-lateral slip, generally decreasing southward from 8.5 ± 0.9 mm/yr offshore Hokkaido and northern Honshu to less than 1 mm/yr near the Noto Peninsula (Figures 7–9).

5.7. Variations in Interplate Coupling

[44] In addition to the plate convergence rates described above, we also image the degree of coupling along the Japan, Nankai, and Sagami subduction interfaces by solving for the slip distribution on triangular elements (Figure 10). The sign convention we adopt is that positive dip slip represents coseismic slip deficit on the subduction interface, and negative dip slip reflects thrust or coseismic sense slip; the strike-slip sign convention is the same as for rectangular fault segments. Linearly estimating subduction interface slip [*Meade and Loveless*, 2009] differs from previous analyses' nonlinear estimates, which solve for the coupling coefficient, χ, on the fault [*Mazzotti et al.*, 2000; *McCaffrey*, 2002]. The coupling coefficient represents the slip magnitude on a fault element, $|\mathbf{t}|$, normalized by the plate convergence rate, u_{PC}: $\chi = |\mathbf{t}|/u_{PC}$. Such solutions are sometimes constrained such that $0 \leq \chi \leq 1$, that is, the coseismic slip deficit on no portion of the plate boundary can occur at a rate faster than plate convergence, and no element can have forward slip [e.g., *Bürgmann et al.*, 2005; *McCaffrey et al.*, 2007]. By explicitly solving for the slip distribution on an array of triangular dislocation elements tessellating the subduction zone interface, we permit forward slip and thus can resolve regions experiencing extremely low coupling, postseismic deformation following large subduction zone earthquakes [e.g., *Heki et al.*, 1997; *T. Nishimura et al.*, 2004], and ongoing very long period slow, or silent, slip events. We calculate χ for each element by dividing the magnitude of estimated TDE slip by the magnitude of slip given by projecting relative block motions onto the TDE geometry (Figure 10c).

[45] Along the Japan-Kuril Trench, we image concentrations of ~100% coupling offshore southeast Hokkaido near the rupture area of the 2003 M_w = 8.3 Tokachi-oki earthquake, and offshore Sendai at 38°S latitude, where four $M_w \geq 7$ earthquakes have occurred since 2003. Although finite slip persists to 70–80 km depth, deeper than the nominal seismogenic zone, most coupling is concentrated between 20 and 60 km depth, consistent with previous coupling analyses of the Japan Trench subduction interface [*Mazzotti et al.*, 2000; *T. Nishimura et al.*, 2004; *Suwa et al.*, 2006]. Near the southern edge of the modeled subduction interface (35°N), coupling is moderate (30–60%) and is restricted to depths shallower than ~30 km, consistent with the findings of *Nishimura et al.* [2007]. Below this depth, the estimated dip slip rates are negative, which we suggest may be an artifact of our inversion, as no substantial postseismic or aseismic deformation has been reported in the region. Nonetheless, observed coastal velocities north of the Boso Peninsula are substantially slower than at stations to the north and south, despite being located closer to the trench (Figure 2), suggesting less interplate coupling. *Mochizuki et al.* [2008] describe the interplate coupling around a large subducted seamount offshore Ibaraki Prefecture (36.0–36.5°N) as spatially heterogeneous, with strong coupling at the leading edge of the subducting feature and weak coupling in its wake. They further suggest that the coupling of the subduction interface around the seamount is perturbed and dictates the pattern of seismicity, which is characterized by moderate earthquakes ($M \sim 7$) repeating every ~20 yr. The source region for such events, including the 1982 M = 7.0 and May 2008 earthquakes, lies in an area of ~25% coupling (Figure 10), suggesting that this low degree of coupling, if persistent through time, may represent plate

interface behavior capable of producing only moderate earthquakes.

[46] A zone of up to 25 mm/yr of thrust sense slip is resolved beneath northernmost Honshu and may reflect postseismic deformation triggered by the 1994 M_w = 7.7 Sanriku-oki earthquake [*Heki et al.*, 1997; *T. Nishimura et al.*, 2000, 2004]. The forward slipping region is restricted to depths greater than ~35 km, while previous estimates of the extent of afterslip incorporate regions as shallow as 17 km [*Heki et al.*, 1997]. However, previous estimates have relied on a GPS velocity field describing motion for only about 1 year following the earthquakes, while the 1997–2000 time series used in our model captures the combined effects of the afterslip, other postseismic deformation mechanisms (such as viscoelastic relaxation), and resumption of interseismic strain accumulation. We note that the zone of resolved forward sense slip in reference model JB1 occurs exclusively downdip of the centroid moment tensor for the 1994 earthquake (focal mechanism shown in Figure 10b), as well as that of a local M_w = 7.4 earthquake in 1989. Above 35 km depth, and therefore coincident with the inferred rupture area of the Sanriku-oki earthquake, we estimate a local minimum in coupling (~25%) between the regions of near complete coupling to the north and south (Figure 10c). This low degree of coupling in the Sanriku-oki region is consistent with postseismic deformation characterizing the early stage of the seismic cycle on this particular segment of the plate boundary [e.g., *Hetland et al.*, 2010].

[47] On the Sagami subduction interface, we estimate a single concentration of coseismic slip deficit reaching ~25 mm/yr centered beneath the Boso Peninsula. Immediately to the west, we image a concentration in right-lateral slip on the interface below the Miura Peninsula, with slip rates reaching ~35 mm/yr, giving a coupling value greater than 100% (Figure 10). Estimation of slip rates on the Sagami interface are hindered by the complicated plate configuration, including the possible presence of a Pacific Plate slab fragment beneath Tokyo [*Toda et al.*, 2008] and uncertainty in the interface geometry [*Ishida*, 1992; *Sato et al.*, 2005]. *Nyst et al.* [2006] estimate that coseismic slip characterizing the 1923 M ~ 7.9 Kanto earthquake occurred on two patches: one of dominantly right-lateral slip beneath the Miura Peninsula and the Odawara region (north of the east coast of the Izu Peninsula), and one of right-lateral reverse oblique slip beneath Tokyo Bay and the Boso Peninsula. This inferred variation in rake is consistent with the geodetically constrained slip rate distribution that we estimate through the interseismic period on the Sagami subduction zone interface.

[48] Along the Nankai Trough, we image a spatial distribution of interplate coupling that is broadly consistent with previous studies [e.g., *Hyndman et al.*, 1995; *Ito et al.*, 1999], including a segmented slip distribution (Figure 10) similar to inferred seismic asperities on the Nankai interface, mapped by *Kodaira et al.* [2006] using wide-angle seismic data and frictional modeling. They found a plutonic body off the southeast tip of the Kii Peninsula and suggested that it serves as a "strong patch," segmenting great earthquake rupture areas. We estimate greatest coupling of ~100% in a kidney-shaped region beneath and immediately southwest of Shikoku, a local minimum in coupling between Shikoku and the Kii Peninsula (down to 70%), a local maximum of 90% offshore the bulk of the Kii Peninsula, and another local decrease to 60% between the peninsula and the Tokai region. The local maxima that we observe from southwest to northeast correspond to the Tonankai, Nankai, and Tokai asperities described by *Kodaira et al.* [2006].

[49] We estimate slow ($\leq$5 mm/yr offshore Shikoku, $\leq$10 mm/yr offshore the Kii Peninsula, and $\leq$20 mm/yr offshore Tokai) forward slip around the downdip extent of the modeled Nankai subduction interface. While this could reflect a numerical artifact of the inversion, we note that our method allows forward slip to be imaged on multiyear timescales, and we suggest that it may be indicative of an ongoing, very long period episode of aseismic slip or silent earthquake. Short-period slow slip phenomena have previously been identified near the Bungo Channel and beneath Shikoku, commonly at depths greater than those typical of seismogenesis (0–30 km [e.g., *Ozawa et al.*, 2001; *Shelly et al.*, 2006]).

[50] In addition to slow forward slip at the downdip extent of much of the Nankai Trough, there is also a region of more substantial (up to 58 mm/yr) forward slip at the southwest extreme of the region meshed using TDEs (Figure 10b). As described in section 3, GPS velocities in southern Kyushu contain some contribution from known postseismic deformation following the 1996 Hyuga-nada earthquakes. The subduction interface offshore Ryukyu is inferred to be uncoupled [*S. Nishimura et al.*, 2004], which means that in block theory, the relative motions of crustal blocks across creeping faults are the exclusive source of interseismic GPS velocity.

5.7.1. Effects of Slip Smoothing

[51] The smoothing weighting factor, β, serves to control the balance between an oscillating (and thus presumably unphysical) slip rate distribution on the TDE mesh that minimizes the misfit between the data and model, and a homogeneous slip rate distribution that results in large residual velocities. To objectively find a β value that results in both a physically based slip distribution consistent with plate convergence rates and a reasonable fit to the constraining data, without imposing finite, a priori limits on slip magnitude, we consider block models with a range of β values with all other parameters held constant and examine the resulting slip rate distributions on the triangulated surfaces. We assume that the portion of the Japan subduction zone that slipped during the 2003 Tokachi-oki earthquake was fully coupled in the years preceding that event. Thus, our analysis using the 1997–2000 velocity field is taken to represent the preseismic, fully coupled state in that region. Additionally, we assume that the region on the Nankai subduction zone, inferred to have slipped during the 1946 Nankaido earthquake, was also fully coupled during 1997–2000. For a given realization of β, we find the TDE elements that lie in the 90th percentile of the estimated slip rate distribution (i.e., those that are most strongly coupled). For β values between 0.045 and 100, these threshold elements highlight the Tokachi-oki and/or Miyagi-oki rupture zones on the Japan Trench, and the Nankaido region on the Nankai subduction zone interface. As a reference state, we select the fastest slipping elements for β = 0.25 to represent the Tokachi-oki and Nankaido earthquake asperities, calculate the maximum, minimum,

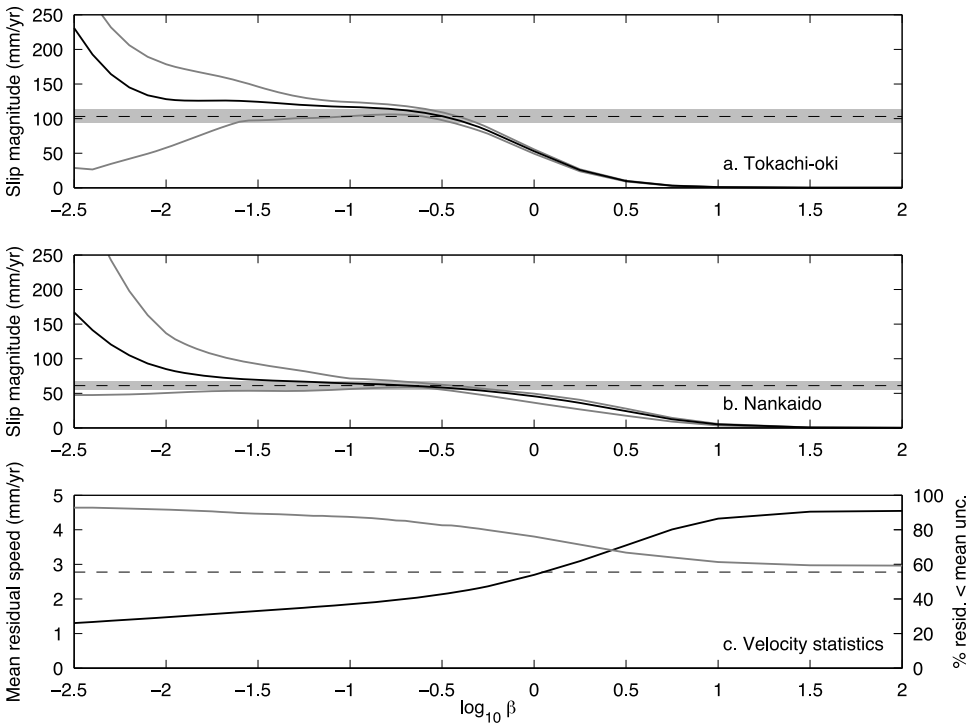

Figure 14. Results of the smoothing iteration tests. A full block model was run using a variety of values of β, with all other parameters held constant. We calculate the minimum, maximum, and mean slip on two clusters of elements that we take to represent the (a) Tokachi-oki and (b) Nankaido earthquake asperities; the extrema are shown as gray lines, and the mean is shown as a black line. The relative block motion velocity calculated at the trench and projected onto the dipping asperity plane is shown by the horizontal dashed black line, with the gray shading indicating ±10% of this value. (c) Plot of statistics of the modeled velocity field as a function of β. In Figure 14c, the black line represents the mean residual velocity magnitude (speed), and the gray line shows the percentage of residual speeds less than the mean observed uncertainty speed; the mean uncertainty is shown as the horizontal black dashed line. See the text for more details regarding the selection of β.

and mean slip magnitudes resolved for all trial values of β, and find the range of β values within which the slip magnitude statistics are physically meaningful with respect to the long-term plate motion as estimated using the block modeling theory.

[52] For very low smoothing values ($\beta \sim 10^{-5}$), the estimated slip rates are unrealistically high (order 10^4 mm/yr) and randomly distributed across the TDE mesh. With increasing β, slip rate amplitudes decrease and the estimated slip distribution becomes smoother. For strong smoothing ($\beta \geq 1$) and with the zero-slip boundary conditions imposed along the updip and downdip limits of the TDE meshes, the maximum, minimum, and mean asperity slip rates converge toward zero (Figures 14a and 14b). We find that the mean slip rates on the Tokachi-oki and Nankaido earthquake asperity elements reach a low slope over the range $10^{-2} \leq \beta \leq 10^{-0.5}$ (Figures 14a and 14b). Within these bounds, the mean slip rates are approximately equal to the long-term convergence rate given by the relative block motions. We show the approximate block motion in the vicinity of the asperities (horizontal dashed lines in Figures 14a and 14b) by projecting the rates calculated at the trench (e.g., Figure 9) onto the dipping elements. We use the average dip of the asperity cluster elements to represent the fault geometry: 27° and 12° for Tokachi-oki and Nankaido, respectively, giving approximate block motion rates of 103 and 61 mm/yr. As β increases, the estimated slip rate distribution on triangular elements is more strongly influenced by the Laplacian minimization criterion, thus increasing the misfit to the GPS data. This trend can be seen in two ways. The black curve in Figure 14c shows the mean residual magnitude, and the gray curve shows the percentage of stations whose residual velocity magnitude is less than the mean uncertainty magnitude of the GPS observations; this value is shown as the horizontal dashed line (on the left axis). Given the monotonic decrease in the quality of fit to the data with increasing β, we select a $\beta = 0.1$ smoothing weight for reference model JB1, as it provides a good fit to the data while still satisfying the plate boundary slip rate constraints.

[53] Slip rates on triangular elements are estimated without kinematic consistency constraints. Nonetheless, the constant value of mean slip on the asperity patches over a range of smoothing factors suggests the resolving power of the GPS data. Had we no a priori knowledge of the long-term block rates, a simple approach would be to identify a range of β values within which the estimated asperity slip rates were roughly constant, as that range suggests estimated slip rate solutions that are reasonably insensitive to changes in the applied smoothing constraints and instead are dictated by the GPS data. For reference model JB1, we

set $\beta = 0.1$ on all subduction interfaces, resulting in (1) mean slip rates on the Tokachi-oki and Nankaido asperity clusters of 105 and 60 mm/yr, respectively, approximately equal to the block motion rates and within the low slope parts of the slip rate versus β curves, (2) small spread between the maximum and minimum slip rates within the clusters of coupled TDEs, and (3) a mean residual surface velocity magnitude of 1.84 mm/yr, less than the mean uncertainty magnitude of the observations (3.35 mm/yr). We note that applying a relaxed smoothing constraint ($\beta \leq 10^{-2.5}$) results in unrealistically high slip rate magnitudes ($\geq$200 mm/yr on the Tokachi-oki asperity) while providing only a slight improvement in the quality of fit to the data over β values that yield asperity slip rates consistent with plate motion (mean residual of 1.27 mm/yr for $\beta = 10^{-2.5}$).

[54] We note that an alternative choice for the optimal β value is that which gives a maximum slip value within the coupled TDE clusters equal to the local plate convergence rate, which, in the case of our tests, would be $\beta \sim 0.5$ ($10^{-0.3}$, Figure 14). Selecting this value would result in a single asperity TDE being fully coupled, as the geometric properties of the smoothing operator would force all surrounding elements to be less than the plate convergence rate. Although some TDEs in the asperity clusters of model JB1 have coupling greater than 100% (Figure 10c), coupling on average within the clusters is less than or equal to 100%. We argue that although isolated occurrence of TDEs with estimated coupling greater than 100% is physically unrealistic, restricting complete coupling to a single element, as would be the case for $\beta \sim 0.5$, is similarly unreasonable. Furthermore, using $\beta = 0.1$ allows for resolution of slip patterns on the order of 150 km in linear dimension while $\beta = 0.5$ oversmooths patterns of that size (Appendix B and Figure B1). We therefore suggest that the selection of $\beta = 0.1$ places sufficient physical constraint on the estimated slip distribution while allowing for resolution of slip patterns with spatial scales of $\sim$150 km.

6. Discussion

6.1. Revised Plate Tectonic Setting

[55] While each block in our model represents a distinct microplate, estimates of Euler pole locations and rotation rates provides a means for comparing the detailed block geometry with larger-scale plate tectonic setting models [e.g., *Seno*, 1985; *DeMets*, 1992b; *Seno et al.*, 1996; *Bird*, 2003]. *Heki et al.* [1990] questioned the concept of a plate tectonic setting at a weak island arc, and asserted that a combination of relative plate motion and intraplate deformation was the most likely explanation for the geodetic velocities in northern Honshu. Block modeling theory [*Matsu'ura et al.*, 1986; *Hashimoto and Jackson*, 1993; *Souter*, 1998; *McCaffrey*, 2002; *Meade and Hager*, 2005; *Meade and Loveless*, 2009] provides a means for systematically separating the effects of elastic strain accumulation resulting from locking at plate boundaries and on crustal faults and the long-term relative plate motions more typically used to define tectonic setting models without having to assume the partitioning of deformation a priori. We isolate the block motion contribution to the interseismic velocity field, $\mathbf{v}_B = \mathbf{R}_B\boldsymbol{\Omega}^{est}$, where $\mathbf{R}_B$ is a linear cross-product operator and show representative velocities for each block in the greater Japan region in Figure 15a. We selectively remove segments and blocks from JB1 so that the geometry is similar to that of several previously proposed plate tectonic setting models [e.g., *Seno et al.*, 1996; *Heki et al.*, 1990, 1999; *Bird*, 2003] in order to explore the capacity of the geodetic data, including GEONET velocities, data to discriminate between these models. *Seno et al.* [1996] presents four possible plate configurations around Japan involving NAM, EU, PS, PAC, OK, and northern Honshu plate (NH). When the boundary between NAM and EU is placed through central Hokkaido [*Chapman and Solomon*, 1976], Japan lies primarily on EU and block motion velocities are $\sim$15 mm/yr to the east in northern Honshu and to the ESE in western Honshu, Kyushu, and Shikoku (Figure 15b). When the boundary between NAM and EU is shifted to the eastern margin of the Sea of Japan and the ISTL [*Seno et al.*, 1996, Figure 2b], velocities on northern Honshu and Hokkaido (part of NAM) are <5 mm/yr to the northeast and 15 mm/yr ESE west of the ISTL (i.e., the part of Japan that lies on EU; Figure 15c). Using this same geometry but including a distinct OK plate, we find velocities that are nearly identical (Figure 15d). That is, using these simple plate boundary configurations, we cannot distinguish OK from NAM using GPS data. With a model that isolates northern Honshu between the ISTL and central Hokkaido as a microplate (Figure 15e and Figure 2d of *Seno et al.* [1996]), we estimate block motion velocities west of the ISTL and in northern Honshu that are very similar to those of Figure 15d (6 mm/yr compared to 5 mm/yr), while velocities in eastern Hokkaido (part of OK) are $\sim$3 mm/yr directed to the SE (Figure 15e). If we consider the plate geometry proposed by *Bird* [2003], which includes PAC, OK, AM, PS, and the Okinawa Plate (Figure 15f and Figure 2 of *Bird* [2003]), we find block velocities in western and northern Honshu similar to those in Figures 15c, 15d, and 15e, while velocities along the Ryukyu Islands, which lie on the Okinawa Plate in this model, move SE at 25–30 mm/yr (Figure 15f). Our study of the effect of adding a block boundary between the Nankai and Ryukyu fore-arc blocks (sections 5.2 and 5.3) shows a very different pattern of block motions as compared to JB1. In JB1, clockwise motion of the combined Ryukyu-Nankai fore arc produces SE directed velocities along the Ryukyu Islands, Kyushu, and Shikoku, ESE velocities on the Kii Peninsula, and NE velocities in Tokai (Figure 4c). However, if the Nankai fore arc is modeled as a distinct block, velocities on it are directed uniformly northward, while motions of the surrounding blocks are little changed. If we test the distinction of the AM from EU using the geometry proposed by *Heki et al.* [1999] (Figure 15g), we find that eastward motion of AM is reduced by about 1 mm/yr relative to the equivalent geometry in which eastern mainland Asia is instead considered part of EU (Figure 15c). Testing a plate configuration involving both AM and OK (Figure 15h) shows a reduction of about 1 mm/yr in NE directed velocities in northern Honshu and Hokkaido as compared to the model in which they are considered to lie on NAM rather than OK (Figure 15g). Finally, we test the *Heki et al.* [1990] model in which northern Honshu is considered to lie on a deformable NAM rather than on a rigidly moving OK (Figure 15i) by estimating a homogeneous strain tensor for NAM. We find block motion velocities on all plates that are nearly

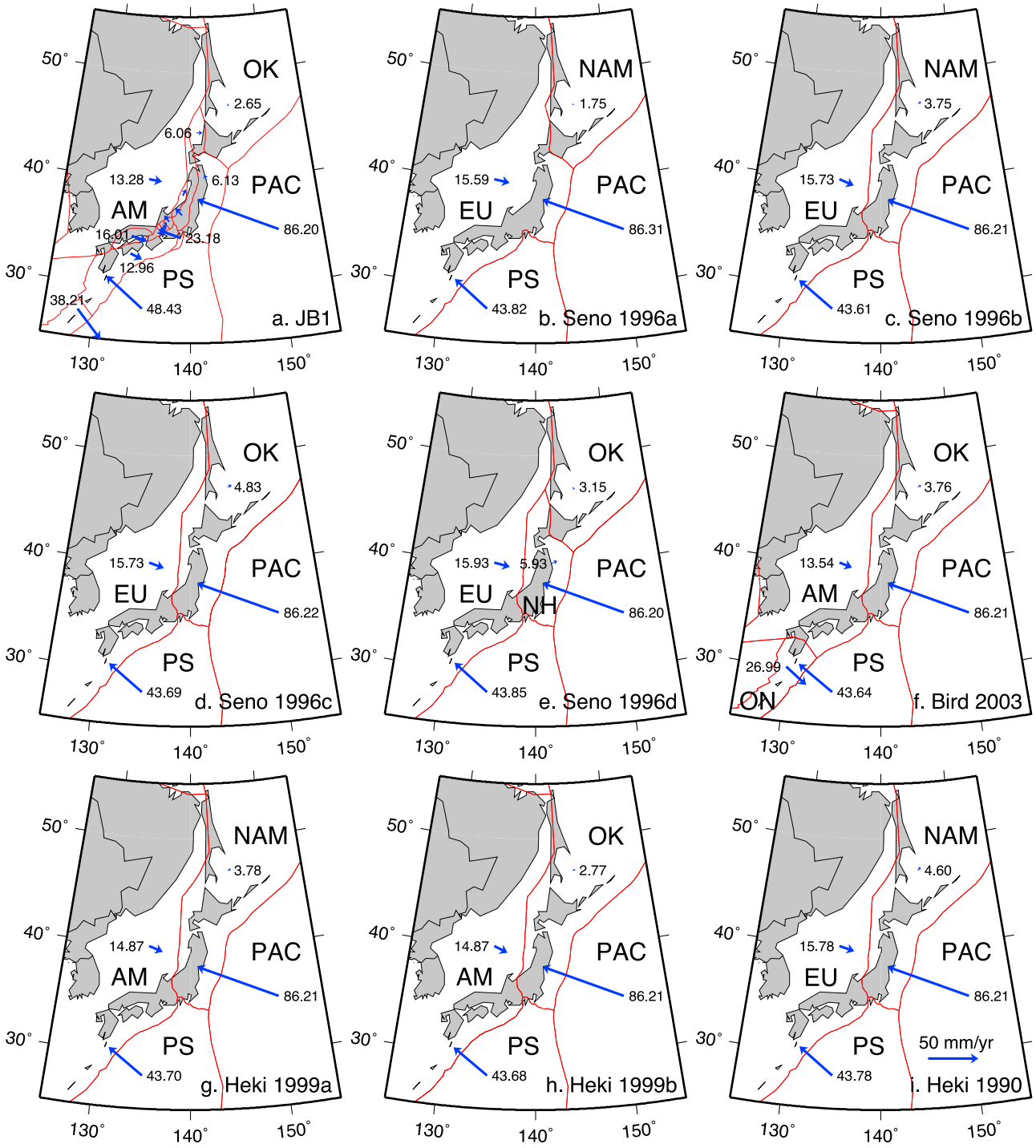

Figure 15. Surface velocities due to long-term block motions. A single velocity was calculated using the estimated Euler pole for each block to show its representative motion relative to stable Eurasia. The velocity magnitude is shown at the vector tail. (a) Model JB1. (b–i) Segments and blocks were selectively removed from model JB1 such that the block geometry agreed with previously proposed plate configurations. Figures 15b, 15c, 15d, and 15e approximate Figures 2a, 2b, 2c, and 2d, respectively, of *Seno et al.* [1996], while Figure 15f mimics the geometry proposed by *Bird* [2003]. Figures 15g and 15h test the plate configurations of *Heki et al.* [1999], and Figure 15i shows the geometry of *Heki et al.* [1990]. See section 6.1 for details. Red lines indicate the block geometry. Block names are abbreviated as follows: NAM, North America; PAC, Pacific; EU, Eurasian; AM, Amurian; PS, Philippine Sea; OK, Okhotsk; ON, Okinawa. The vector scale shown in Figure 15i applies to all plots.

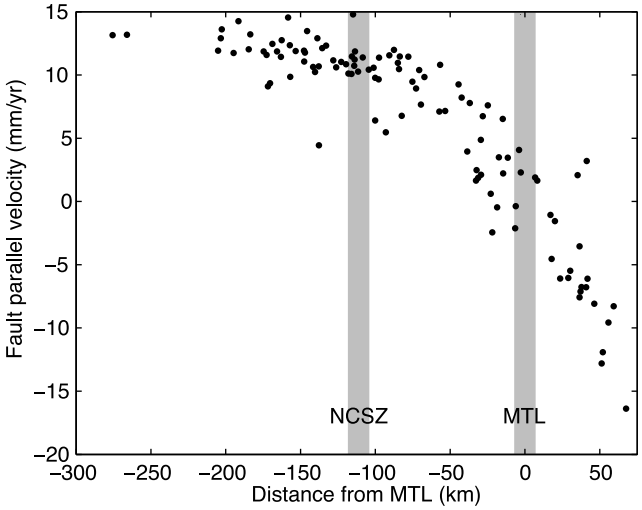

Figure 16. Approximately fault-parallel velocities at stations surrounding the Median Tectonic Line (MTL) and North Chugoku Shear Zone (NCSZ). Velocities across the MTL show a sharp gradient, while no such pattern is evident across the NCSZ.

equivalent to those in Figure 15d, indicating that with the appropriate local plate configuration, and GPS data concentrated on the Japanese Islands, it is difficult to distinguish whether or not northern Honshu should be considered part of a rotating OK or a deformable NAM.

[56] We propose that deformation across Japan can be described as resulting from the motions of 20 plates with a residual velocity magnitude of 1.84 mm/yr. Model JB1 shows a dramatic difference in the block motion velocities between Hokkaido and northern Honshu (Figure 4c), suggesting that the Hidaka Range fault and its continuation northward to Sakhalin Island marks a plate boundary [*Chapman and Solomon*, 1976; *Seno et al.*, 1996]. We propose that the Nankai forearc/Tokai and Chubu region blocks represent a region that moves reasonably coherently (Figure 4c) and is separated from the greater Amurian Plate by the NKTZ and MTL, and from northern Honshu by the ISTL; these boundaries define northern Honshu as a distinct microplate [*Seno*, 1985]. Our models suggest that the Kyushu fore arc is part of the same block that comprises the Nankai fore arc, while the Ryukyu fore arc is segmented into two blocks. The boundary between the Ryukyu blocks and the greater Amurian/Yangtze Plate region is the Okinawa Trough. Stations on northern Kyushu and north of the MTL-NKTZ system lie on the southeastern edge of AM.

6.2. Partitioning of Deformation

[57] The trench-parallel component of the oblique convergence between PS and the Nankai fore-arc region is accommodated by right-lateral slip on both the subduction interface and the MTL, which bound the Nankai fore-arc block. Slip on the central MTL is relatively uniform at about 7 mm/yr, while the strike-slip component of motion across the Nankai Trough averages 22.9 mm/yr (section 5.6.3). Across the NCSZ, which is arcuate in shape but generally parallel to the MTL and Nankai Trough, we estimate negligible relative motion (0–1 ± 1 mm/yr left-lateral), which suggests that the available GPS data cannot distinguish the western Honshu block (between the MTL and NCSZ) from AM.

[58] Several studies have documented the worldwide occurrence of partitioning of oblique convergence between the subduction interface and upper plate strike-slip faults [e.g., *Fitch*, 1972; *Beck*, 1991; *McCaffrey*, 1996]. The "flat slab" subduction that takes place beneath Shikoku and western Honshu is interpreted to influence the pattern of slip partitioning along the Nankai Trough. Because of the shallow dip of the subducted plate, arc volcanism occurs farther from the trench than it would above a more steeply dipping slab. The thermally weakened line of arc volcanoes may be exploited as a region of concentrated strain, in some cases accommodating part or all of the margin-parallel component of deformation in an obliquely converging margin. *Gutscher and Lallemand* [1999] suggest that the NCSZ represents the locus of active strain partitioning, noting the relatively frequent occurrence of moderate earthquakes along it (15 M $\geq$ 5 earthquakes in the last 150 years), although the shear zone is not evident as a major surface breaking fault. Furthermore, they note that the MTL, while commonly cited as a type example of strain partitioning, has not experienced a destructive earthquake since the early 8th century [*Tsutsumi et al.*, 1991]. *Gutscher and Lallemand* [1999] suggest that the reason that the NCSZ has not been recognized as a major gradient in geodetic data is that the fault system is locked during the interseismic period thus relative motion across it would only be apparent after decades observation.

[59] Conversely, block theory addresses this problem directly by providing a framework for resolving both long-term block motions and elastic strain accumulation across block bounding faults. The classic arctangent fault perpendicular velocity pattern characteristic of a locked strike-slip fault [*Savage and Burford*, 1973] is absent across the NCSZ yet evident across the MTL (Figure 16). The geodetic, geologic, and seismologic observations present a paradox: the clear gradient in GPS velocities across the MTL suggests accumulating elastic strain, but crustal seismicity is concentrated along the NCSZ and virtually absent along the MTL. Similarly, the MTL is expressed clearly as a continuous, surface breaking fault with evidence of motion throughout the Quaternary [e.g., *Tsutsumi et al.*, 1991], while the seismically active NCSZ lacks a prominent surface trace [*Gutscher and Lallemand*, 1999]. In 1596, a $M \sim 7.5$ earthquake occurred on the eastern segment of the MTL four days after a $M \sim 7$ event on the western segment. Trench excavation suggests that the central segment of the MTL slipped during one or both of these events, yet there is no record of damage from radiated seismic waves immediately surrounding that part of the fault. *Kanaori et al.* [1994] suggest that these observations can be explained if the central segment of the MTL slips aseismically during and/or following large earthquakes on adjacent segments. If true, this could explain why the MTL marks a prominent gradient in the GPS velocity field, indicating elastic strain accumulation, but shows scarce historical seismicity, particularly compared to the NCSZ. Alternatively, it could be that the recurrence interval of earthquakes on the central segment is very long and it presently represents a seismic gap [*Kanaori et al.*, 1994]. Another possibility is that the low-velocity gradient across the NCSZ results from viscoelastic earthquake cycle effects caused by a relatively low viscosity

lower crust/upper mantle or relatively long mean earthquake repeat time that causes most strain accumulation to occur in the first 30% of the interseismic period following the last earthquake [*Savage and Prescott*, 1978; *Savage*, 2000].

[60] No clear change in speed or azimuth is observed in the GPS velocity field at the Hokkaido fore arc. As discussed in section 5.5, we find that a Kuril fore-arc sliver is not resolvable using the current data, as alternative block models that explicitly include this structure yield estimate slip rates at odds with the known sense of long-term slip at the Hidaka Fold-and-Thrust Belt and the reportedly right-lateral Kuril sliver fault itself. We propose that translation of the eastern Hokkaido and Kuril fore arcs is accommodated by right-lateral slip on the subduction interface, although we cannot rule out the possibility that lateral motion is distributed amongst several small crustal faults below the spatial resolution of the local GPS data. The rake of slip deficit on the subduction interface agrees with the slip vector estimated for the 2003 M_w = 8.3 Tokachi-oki earthquake based on GPS data [e.g., *Ozawa et al.*, 2004; *Miyazaki and Larson*, 2008], indicating that earthquakes on this part of the plate interface can accommodate oblique convergence. Additionally, the 5–10 mm/yr of shortening we resolve across the NE dipping thrust faults at the Hidaka Mountains is consistent with estimates of contemporary relative motion of the Kuril fore arc inferred from a comparison between the NUVEL-1 plate motion model [*DeMets et al.*, 1990] and a local catalog of earthquake slip vectors [*DeMets*, 1992a].

7. Conclusions

[61] We use spherical linear block theory [*Matsu'ura et al.*, 1986; *Hashimoto and Jackson*, 1993; *Souter*, 1998; *McCaffrey*, 2002; *Meade and Hager*, 2005; *Meade and Loveless*, 2009] to describe and interpret the interseismic GEONET GPS velocity field in Japan as the summed effects of block or microplate rotational motion, elastic strain accumulation about upper plate faults, and spatially variable coupling on the bounding subduction zones.

[62] 1. The reference Japan block model (JB1, consisting of 20 blocks) explains geodetically observed velocities around Japan with a mean residual velocity magnitude of 1.84 mm/yr, less than the 3.35 mm/yr mean uncertainty magnitude in the station observations.

[63] 2. Estimates of elastic coupling on geometrically accurate representations of the subduction zone interfaces show spatial correlations with the rupture areas of known earthquakes: concentrations of strain accumulation along the Japan Trench coincide with the locations of the 2003 Tokachi-oki earthquake off Hokkaido and the series of M_w > 7 earthquakes off the coast of Sendai, and strong coupling on the Nankai Trough is consistent with the Nankaido, Tonankai, and Tokai earthquake rupture zones.

[64] 3. Regions of thrust sense slip at depths >35 km offshore northern Honshu reflect postseismic deformation following the 1994 Sanriku-oki earthquake.

[65] 4. We confirm the hypotheses that the NKTZ and ISTL are major tectonic boundaries in central Honshu accommodating >15 mm/yr of motion. Further, geodetic slip rate estimates on the western half of the Gofukuji segment are less than half of geologic estimates suggesting the possibility of slip rate variability over late Pleistocene–Holocene scales.

[66] 5. Fast (~7 mm/yr) right-lateral slip on the Median Tectonic Line and its westward extension on Kyushu accounts for about 1/4 of the margin-parallel motion across the Nankai Trough, with the remaining 3/4 taken up by strike-slip motion on the subduction interface itself. Conversely, we cannot resolve right-lateral slip across a discrete structure defining a Kuril fore-arc sliver in Hokkaido. Instead, oblique convergence there is taken up exclusively by slip on the subduction interface and/or is distributed amongst crustal faults that are too small and/or slowly slipping to be resolved with the available data.

[67] 6. In extreme southeast Hokkaido, we estimate 5–10 mm/yr of shortening across the Hidaka Range Fold-and-Thrust Belt, consistent with geologic estimates.

[68] 7. Faults in western Hokkaido and their continuations throughout the Ou Backbone Range of northern Honshu are in general characterized by reverse slip, consistent with the mechanism of recent crustal earthquakes, including the 2007 Iwata Prefecture event. Slow normal slip on segments in northernmost Honshu may reflect crustal effects of the Sanriku-oki postseismic deformation.

[69] 8. Near Nagano, we find several GPS stations with anomalously fast velocities, which can be explained by a ~40 km long creeping fault segment.

[70] As a whole these models provide the highest resolution image of present-day fault system activity across Japan deformation across and provide critical constraints for both time-dependent seismic hazard analysis and comparisons with geologic fault slip rate estimates to assess the fault system evolution.

Appendix A: Combination of Disparate GPS Velocity Fields Into a Common Reference Frame

[71] The proliferation of GPS velocity data sets over the past 15 years has provided an unprecedented view of contemporary deformation in many tectonically active regions. Initial publication of GPS data generally provides a first-order interpretation of the velocity field in terms of the geological processes driving the motion. In many cases, raw GPS data are processed in such a way that the resulting published velocity field describes surface motion of one particular region relative to a chosen reference frame. While such a field is useful for constraining the geologic processes acting on the local region, variations in reference frame realizations make it difficult to combine multiple velocity fields in order to examine motion at a larger spatial scale. Reprocessing the raw data from one network in tandem with those from another [e.g., *Kendrick et al.*, 2001] is one way of expressing GPS velocities in a common reference frame, but access to these data may be limited.

[72] Here we present a simple way of combining multiple GPS velocity fields containing collocated stations in a single reference frame.We do this by solving for a rotation and translation vector that minimizes the misfit between velocities at collocated stations. The technique allows velocity fields in different reference frames to be combined, so long as each field shares a sufficient number of stations with at least one other field in order to adequately constrain the best fitting transformation vectors.

A1. Velocity Field Combination

[73] We first consider the case of two velocity fields, represented by vectors $\mathbf{V}_{A(A)}$ and $\mathbf{V}_{B(B)}$, where the first and second subscripts identify the particular velocity field and the reference frame in which it is defined, respectively. While $\mathbf{V}_{A(A)}$ and $\mathbf{V}_{B(B)}$ may have different lengths the vectors containing the subset of stations that are collocated, $\mathbf{v}^B_{A(A)}$ and $\mathbf{v}^A_{B(B)}$ (where the superscript denotes the comparison field), are the same length. Assuming that the discrepancies between $\mathbf{v}^B_{A(A)}$ and $\mathbf{v}^A_{B(B)}$ are due purely to differences in the reference frame, we can align the two velocity fields into a common reference frame by minimizing the residual velocities with respect to a reference frame correction model. While this can be generalized as a seven-parameter model, considering the rotation (three parameters), translation (three parameters), and scaling (one parameter) required to align the fields, we use a six-parameter estimator, which neglects scaling. In this case the differential velocities at collocated stations may be written as

$$\mathbf{v}^B_{A(A)} - \mathbf{v}^A_{B(B)} = \Delta\mathbf{v}_{A,B(A)} = \mathbf{R}_{A,B}\boldsymbol{\Omega}_{A,B(A)} + \mathbf{d}_{A,B(A)} \tag{A1}$$

where $\mathbf{R}_{A,B}$ contains the partial derivatives of the east and north velocities with respect to the Cartesian rotation vector, $\boldsymbol{\Omega}_{A,B(A)}$, and $\mathbf{d}_{A,B(A)}$ is the translation vector. We rewrite this equation as a single matrix expression by combining the terms on the right-hand side:

$$\Delta\mathbf{v}_{A,B(A)} = [\,\mathbf{R}_{A,B} \quad \mathbf{I}\,]\begin{bmatrix}\boldsymbol{\Omega}_{A,B(A)}\\ \mathbf{d}_{A,B(A)}\end{bmatrix} = \mathbf{G}_{A,B}\mathbf{m}_{A,B(A)}, \tag{A2}$$

where $\mathbf{I}$ is the identity matrix and $\mathbf{G}_{A,B}$ and $\mathbf{m}_{A,B(A)}$ represent the combined design matrices and model parameters, respectively. The combined transformation vector $\mathbf{m}_{A,B(A)}$ that minimizes the misfit between the collocated stations can be estimated in a classic least squares sense,

$$\mathbf{m}^{\text{est}}_{A,B(A)} = \left(\mathbf{G}^{\mathrm{T}}_{A,B}\mathbf{W}_{A,B}\mathbf{G}_{A,B}\right)^{-1}\mathbf{W}_{A,B}\mathbf{G}^{\mathrm{T}}_{A,B}\Delta\mathbf{v}_{A,B(A)}, \tag{A3}$$

where $\mathbf{W}_{A,B}$ represents a data weighting matrix composed of the data uncertainties. Solving for $\mathbf{m}^{\text{est}}_{A,B(A)}$ gives the transformation vector that will align the $\mathbf{V}_{B(B)}$ velocities into the A reference frame. The solution for the rotated velocities is

$$\mathbf{V}_{B(A)} = \mathbf{V}_{B(B)} + \mathbf{G}_{A,B}\mathbf{m}^{(est)}_{A,B(A)}. \tag{A4}$$

[74] Now for the case of three velocity fields $\mathbf{V}_{A(A)}$, $\mathbf{V}_{B(B)}$, and $\mathbf{V}_{C(C)}$. The subsets of overlapping velocities are between the A and B fields: $\mathbf{v}^B_{A(A)}$, $\mathbf{v}^A_{B(B)}$; between the A and C fields: $\mathbf{v}^C_{A(A)}$, $\mathbf{v}^A_{C(C)}$; and between the B and C fields: $\mathbf{v}^C_{B(B)}$, $\mathbf{v}^B_{C(C)}$. The difference in velocity between each set of collocated station can again be written in terms of a rotation vector that aligns the two reference frames,

$$\mathbf{v}^B_{A(A)} - \mathbf{v}^A_{B(B)} = \Delta\mathbf{v}_{A,B(A)} = \mathbf{G}_{A,B}\mathbf{m}_{A,B(A)}, \tag{A5a}$$

$$\mathbf{v}^C_{A(A)} - \mathbf{v}^A_{C(C)} = \Delta\mathbf{v}_{A,C(A)} = \mathbf{G}_{A,C}\mathbf{m}_{A,C(A)}, \tag{A5b}$$

$$\mathbf{v}^C_{B(B)} - \mathbf{v}^B_{C(C)} = \Delta\mathbf{v}_{B,C(B)} = \mathbf{G}_{B,C}\mathbf{m}_{B,C(B)}. \tag{A5c}$$

Each of these can be solved for the rotation vectors through a weighted least squares inversion:

$$\mathbf{m}^{\text{est}}_{A,B(A)} = \left(\mathbf{G}^{\mathrm{T}}_{A,B}\mathbf{W}_{A,B}\mathbf{G}_{A,B}\right)^{-1}\mathbf{W}_{A,B}\mathbf{G}^{\mathrm{T}}_{A,B}\Delta\mathbf{v}_{A,B(A)}, \tag{A6a}$$

$$\mathbf{m}^{\text{est}}_{A,C(B)} = \left(\mathbf{G}^{\mathrm{T}}_{A,C}\mathbf{W}_{A,C}\mathbf{R}_{A,C}\right)^{-1}\mathbf{W}_{A,C}\mathbf{G}^{\mathrm{T}}_{A,C}\Delta\mathbf{v}_{A,C(A)}, \tag{A6b}$$

$$\mathbf{m}^{\text{est}}_{B,C(B)} = \left(\mathbf{G}^{\mathrm{T}}_{B,C}\mathbf{W}_{B,C}\mathbf{G}_{B,C}\right)^{-1}\mathbf{W}_{B,C}\mathbf{G}^{\mathrm{T}}_{B,C}\Delta\mathbf{v}_{B,C(B)}. \tag{A6c}$$

This allows us to rotate both the B and C velocity fields into the A frame,

$$\mathbf{V}_{B(A)} = \mathbf{V}_{B(B)} + \mathbf{G}_{A,B}\mathbf{m}^{\text{est}}_{A,B(A)}, \tag{A7a}$$

$$\mathbf{V}_{C(A)} = \mathbf{V}_{C(C)} + \mathbf{G}_{A,C}\mathbf{m}^{\text{est}}_{A,C(A)}, \tag{A7b}$$

or the C velocity field into the B frame,

$$\mathbf{V}_{C(B)} = \mathbf{V}_{C(C)} + \mathbf{G}_{B,C}\mathbf{m}^{\text{est}}_{B,C(B)}. \tag{A7c}$$

[75] One of the most common and interesting cases is where the C field has stations collocated with the B field stations but not with the A field stations. In this case we can rotate the C velocities into the B frame then rotate the resulting set of velocities into the A frame using the rotation vector that was used to align the A and B frames,

$$\mathbf{V}_{C(A)} = \mathbf{V}_{C(B)} + \mathbf{G}_{B,C}\mathbf{m}^{\text{est}}_{A,B(A)} = \mathbf{V}_{C(C)} + \mathbf{G}_{B,C}\left(\mathbf{m}^{\text{est}}_{B,C(B)} + \mathbf{m}^{\text{est}}_{A,B(A)}\right) \tag{A8}$$

where the rotation vectors from the necessary transforms are simply summed. For the more general case where the path of overlaps to transform velocities from a frame i to a frame j through N transformations the total fully aligned velocity can be written as:

$$\mathbf{V}_{i(j)} = \mathbf{V}_{i(i)} + \mathbf{G}_{i,j}\sum_{k=1}^{N}\mathbf{m}^{\text{est}}_{k-1,k(k-1)} \tag{A9}$$

[76] For any number of velocity fields, each of which shares a subset of stations with at least one of the other fields, there exists a "connection tree" defining the collocated stations that tie each field to another. In the case described by equation (A7), velocity field C is connected to field A via field B. By establishing this connection tree, all of the fields can be rotated such that station velocities are expressed in a common reference frame. This reference frame can either be the existing reference frame of one of

	Apel, 2006	Calais, 2006	Kogan, 2000 (EU)	Kogan, 2001 (NAM)	Shen, 2005	Wang, 2001	Zhang, 2004	GEONET 1997–2000
Apel, 2006		39	14	10	0	23	0	19
Calais, 2006	0.35		4	1	45	114	62	1
Kogan, 2000 (EU)	0.87	---		2	0	6	0	0
Kogan, 2000 (NAM)	1.14	---	---		0	1	0	0
Shen, 2005	---	0.35	---	---		78	224	0
Wang, 2001	0.37	0.70	---	---	0.69		119	2
Zhang, 2004	---	0.70	---	---	0.63	0.58		0
GEONET 1997–2000	0.42	---	---	---	---	---	---	

Figure A1. Velocity field combination matrix used in model JB1. The entries in the upper triangular part of the matrix show the number of collocated stations between the velocity fields, while the lower triangular entries give the mean residual velocity magnitude between the rotated and reference fields. Boxes containing gray diagonal lines indicate velocity field pairs that were not combined because of the number of collocated stations; we only rotated fields sharing 10 or more stations. Not all stations for each field were used in the block modeling.

the fields, or an arbitrary point on the globe. To define the latter, we assume that some subset of stations in the combined velocity field, $\mathbf{v}_{ST(j)}$ represents a stable region, and we seek to minimize the velocities of these stations. We do so by again finding the best fitting rotation vector that is a solution to the equation

$$0 = \mathbf{v}_{ST(ST)} = \mathbf{v}_{ST(j)} + \mathbf{m}_{ST,j}\mathbf{G}^{\text{est}}_{ST,j(ST)}. \tag{A10}$$

We then rotate all vectors in the combined velocity field into the stable reference frame *ST*, resulting in a combined field expressed relative to an arbitrary position that is assumed stable.

A2. Application: A Eurasian-Pacific GPS Velocity Field

[77] We apply the reference frame alignment scheme to several recently published GPS data sets that characterize the contemporary motion of Eurasia and the western Pacific rim. We combine our GEONET velocity field with data from northeast Asia and the Pacific plate [*Kogan et al.*, 2000; *Apel et al.*, 2006], east Asia [*Shen et al.*, 2000; *Calais et al.*, 2006], greater China [*Wang et al.*, 2001], and the Tibetan plateau [*Zhang et al.*, 2004; *Calais et al.*, 2006], and rotate all velocities into the reference frame used by *Apel et al.* [2006].

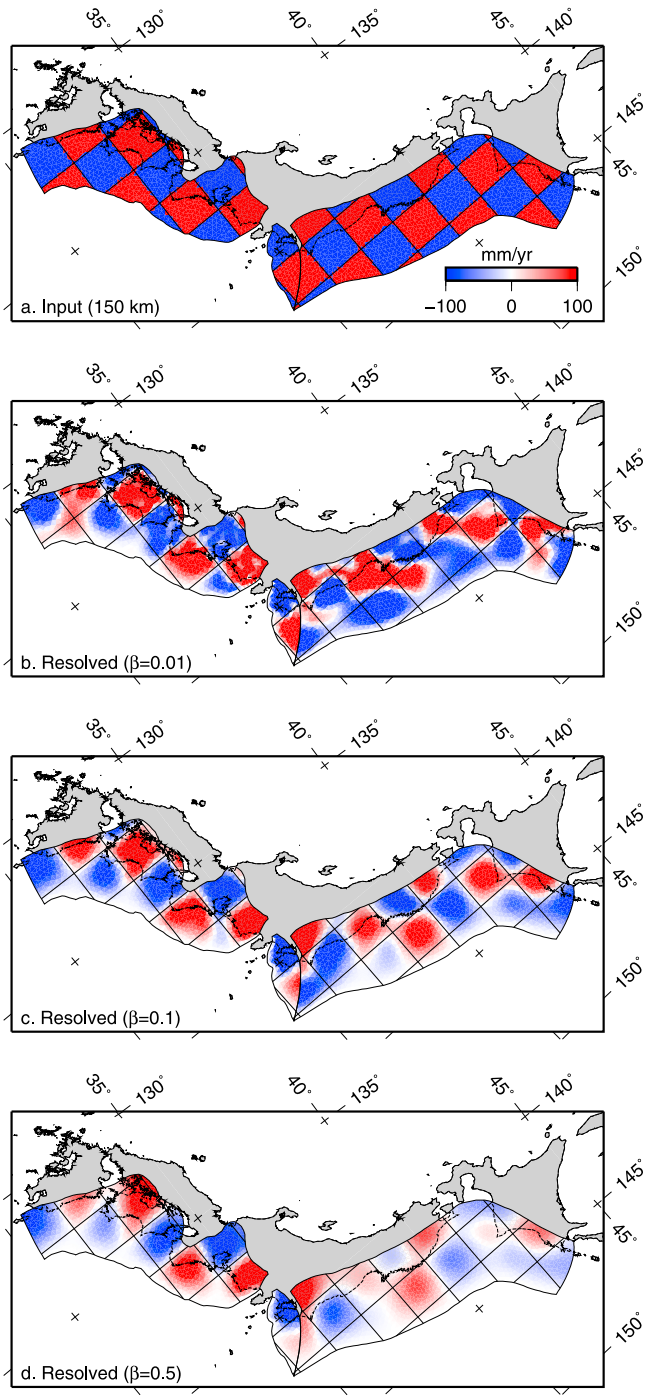

Figure B1. Input and estimated slip distributions for "checkerboard" resolution tests. (a) Input slip distribution, with −100 and 100 mm/yr of dip slip applied to alternating patches approximately 150 × 150 km in size on the discretized subduction zone geometries. We use this slip distribution to calculate a forward model of predicted surface velocities at GEONET GPS station. (b–d) Slip distribution estimated from the inversion of the synthetic velocity field to which we applied Gaussian noise with mean and standard deviation equal to those of the formal uncertainties on the real GEONET data. For Figures B1b–B1d, the results are shown with a different weighting value, β, of the smoothing operator.

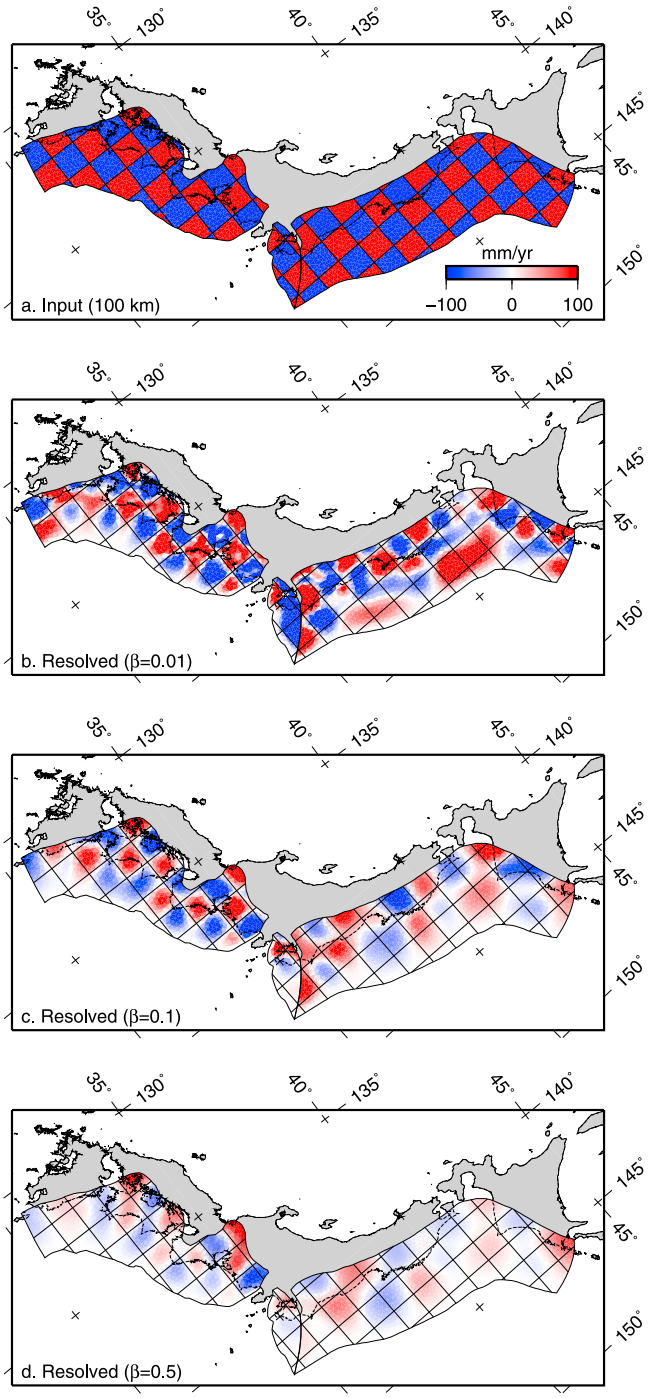

Figure B2. Same as Figure B1 except results of the checkerboard test for patches approximately 100 × 100 km in size.

[78] Figure A1 shows the number of collocated stations, as well as the goodness of fit of each velocity field combination.

Appendix B: Resolution Tests for Subduction Zone Slip Distributions

[79] To assess how well the GEONET GPS data can resolve spatial variations in the interseismic slip distribution on the subduction zone interfaces that we model using triangular dislocation elements, we use so-called "checkerboard" tests. We apply binary slip patterns, arranged in a checkerboard fashion, to the discretized plate boundary geometry, calculate the surface velocities at GEONET station coordinates that would result from the simulated slip pattern, add Gaussian noise to these velocities, and invert them for slip on the interfaces, examining the degree to which we can recover the input checkerboard slip

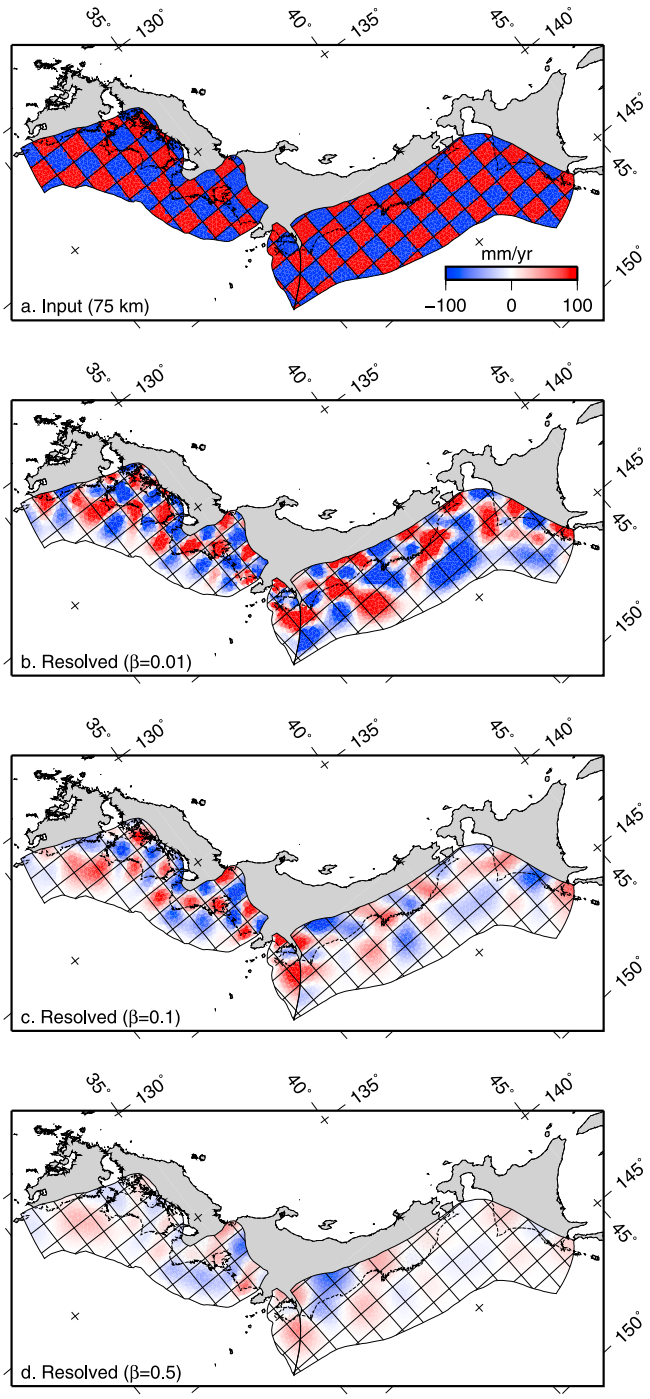

Figure B3. Same as Figure B1 except results of the checkerboard test for patches approximately 75 × 75 km in size.

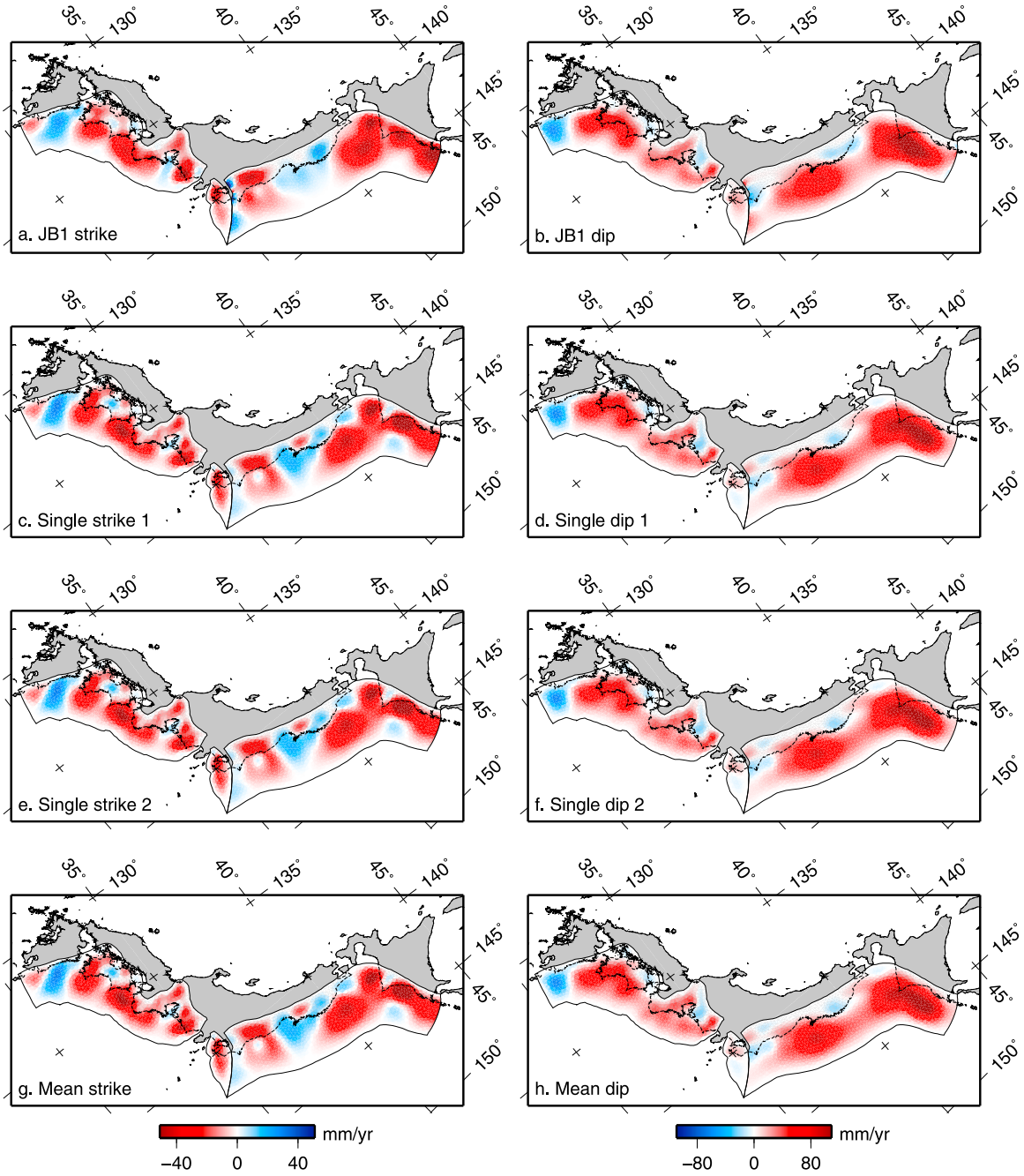

Figure B4. Recovery tests of the JB1 triangular slip distribution. We use the velocity field predicted by the slip on triangular dislocation elements for JB1, add Gaussian noise with mean and standard deviation similar to those of the formal uncertainties on GEONET stations, and invert using the same smoothing parameters as those of JB1. (a and b) The strike-slip and dip-slip distribution from JB1, (c, d, e, and f) the slip recovered from inversion of the velocity field subject to two instances of random noise, and (g and h) the mean slip distribution averaged over 25 trials, each with a different instance of noise applied to the constraining velocity field.

distribution. We test square checkerboard cells of approximately 150, 100, and 75 km in linear dimension to which an alternating pattern of −100 and 100 mm/yr of dip slip is applied. Such slip magnitudes result in predicted synthetic surface velocities on the order of 10 mm/yr, comparable to the mean interseismic speed of interseismic GEONET stations (∼20 mm/yr). We apply Gaussian noise to the synthetic velocity field, characterized by mean and standard deviation values equal to those of the formal uncertainties on the GEONET observations. We then invert the noisy velocity field for slip on the subduction thrusts, subject to the smoothing constraints described in section 2. We examine the results for inversions subject to several different values of the smoothing parameter β.

[80] The results of the checkerboard tests are shown in Figures B1–B3. We find that using a smoothing weighting

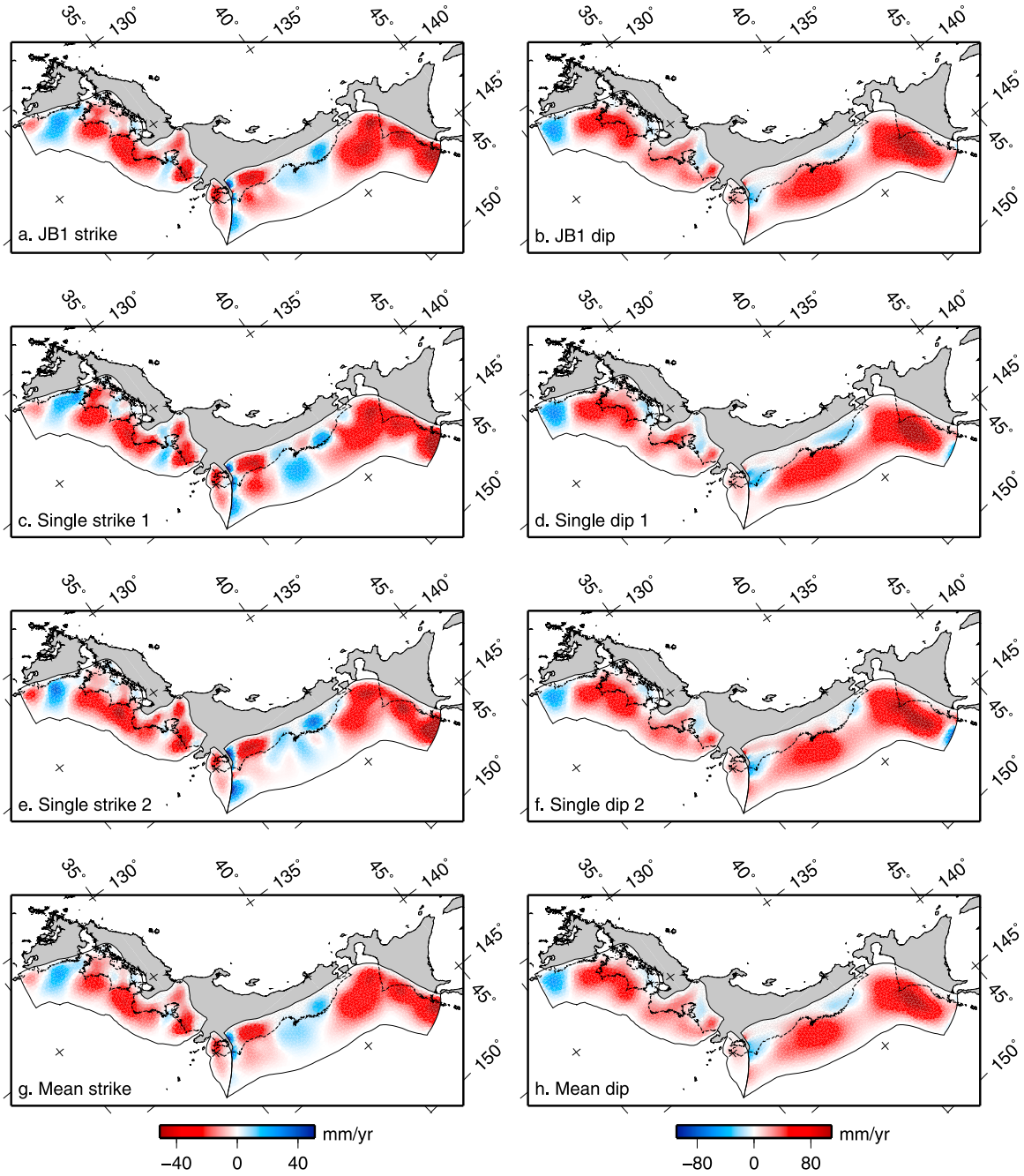

Figure B5. Same as Figure B4 except recovery tests of the JB1 triangular slip distribution, using the total velocity field predicted by model JB1, subject to instances of Gaussian noise, as described for Figure B4. Rather than inverting only for the slip distribution, we use the noisy model velocity field as the constraint for full block model runs and here show the slip distributions estimated by these simulations.

parameter of $\beta = 0.1$, we can recover the input pattern of slip applied to grid cells approximately 150 km on a side along all three subduction zones (Figure B1c), but for smaller checkerboard grid cells, the pattern can only be resolved on portions of the subduction zone that lie beneath the coastline, where geodetic stations are located (Figures B2c and B3c); in all cases, the slip distribution on the Nankai subduction zone is best recovered in the inversion owing to the large proportion of the fault interface that extends beneath land.

[81] In addition to these synthetic "checkerboard" tests, we are interested in evaluating our confidence in features of the slip distribution resolved in model JB1. To do so, we follow a similar method as that employed for the checkerboard tests. We use the estimated velocity field due only to slip on the triangulated surfaces (i.e., the field of Figure 4f), add Gaussian noise with a distribution similar to that of the uncertainties on the GEONET observations, and invert this noisy velocity field for subduction zone slip, subject to the same smoothing constraints that we applied in the original

JB1 inversion. We find that the major features of the slip distribution that we discuss in section 5.7 can be resolved using this method, giving us confidence that they are more likely to reflect variations in coupling rather than numerical artifacts of the inversion (Figure B4). We note that the features of the dip-slip distribution are recovered better than those of the strike-slip distribution; individual instances of random noise introduce patterns of strike slip that vary from those of JB1, but the average slip distribution recovered from inverting 25 instances of random noise yields a distribution very similar to that of JB1. One exception is the near-trench strike-slip distribution offshore northern Honshu: whereas JB1 shows a patch of left-lateral slip across nearly the entire width of the fault around 40°N, such slip is limited to depth in the average recovered distribution.

[82] We also test the resolution of the triangular element slip distribution by using the total velocity field predicted by JB1, adding noise, and inverting using the full block model theory (Figure B5). By doing this, we examine how the solution is modulated by the subduction zones as well as the other faults comprising the block geometry.

[83] **Acknowledgments.** We thank Wayne Thatcher, an anonymous referee, and the Associate Editor for thorough, thoughtful reviews that helped to improve the paper. We thank the Geographical Survey Institute of the Government of Japan for making GEONET data available. We used the open source meshing program Gmsh [*Geuzaine and Remacle*, 2009] to construct the triangulated fault zone surfaces. Most figures were prepared using the Generic Mapping Tools [*Wessel and Smith*, 1998]. This research is supported by funding from Harvard University.

References

Apel, E. V., R. Burgmann, G. Steblov, N. Vasilenko, R. King, and A. Prytkov (2006), Independent active microplate tectonics of northeast Asia from GPS velocities and block modeling, *Geophys. Res. Lett.*, *33*, L11303, doi:10.1029/2006GL026077.

Azuma, T., K. Shimokawa, A. Sangawa, Y. Sugiyama, T. Kuwabara, K. Okumura, H. Kurosawa, and A. Miwa (2003), Paleoseismological study on the Kuromatsunai fault zone in southwestern Hokkaido, northern Japan (in Japanese with English abstract), *Annu. Rep. Active Fault Paleoearthquake Res.*, *3*, 1–22.

Azuma, T., et al. (2004), Timing of faulting events and subsurface structures of the Kuromatsunai-teichi fault zone, southwestern Hokkaido, Japan (in Japanese with English abstract), *Annu. Rep. Active Fault Paleoearthquake Res.*, *4*, 45–64.

Beck, M. (1991), Coastwise transport reconsidered: Lateral displacements in oblique subduction zones, and tectonic consequences, *Phys. Earth Planet. Inter.*, *68*(1–2), 1–8, doi:10.1016/0031-9201(91)90002-Y.

Bevis, M., and S. J. Martel (2001), Oblique plate convergence and interseismic strain accumulation, *Geochem. Geophys. Geosyst.*, *2*(8), 1033, doi:10.1029/2000GC000125.

Bird, P. (2003), An updated digital model of plate boundaries, *Geochem. Geophys. Geosyst.*, *4*(3), 1027, doi:10.1029/2001GC000252.

Bürgmann, R., M. G. Kogan, G. M. Steblov, G. Hilley, V. E. Levin, and E. Apel (2005), Interseismic coupling and asperity distribution along the Kamchatka subduction zone, *J. Geophys. Res.*, *110*, B07405, doi:10.1029/2005JB003648.

Calais, E., L. Dong, M. Wang, Z. Shen, and M. Vergnolle (2006), Continental deformation in Asia from a combined GPS solution, *Geophys. Res. Lett.*, *33*, L24319, doi:10.1029/2006GL028433.

Chapman, M. E., and S. C. Solomon (1976), North American-Eurasian plate boundary in northeast Asia, *J. Geophys. Res.*, *81*(5), 921–930, doi:10.1029/JB081i005p00921.

Cook, D. B., K. Fujita, and C. A. McMullen (1986), Present-day plate interactions in northeast Asia: North American, Eurasian, and Okhotsk plates, *J. Geodyn.*, *6*(1–4), 33–51, doi:10.1016/0264-3707(86)90031-1.

DeMets, C. (1992a), Oblique convergence and deformation along the Kuril and Japan trenches, *J. Geophys. Res.*, *97*(B12), 17,615–17,625, doi:10.1029/92JB01306.

DeMets, C. (1992b), A test of present-day plate geometries for northeast Asia and Japan, *J. Geophys. Res.*, *97*(B12), 17,627–17,635, doi:10.1029/92JB01335.

DeMets, C., R. G. Gordon, D. F. Argus, and S. Stein (1990), Current plate motions, *Geophys. J. Int.*, *101*(2), 425–478, doi:10.1111/j.1365-246X.1990.tb06579.x.

Feigl, K. L., et al. (1993), Space geodetic measurement of crustal deformation in central and southern California, *J. Geophys. Res.*, *98*(B12), 21,677–21,712, doi:10.1029/93JB02405.

Fitch, T. J. (1972), Plate convergence, transcurrent faults, and internal deformation adjacent to southeast Asia and the western Pacific, *J. Geophys. Res.*, *77*(23), 4432–4460, doi:10.1029/JB077i023p04432.

Fournier, M., J. Angelier, J. Cadet, and O. Fabbri (2001), Regional seismicity and on land deformation in the Ryukyu arc- Implications for the kinematics of opening of the Okinawa Trough, *J. Geophys. Res.*, *106*(B7), 13,751–13,768, doi:10.1029/2001JB900010.

Fukao, Y., and M. Furumoto (1975), Mechanism of large earthquakes along the eastern margin of the Japan sea, *Tectonophysics*, *26*(3–4), 247–266, doi:10.1016/0040-1951(75)90093-1.

Furuse, N., and Y. Kono (2003), Slab residual gravity anomaly: Gravity reduction due to subducting plates beneath the Japanese Islands, *J. Geodyn.*, *36*, 497–514, doi:10.1016/S0264-3707(03)00062-0.

Geuzaine, C., and J.-F. Remacle (2009), Gmsh: A three-dimensional finite element mesh generator with built-in pre- and post-processing facilities, *Int. J. Numer. Methods Eng.*, *79*(11), 1309–1331, doi:10.1002/nme.2579.

Gomez, F., et al. (2007), Global Positioning System measurements of strain accumulation and slip transfer through the restraining bend along the Dead Sea fault system in Lebanon, *Geophys. J. Int.*, *168*(3), 1021–1028, doi:10.1111/j.1365-246X.2006.03328.x.

Gutscher, M. A., and S. Lallemand (1999), Birth of a major strike-slip fault in SW Japan, *Terra Nova*, *11*(5), 203–209, doi:10.1046/j.1365-3121.1999.00247.x.

Hager, B. H., R. W. King, and M. H. Murray (1991), Measurement of Crustal Deformation Using the Global Positioning System, *Annu. Rev. Earth Planet. Sci.*, *19*(1), 351–382, doi:10.1146/annurev.ea.19.050191.002031.

Hashimoto, M., and D. D. Jackson (1993), Plate tectonics and crustal deformation around the Japanese islands, *J. Geophys. Res.*, *98*(B9), 16,149–16,166, doi:10.1029/93JB00444.

Hashimoto, M., S. Miyazaki, and D. D. Jackson (2000), A block-fault model for deformation of the Japanese Islands derived from continuous GPS observation, *Earth Planets Space*, *52*, 1095–1100.

Heki, K., and S. Miyazaki (2001), Plate convergence and long-term crustal deformation in central Japan, *Geophys. Res. Lett.*, *28*(12), 2313–2316, doi:10.1029/2000GL012537.

Heki, K., Y. Takahashi, and T. Kondo (1990), Contraction of northeastern Japan: Evidence from horizontal displacement of a Japanese station in global very long baseline interferometry networks, *Tectonophysics*, *181*(1–4), 113–122, doi:10.1016/0040-1951(90)90011-V.

Heki, K., S. Miyazaki, and H. Tsuji (1997), Silent fault slip following an interplate thrust earthquake at the Japan Trench, *Nature*, *386*, 595–597, doi:10.1038/386595a0.

Heki, K., S. Miyazaki, H. Takahashi, M. Kasahara, F. Kimata, S. Miura, N. Vasilenko, A. Ivashchenko, and K. An (1999), The Amurian Plate motion and current plate kinematics in eastern Asia, *J. Geophys. Res.*, *104*(B12), 29,147–29,155, doi:10.1029/1999JB900295.

Hetland, E. A., M. Simons, and E. M. Dunham (2010), Postseismic and interseismic fault creep I: Model description, *Geophys. J. Int.*, in press.

Hirose, F., J. Nakajima, and A. Hasegawa (2008), Three-dimensional seismic velocity structure and configuration of the Philippine Sea slab in southwestern Japan estimated by double-difference tomography, *J. Geophys. Res.*, *113*, B09315, doi:10.1029/2007JB005274.

Hirose, H., K. Hirahara, F. Kimata, N. Fujii, and S. Miyazaki (1999), A slow thrust slip even following the two 1996 Hyuganada earthquakes beneath the Bungo Channel, southwest Japan, *Geophys. Res. Lett.*, *26*(21), 3237–3240, doi:10.1029/1999GL010999.

Hyndman, R. D., K. Wang, and M. Yamano (1995), Thermal constraints on the seismogenic portion of the southwestern Japan subduction thrust, *J. Geophys. Res.*, *100*(B8), 15,373–15,392, doi:10.1029/95JB00153.

Hyodo, M., and K. Hirahara (2003), A viscoelastic model of interseismic strain concentration in Niigata-Kobe Tectonic Zone of central Japan, *Earth Planets Space*, *55*, 667–675.

Iio, Y., T. Sagiya, Y. Kobayashi, and I. Shiozaki (2002), Water-weakened lower crust and its role in the concentrated deformation in the Japanese Islands, *Earth Planet. Sci. Lett.*, *203*, 245–253, doi:10.1016/S0012-821X(02)00879-8.

Ishida, M. (1992), Geometry and Relative Motion of the Philippine Sea plate and Pacific plate beneath the Kanto-Tokai District, *J. Geophys. Res.*, *97*(B1), 489–513, doi:10.1029/91JB02567.

Ito, T., T. Ikawa, S. Yamakita, and T. Maeda (1996), Gently north-dipping Median Tectonic Line (MTL) revealed by recent seismic reflection studies, southwest Japan, *Tectonophysics*, *264*(1–4), 51–63, doi:10.1016/S0040-1951(96)00117-5.

Ito, T., S. Yoshioka, and S. Miyazaki (1999), Interplate coupling in southwest Japan deduced from inversion analysis of GPS data, *Phys. Earth Planet. Inter.*, *115*(1), 17–34, doi:10.1016/S0031-9201(99)00063-1.

Ito, T., S. Yoshioka, and S. Miyazaki (2000), Interplate coupling in northeast Japan deduced from inversion analysis of GPS data, *Earth Planet. Sci. Lett.*, *176*(1), 117–130, doi:10.1016/S0012-821X(99)00316-7.

Itoh, Y., T. Ishiyama, and Y. Nagasaki (2005), Deformation mode in the frontal edge of an arc-arc collision zone: Subsurface geology, active faults and paleomagnetism in southern central Hokkaido, Japan, *Tectonophysics*, *395*(1–2), 81–97, doi:10.1016/j.tecto.2004.09.003.

Kanaori, Y. (1990), Late mesozoic-cenozoic strike-slip and block rotation in the inner belt of southwest Japan, *Tectonophysics*, *177*(4), 381–399, doi:10.1016/0040-1951(90)90397-Q.

Kanaori, Y., Y. Endo, K. Yairi, and S.-I. Kawakami (1990), A nested fault system with block rotation caused by left-lateral faulting: The Neodani and Atera faults, central Japan, *Tectonophysics*, *177*(4), 401–418, doi:10.1016/0040-1951(90)90398-R.

Kanaori, Y., S. Kawakami, and K. Yairi (1991), Space-time distribution patterns of destructive earthquakes in the inner belt of central Japan: Activity intervals and locations of earthquakes, *Eng. Geol.*, *31*, 209–230, doi:10.1016/0013-7952(91)90009-A.

Kanaori, Y., S. Kawakami, and K. Yairi (1992), The block structure and Quaternary strike-slip block rotation of central Japan, *Tectonics*, *11*(1), 47–56, doi:10.1029/91TC01511.

Kanaori, Y., S. Kawakami, and K. Yairi (1993), Space-time correlations between inland earthquakes in central Japan and great offshore earthquakes along the Nankai trough: Implication for destructive earthquake prediction, *Eng. Geol.*, *33*, 289–303, doi:10.1016/0013-7952(93)90031-7.

Kanaori, Y., S. Kawakami, and K. Yairi (1994), Seismotectonics of the Median Tectonic Line in southwest Japan: Implications for coupling among major fault systems, *Pure Appl. Geophys.*, *142*(3–4), 589–607, doi:10.1007/BF00876056.

Kaneda, H., and A. Okada (2008), Long-term seismic behavior of a fault involved in a multiple-fault rupture: Insights from tectonic geomorphology along the Neodani Fault, central Japan, *Bull. Seismol. Soc. Am.*, *98*(5), 2170–2190, doi:10.1785/0120070204.

Kato, A., E. Kurashimo, N. Hirata, S. Sakai, T. Iwasaki, and T. Kanazawa (2005), Imaging the source region of the 2004 mid-Niigata prefecture earthquake and the evolution of a seismogenic thrust-related fold, *Geophys. Res. Lett.*, *32*(7), L07307, doi:10.1029/2005GL022366.

Kato, N., H. Sato, M. Orito, K. Hirakawa, Y. Ikeda, and T. Ito (2004), Has the plate boundary shifted from central Hokkaido to the eastern part of the Sea of Japan?, *Tectonophysics*, *388*(1–4), 75–84, doi:10.1016/j.tecto.2004.04.030.

Kendrick, E., M. Bevis, R. Smalley Jr., and B. Brooks (2001), An integrated crustal velocity field for the central Andes, *Geochem. Geophys. Geosyst.*, *2*(11), 1066, doi:10.1029/2001GC000191.

Kimura, G. (1986), Oblique subduction and collision: Forearc tectonics of the Kuril Arc, *Geology*, *14*(5), 404–407, doi:10.1130/0091-7613(1986)14<404:OSACFT>2.0.CO;2.

Kimura, G., and K. Tamaki (1986), Collision, rotation, and back-arc spreading in the region of the Okhotsk and Japan seas, *Tectonics*, *5*(3), 389–401, doi:10.1029/TC005i003p00389.

Kodaira, S., et al. (2006), A cause of rupture segmentation and synchronization in the Nankai trough revealed by seismic imaging and numerical simulation, *J. Geophys. Res.*, *111*, B09301, doi:10.1029/2005JB004030.

Kogan, M. G., G. M. Steblov, R. W. King, T. A. Herring, D. I. Frolov, S. G. Egorov, V. Y. Levin, A. Lerner-Lam, and A. Jones (2000), Geodetic constraints on the rigidity and relative motion of Eurasia and North America, *Geophys. Res. Lett.*, *27*(14), 2041–2044, doi:10.1029/2000GL011422.

Kusunoki, K., and G. Kimura (1998), Collision and extrusion at the Kuril-Japan arc junction, *Tectonics*, *17*(6), 843–858, doi:10.1029/98TC02699.

Le Pichon, X., S. Mazzotti, P. Henry, and M. Hashimoto (1998), Deformation of the Japanese Islands and seismic coupling: An interpretation based on GSI permanent GPS observations, *Geophys. J. Int.*, *134*(2), 501–514, doi:10.1046/j.1365-246x.1998.00595.x.

Maerten, F., P. Resor, D. D. Pollard, and L. Maerten (2005), Inverting for slip on three-dimensional fault surfaces using angular dislocations, *Bull. Seismol. Soc. Am.*, *95*(5), 1654–1665, doi:10.1785/0120030181.

Matsu'ura, M., D. D. Jackson, and A. Cheng (1986), Dislocation model for aseismic crustal deformation at Hollister, California, *J. Geophys. Res.*, *91*(B12), 12,661–12,674, doi:10.1029/JB091iB12p12661.

Matsuzaki, M., S. Kawakami, Y. Kanaori, and K. Yairi (1996), Modeling of the interaction between destructive inland earthquakes and large off coast earthquakes in central and south-west Japan, *Eng. Geol.*, *43*(2–3), 169–176, doi:10.1016/0013-7952(96)00058-0.

Mazzotti, S., X. Le Pichon, P. Henry, and S. Miyazaki (2000), Full interseismic locking of the Nankai and Japan-west Kurile subduction zones: An analysis of uniform elastic strain accumulation in Japan constrained by permanent GPS, *J. Geophys. Res.*, *105*(B6), 13,159–13,177, doi:10.1029/2000JB900060.

Mazzotti, S., P. Henry, and X. Le Pichon (2001), Transient and permanent deformation of central Japan estimated by GPS: 2. Strain partitioning and arc-arc collision, *Earth Planet. Sci. Lett.*, *184*(2), 455–469, doi:10.1016/S0012-821X(00)00336-8.

McCaffrey, R. (1992), Oblique plate convergence, slip vectors, and forearc deformation, *J. Geophys. Res.*, *97*(B6), 8905–8915, doi:10.1029/92JB00483.

McCaffrey, R. (1993), On the role of the upper plate in great subduction zone earthquakes, *J. Geophys. Res.*, *98*(B7), 11,953–11,966, doi:10.1029/93JB00445.

McCaffrey, R. (1996), Estimates of modern arc-parallel strain rates in fore arcs, *Geology*, *24*(1), 27–30, doi:10.1130/0091-7613(1996)024<0027:EOMAPS>2.3.CO;2.

McCaffrey, R. (2002), Crustal block rotations and plate coupling, in *Plate Boundary Zones*, *Geodyn. Ser.*, vol. 30>, edited by S. Stein and J. T. Freymueller, pp. 101–122, AGU, Washington, D. C.

McCaffrey, R., A. Qamar, R. King, R. Wells, G. Khazaradze, C. Williams, C. Stevens, J. Vollick, and P. Zwick (2007), Fault locking, block rotation and crustal deformation in the Pacific Northwest, *Geophys. J. Int.*, *169*(3), 1315–1340, doi:10.1111/j.1365-246X.2007.03371.x.

McClusky, S., et al. (2000), Global Positioning System constraints on plate kinematics and dynamics in the eastern Mediterranean and Caucasus, *J. Geophys. Res.*, *105*(B3), 5695–5720.

Meade, B. J., and B. H. Hager (2005), Block models of crustal motion in southern California constrained by GPS measurements, *J. Geophys. Res.*, *110*, B03403, doi:10.1029/2004JB003209.

Meade, B. J., and J. P. Loveless (2009), Block modeling with multiple fault network geometries and a linear elastic coupling estimator in spherical coordinates, *Bull. Seismol. Soc. Am.*, *99*(6), 3124–3139.

Miura, S., T. Sato, K. Tachibana, Y. Satake, and A. Hasegawa (2002), Strain accumulation in and around the Ou Backbone Range, northeastern Japan as observed by a dense GPS network, *Earth Planets Space*, *54*, 1071–1076.

Miura, S., T. Sato, A. Hasegawa, Y. Suwa, K. Tachibana, and S. Yui (2004), Strain concentration zone along the volcanic front derived by GPS observations in NE Japan arc, *Earth Planets Space*, *56*(12), 1347–1355.

Miyazaki, S., and K. Heki (2001), Crustal velocity field of southwest Japan: Subduction and arc-arc collision, *J. Geophys. Res.*, *106*(B3), 4305–4326, doi:10.1029/2000JB900312.

Miyazaki, S., and K. M. Larson (2008), Coseismic and early postseismic slip for the 2003 Tokachi-oki earthquake sequence inferred from GPS data, *Geophys. Res. Lett.*, *35*(4), L04302, doi:10.1029/2007GL032309.

Mochizuki, K., T. Yamada, M. Shinohara, Y. Yamanaka, and T. Kanazawa (2008), Weak Interplate Coupling by Seamounts and Repeating M ~ 7 Earthquakes, *Science*, *321*(5893), 1194–1197, doi:10.1126/science.1160250.

Nakamura, K. (1983), Possible nascent trench along the eastern Japan Sea as the convergent boundary between Eurasian and North American plates, *Bull. Earthquake Res. Inst. Univ. Tokyo*, *58*(3), 711–722.

Nakamura, M. (2004), Crustal deformation in the central and southern Ryukyu Arc estimated from GPS data, *Earth Planet. Sci. Lett.*, *217*(3–4), 389–398, doi:10.1016/S0012-821X(03)00604-6.

Nakata, T., and T. Imaizumi (Eds.) (2002), Digital active fault map of Japan, Univ. of Tokyo Press, Tokyo.

Nishimura, S., and M. Hashimoto (2006), A model with rigid rotations and slip deficits for the GPS-derived velocity field in Southwest Japan, *Tectonophysics*, *421*(3–4), 187–207, doi:10.1016/j.tecto.2006.04.017.

Nishimura, S., M. Hashimoto, and M. Ando (2004), A rigid block rotation model for the GPS derived velocity field along the Ryukyu arc, *Phys. Earth Planet. Inter.*, *142*(3–4), 185–203, doi:10.1016/j.pepi.2003.12.014.

Nishimura, T., et al. (2000), Distribution of seismic coupling on the subducting plate boundary in northeastern Japan inferred from GPS observations, *Tectonophysics*, *323*(3–4), 217–238, doi:10.1016/S0040-1951(00)00108-6.

Nishimura, T., T. Hirasawa, S. Miyazaki, T. Sagiya, T. Tada, S. Miura, and K. Tanaka (2004), Temporal change of interplate coupling in northeastern Japan during 1995–2002 estimated from continuous GPS observations, *Geophys. J. Int.*, *157*(2), 901–916, doi:10.1111/j.1365-246X.2004.02159.x.

Nishimura, T., T. Sagiya, and R. S. Stein (2007), Crustal block kinematics and seismic potential of the northernmost Philippine Sea plate and Izu microplate, central Japan, inferred from GPS and leveling data, *J. Geophys. Res.*, *112*, B05414, doi:10.1029/2005JB004102.

Nyst, M., T. Nishimura, F. Pollitz, and W. Thatcher (2006), The 1923 Kanto earthquake reevaluated using a newly augmented geodetic data set, *J. Geophys. Res.*, *111*(B11), B11306, doi:10.1029/2005JB003628.

Okumura, K. (2001), Paleoseismology of the Itoigawa-Shizuoka tectonic line in central Japan, *J. Seismol.*, *5*(3), 411–431, doi:10.1023/A:1011483811145.

Okamura, Y., K. Satake, K. Ikehara, A. Takeuchi, and K. Arai (2005), Paleoseismology of deep-sea faults based on marine surveys of northern Okushiri ridge in the Japan Sea, *J. Geophys. Res.*, *110*, B09105, doi:10.1029/2004JB003135.

Ozawa, S., M. Murakami, and T. Tada (2001), Time-dependent inversion study of the slow thrust event in the Nankai trough subduction zone, southwestern Japan, *J. Geophys. Res.*, *106*(B1), 787–802, doi:10.1029/2000JB900317.

Ozawa, S., M. Kaidzu, M. Murakami, T. Imakiire, and Y. Hatanaka (2004), Coseismic and postseismic crustal deformation after the Mw 8 Tokachi-oki earthquake in Japan, *Earth Planets Space*, *56*(7), 675–680.

Reilinger, R., et al. (2006), GPS constraints on continental deformation in the Africa-Arabia-Eurasia continental collision zone and implications for the dynamics of plate interactions, *J. Geophys. Res.*, *111*, B05411, doi:10.1029/2005JB004051.

Sagiya, T. (1999), Interplate coupling in the Tokai district, central Japan, deduced from continuous GPS data, *Geophys. Res. Lett.*, *26*(15), 2315–2318, doi:10.1029/1999GL900511.

Sagiya, T. (2004), A decade of GEONET: 1994–2003-The continuous GPS observation in Japan and its impact on earthquake studies, *Earth Planets Space*, *56*(8), XXIX–XLI.

Sagiya, T., S. Miyazaki, and T. Tada (2000), Continuous GPS array and present-day crustal deformation of Japan, *Pure Appl. Geophys.*, *157*(11–12), 2303–2322.

Sagiya, T., T. Nishimura, Y. Iio, and T. Tada (2002), Crustal deformation around the northern and central Itoigawa-Shizuoka Tectonic Line, *Earth Planets Space*, *54*(11), 1059–1063.

Sagiya, T., T. Nishimura, and Y. Iio (2004), Heterogeneous crustal deformation along the central-northern Itoigawa-Shizuoka Tectonic Line Fault System, central Japan, *Earth Planets Space*, *56*(12), 1247–1252.

Sato, H., et al. (2005), Earthquake source fault beneath Tokyo, *Science*, *309*(5733), 462–464, doi:10.1126/science.1110489.

Savage, J. (2000), Viscoelastic-coupling model for the earthquake cycle driven from below, *J. Geophys. Res.*, *105*(B11), 25,525–25,532, doi:10.1029/2000JB900276.

Savage, J., and W. H. Prescott (1978), Asthenosphere readjustment and the earthquake cycle, *J. Geophys. Res.*, *83*(B7), 3369–3376, doi:10.1029/JB083iB07p03369.

Savage, J. C. (1983), A dislocation model of strain accumulation and release at a subduction zone, *J. Geophys. Res.*, *88*(B6), 4984–4996, doi:10.1029/JB088iB06p04984.

Savage, J. C., and R. O. Burford (1973), Geodetic determination of relative plate motion in central California, *J. Geophys. Res.*, *78*(5), 832–845, doi:10.1029/JB078i005p00832.

Semmane, F., F. Cotton, and M. Campillo (2005), The 2000 Tottori earthquake: A shallow earthquake with no surface rupture and slip properties controlled by depth, *J. Geophys. Res.*, *110*(B3), B03306, doi:10.1029/2004JB003194.

Seno, T. (1985), Is northern Honshu a microplate?, *Tectonophysics*, *115*(3–4), 177–196, doi:10.1016/0040-1951(85)90138-6.

Seno, T. (2005), The September 5, 2004 off the Kii Peninsula earthquakes as a composition of bending and collision, *Earth Planets Space*, *57*(4), 327–332.

Seno, T., and T. Takano (1989), Seismotectonics at the trench-trench-trench triple junction off central Honshu, *Pure Appl. Geophys.*, *129*(1–2), 27–40, doi:10.1007/BF00874623.

Seno, T., S. Stein, and A. E. Gripp (1993), A model for the motion of the Philippine Sea Plate consistent with NUVEL-1 and geologic data, *J. Geophys. Res.*, *98*(B10), 17,941–17,948, doi:10.1029/93JB00782.

Seno, T., T. Sakurai, and S. Stein (1996), Can the Okhotsk plate be discriminated from the North American plate?, *J. Geophys. Res.*, *101*(B5), 11,305–11,315, doi:10.1029/96JB00532.

Shelly, D., G. Beroza, S. Ide, and S. Nakamula (2006), Low-frequency earthquakes in Shikoku, Japan, and their relationship to episodic tremor and slip, *Nature*, *442*(7099), 188–191, doi:10.1038/nature04931.

Shen, Z. K., C. K. Zhao, A. Yin, Y. X. Li, D. D. Jackson, P. Fang, and D. N. Dong (2000), Contemporary crustal deformation in east Asia constrained by Global Positioning System measurements, *J. Geophys. Res.*, *105*(B3), 5721–5734, doi:10.1029/1999JB900391.

Shen, Z. K., J. N. Lu, M. Wang, and R. Bürgmann (2005), Contemporary crustal deformation around the southeast borderland of the Tibetan Plateau, *J. Geophys. Res.*, *110*(B11), B11409, doi:10.1029/2004JB003421.

Shen-Tu, B., W. E. Holt, and A. J. Haines (1995), Intraplate deformation in the Japanese Islands: A kinematic study of intraplate deformation at a convergent plate margin, *J. Geophys. Res.*, *100*(B12), 24,275–24,293, doi:10.1029/95JB02842.

Shibutani, T., S. Nakao, R. Nishida, F. Takeuchi, K. Watanabe, and Y. Umeda (2002), Swarm-like seismic activity in 1989, 1990 and 1997 preceding the 2000 Western Tottori Earthquake, *Earth Planets Space*, *54*(8), 831–845.

Shimazaki, K., and Y. Zhao (2000), Dislocation model for strain accumulation in a plate collision zone, *Earth Planets Space*, *52*, 1091–1094.

Souter, B. J. (1998), Comparisons of geologic models to GPS observations in southern California, PhD. thesis, Mass. Inst. of Technol., Cambridge.

Suwa, Y., S. Miura, A. Hasegawa, T. Sato, and K. Tachibana (2006), Interplate coupling beneath NE Japan inferred from three-dimensional displacement field, *J. Geophys. Res.*, *111*(B4), B04402, doi:10.1029/2004JB003203.

Tabei, T., et al. (2002), Subsurface structure and faulting of the Median Tectonic Line, southwest Japan inferred from GPS velocity field, *Earth Planets Space*, *54*, 1065–1070.

Tabei, T., M. M. S. Hashimoto, and Y. Ohta (2003), Present-day deformation across the southwest Japan Arc: Oblique subduction of the Philippine Sea Plate and lateral slip of the Nankai Forearc, *Earth Planets Space*, *55*(10), 643–647.

Takayama, H., and A. Yoshida (2007), Crustal deformation in Kyushu derived from GEONET data, *J. Geophys. Res.*, *112*(B6), B06413, doi:10.1029/2006JB004690.

Tamaki, K., and E. Honza (1985), Incipient subduction and obduction along the eastern margin of the Japan Sea, *Tectonophysics*, *119*(1–4), 381–406, doi:10.1016/0040-1951(85)90047-2.

Toda, S., R. S. Stein, S. H. Kirby, and S. B. Bozkurt (2008), A slab fragment wedged under Tokyo and its tectonic and seismic implications, *Nat. Geosci.*, *1*, 771–776, doi:10.1038/ngeo318.

Toya, Y., and M. Kasahara (2005), Robust and exploratory analysis of active mesoscale tectonic zones in Japan utilizing the nationwide GPS array, *Tectonophysics*, *400*(1–4), 27–53, doi:10.1016/j.tecto.2005.02.003.

Tsutsumi, H., A. Okada, T. Nakata, M. Ando, and T. Tsukuda (1991), Timing and displacement of Holocene faulting on the Median Tectonic Line in central Shikoku, southwest Japan, *J. Struct. Geol.*, *13*, 227–233, doi:10.1016/0191-8141(91)90069-U.

Ueda, H., M. Ohtake, and H. Sato (2003), Postseismic crustal deformation following the 1993 Hokkaido Nansei-oki earthquake, northern Japan: Evidence for a low-viscosity zone in the uppermost mantle, *J. Geophys. Res.*, *108*(B3), 2151, doi:10.1029/2002JB002067.

Wallace, L., S. Ellis, K. Miyao, S. Miura, J. Beavan, and J. Goto (2009), Enigmatic, highly active left-lateral shear zone in southwest Japan explained by aseismic ridge collision, *Geology*, *37*(2), 143–146, doi:10.1130/G25221A.1.

Wang, Q., et al. (2001), Present-day crustal deformation in China constrained by global positioning system measurements, *Science*, *294*(5542), 574–577, doi:10.1126/science.1063647.

Wesnousky, S., C. Scholz, and K. Shimazaki (1982), Deformation of an island arc: Rates of moment release and crustal shortening in intraplate Japan determined from seismicity and Quaternary fault data, *J. Geophys. Res.*, *87*(B8), 6829–6852, doi:10.1029/JB087iB08p06829.

Wessel, P., and W. H. F. Smith (1998), New, improved version of Generic Mapping Tools, *Eos Trans. AGU*, *79*, 579, doi:10.1029/98EO00426.

Yagi, Y., M. Kikuchi, S. Yoshida, and T. Sagiya (1999), Comparison of the coseismic rupture with the aftershock distribution in the Hyuga-nada earthquakes of 1996, *Geophys. Res. Lett.*, *26*(20), 3161–3164, doi:10.1029/1999GL005340.

Yamasaki, T., and T. Seno (2005), High strain rate zone in central Honshu resulting from the viscosity heterogeneities in the crust and mantle, *Earth Planet. Sci. Lett.*, *232*(1–2), 13–27, doi:10.1016/j.epsl.2005.01.015.

Zhang, P. Z., Z. Shen, M. Wang, W. J. Gan, R. Burgmann, and P. Molnar (2004), Continuous deformation of the Tibetan Plateau from Global Positioning System data, *Geology*, *32*(9), 809–812, doi:10.1130/G20554.1.

Zonenshain, L. P., and L. A. Savostin (1981), Geodynamics of the Baikal rift zone and plate tectonics of Asia, *Tectonophysics*, *76*(1–2), 1–45, doi:10.1016/0040-1951(81)90251-1.

J. P. Loveless and B. J. Meade, Department of Earth and Planetary Sciences, Harvard University, 24 Oxford St., Cambridge, MA 02138, USA. (loveless@eps.harvard.edu)